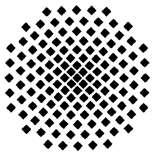

Patch loading resistance of girders with corrugated webs

PhD Dissertation

Balázs KÖVESDI
Budapest University of Technology and Economics

Supervisors:

László DUNAI, DSc
Professor
Budapest University of Technology and Economics, Hungary

Ulrike KUHLMANN, Prof. Dr. -Ing.
Professor
University of Stuttgart, Germany

Budapest, 2010.

Abstract

The corrugated steel plate is a widely used structural element in many fields of application because of its favourable properties. From the 1990's it has been increasingly used as web of steel and composite bridges. When such a bridge is incrementally launched, buckling of the thin steel web may occur. During launching nearly all cross-sections come at least once over a support where a concentrated reaction force is introduced and hereby buckling problems may arise. Bearing stiffeners give no solutions in case of moving, therefore it is necessary to determine the patch loading resistance of the corrugated webs under partial compressive patch loading, what is the topic of the thesis.

On the basis of previous experiments and numerical investigations found in the literature a numerical model is developed. On this model failure mode and ultimate load is determined by geometrical and material nonlinear analysis using geometric imperfections. Model verification is executed by the comparison of the experimental and numerical resistances and failure modes. In the frame of a numerical parametric study the geometric parameters which have influence on the patch loading resistance and on the structural behaviour are analysed, tendencies are determined. Existing design formulas from literature are summarised from the point of view of bridges and enhanced by Braun and Kuhlmann based on the numerical results.

Experimental program on 12 large scale test specimens are designed and tested at the Department of Structural Engineering of the Budapest University of Technology and Economics to analyze the structural behaviour and ultimate loads under patch loading. The aim of the experiments is the determination of the patch loading resistance by different geometrical arrangements, loading lengths and loading positions. Different failure modes and structural behaviours are analyzed and described in the function of the investigated parameters. Based on the test results the design method developed by Braun and Kuhlmann is studied and modified.

Based on the experimental program suggestions for the consideration of the equivalent geometric imperfection in the FEM based design method are collected. The applied equivalent geometric imperfection has a major importance in the FEM based design and there are no recommendations in the current version of the Eurocode 3 for corrugated web girders. In the completed research work different applicable equivalent geometric imperfection shapes are investigated and appropriate scaling factors are developed.

Eccentricities of the patch load with respect to the middle plane of the web are unavoidable during the bridge launching process, therefore the influence of the eccentricities on the patch loading resistance of corrugated web girders is investigated in this thesis. Based on the numerical calculations and based on the own experiments, conclusions for girders with trapezoidal corrugated webs are summarized and design recommendations are proposed concerning bridge launching in case of eccentric patch loading.

During launching of a bridge structure a parallel shear and transverse force are acting on the corrugated web in the same cross section, what should be considered in the design. The interaction behaviour of steel girders subjected to combination of shear and patch loading was studied only scarcely by researchers in the past and there are no standard design interaction equation in the current version of the Eurocode 3. In the frame of a numerical parametric study typical corrugation profiles, different loading lengths and a larger range of web and fold ratios are investigated. The influence of each investigated parameters are studied, tendencies are determined and a design interaction equation is proposed.

Acknowledgement

The research work is completed under the partial financial support of the following projects, foundations and cooperations:

- cooperation between the Budapest University of Technology and Economics (BME), Hungary and the University of Stuttgart, Germany,
- FOSTA Project No. P 645, German Research Association for Steel Application, Germany,
- OTKA - T049305 project, Hungarian National Scientific Research Foundation, Hungary,
- "Research scholarship for PhD students and young researchers", founded by the German Academic Exchange Service DAAD,
- the test specimens were spondored by RUTIN Kft and by Pont-TERV Rt,

which are gratefully acknowledged.

I would like to express my special thanks to my supervisors: *Prof. László Dunai* (Budapest University of Technology and Economics, BME, Department of Structural Engineering) and *Prof. Ulrike Kuhlmann* (University of Stuttgart, Institute of Structural Design) who supervised and supported me to improve the presented research work. I would like to thank their help which covered not only the professional help, but personal advices.

I would like to thank *László Kaltenbach, Dr. Miklós Kálló and Mansour Kachichian* (Structural Laboratory, BME) and all of the laboratory staff for helping me to perform the experimental part of the presented research. They gave me a special experience in the laboratory work what highly developed my researcher aspect.

I would like to give special thanks to *Benjamin Braun* (University of Stuttgart, Institute of Structural Design) who supported my research work with practical advices and helped in several ways and always turned a ready ear to my question.

I would like to thank all kind of help and support to the members of the Department of Structural Engineering of the Budapest University of Technology and Economics, where I spend most of my PhD years.

Thanks are also to the members of the Institute of Structural Design of the University of Stuttgart who helped my integration in the university life in Stuttgart, and who secured me a friendly environment during my study stay in Germany.

Special thanks are also to my family who has emotionally supported me to execute the presented research.

1. Introduction

1.1. Background of the research

The corrugated steel plate has been used in many fields of application for a long time because of its favourable properties. For example in the field of structural engineering it is used as sheet-pile wall or girder web in building structures, in the field of building design it is used for façades or roof structures, and it is a basic component of composite floors. For the last 20 years it has been increasingly used as a beam web. This structural layout has spread in the field of bridges, too, especially in hybrid bridges. This is a special bridge type with concrete decks and steel webs, mostly with corrugated steel webs.

A schematic drawing of this bridge type can be seen in Fig. 1. The first hybrid bridge with trapezoidally corrugated webs was built in France in 1986 (Pont de Cognac bridge). Because of the great number of advantages this structural layout spread very fast especially in Japan, where numerous hybrid bridges have been built or are still under construction.

Figure 1: Corrugated steel web bridges, from [1].

Due to the features of corrugation, the application of corrugated steel webs leads to advantages for hybrid bridge structures. The web has a small stiffness in longitudinal direction, therefore the prestressing force remains in the concrete chords. The resistance against buckling – locally and globally – rises, so the number of stiffeners or diaphragms may be reduced significantly. In comparison to flat webs there is a high bending stiffness in transverse direction, which allows reducing the number of cross frames in box girder bridges. Due to the increased stiffness the web thickness may be reduced, therefore the dead load of the structure may be smaller leading to easier and faster building processes especially in case of incremental launching. An another advantage is that the concreting difficulty of thin reinforced concrete webs disappears, which also results in a faster and easier building process.

The Altwipfergrund-Viaduct in Germany has the same structural layout. The building process of the bridge was finished in 2002. The lateral view can be seen in Fig. 2. This is a three-span-bridge, which spans are on the north bridge 81.47 m + 115 m + 81.35 m = 277.32 m, and on the south bridge 84.55 m + 115.00 m + 80.52 m = 280.00 m [2]. The cross section is a hybrid box girder with corrugated steel webs. The University of Stuttgart had a FOSTA Research Project No. P 645 [3] which was dealing with the structural behaviour of this new type of bridge structure. In one part of this research project the patch loading resistance of girders with corrugated webs was investigated in detail.

The current research started in the frame of this FOSTA Research Project and further continued in the cooperation between the Institute of Structural Design of the University of Stuttgart and the Department of Structural Engineering of the Budapest University of Technology and Economics. In the current PhD thesis only my part of the research cooperation is presented and results of my own research activities are referred. More informations are given in Section 2.5.2 where some research details which are not part of my

own work and those which are absolutely necessary to understand the research steps, are clearly separated.

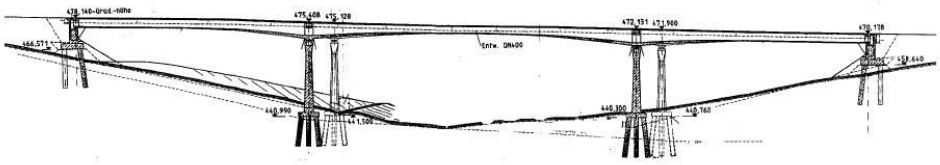

Figure 2: Lateral view of the Altwipfergrund-Viaduct, from [2].

1.2. Motivation of the research

1.2.1. Determination of the patch loading resistance of girders with trapezoidally corrugated webs

From the modern bridge erection methods the incremental launching technique is one of the most competitive. This building process, however, involves a problem with buckling of the thin steel web under patch loading. During launching nearly all cross-sections come at least once over a support where a concentrated reaction force is introduced and hereby buckling problems may arise. Bearing stiffeners give no solutions in case of moving, therefore it is necessary to determine the patch loading resistance of the corrugated webs under partial compressive patch loading.

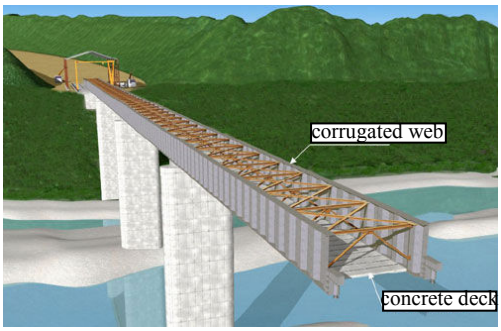

Figure 3: Incremental launching of a corrugated web bridge, from [1].

When launching a bridge the buckling stability due to patch loading is a decisive situation to be considered. There are no rules provided however for patch loading of corrugated web girders in the EN1993-1-5 Annex D [4]. In the literature there are only a few investigations dealing with the patch loading resistance of girders with corrugated webs. The existing experimental, analytical and numerical investigations were analysed from the point of view of bridge constructions. Investigations up to now focused on typical building structures, where the web slenderness is high and the loading length is short. These investigations are extended on typical bridge structures in the current PhD thesis.

On the basis of previous experimental results available from literature a numerical model is developed. In the frame of numerous numerical simulations by finite element method (FEM) the structural behaviour of corrugated web girders under patch loading is analysed and the influence of the geometric parameters on the load bearing capacity are determined. Existing design methods from literature were studied and compared to the previous experimental and current numerical results. The applicability of different design models were analysed and the design method of Kähönen [5] showed the best approach in case of typical bridge structures. On the basis of my numerical calculations the design method of Kähönen is further developed and modified by Braun and Kuhlmann [3]. To justify this modified design method laboratory experiments are performed on 12 steel I-girders at the Budapest University of Technology and

Economics, Department of Structural Design. The previously proposed design method is modified and verified by these test results and by further numerical calculations.

Based on the executed tests recommendations are formulated for a finite element simulation based design method. The aim of the finite element calculations is the direct determination of the design value of the patch loading resistance. In case of design methods based on finite element analysis the consideration of the equivalent geometric imperfection has a major importance. There are no standardized imperfection shapes and scaling factors for corrugated webs. Therefore in the frame of this PhD thesis applicable imperfection shapes and scaling factors are determined for patch loading resistance calculation of corrugated web girders.

1.2.2. Determination of the eccentric patch loading resistance of girders with trapezoidally corrugated webs

During launching of a bridge structure, eccentricities of the patch load with respect to the plane of the web are unavoidable in practice (Fig. 4). The objective of this study is to analyze the influence of the eccentricity on the patch loading resistance of corrugated web girders.

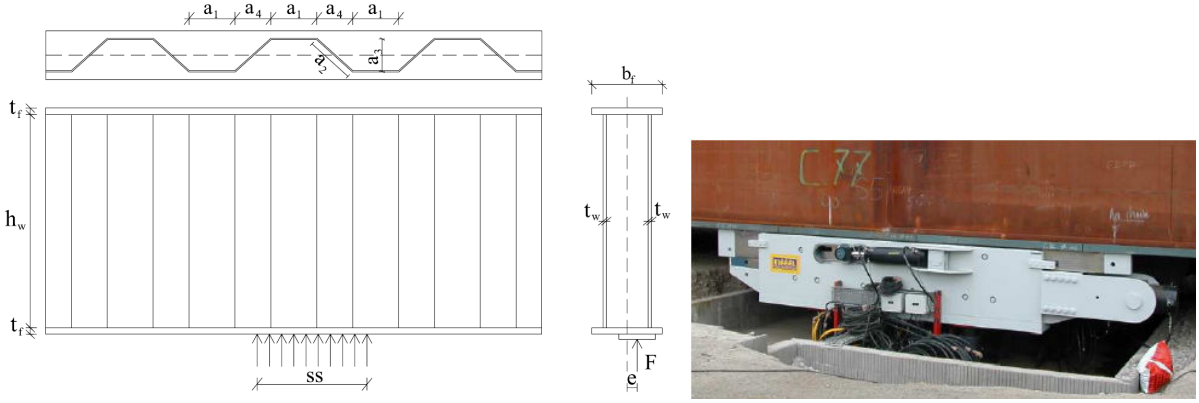

Figure 4: Launching device and eccentric loading, from [6].

As a previous step before analyzing the eccentricity, the effect of the loading width is investigated. The loading width should be smaller than the flange width to be able to analyze eccentricities. Reduced loading width indicates a reduction in the patch loading resistance as well, what should also be taken into account. In the literature no investigations are available dealing with the effect of loading width, therefore a reference experiment and a comprehensive numerical parametric study is conducted in this research field. Based on numerical calculations the parameters which have influence on the patch loading resistance with different loading width are determined and a design proposal is developed.

After the loading width analysis, the resistance reduction effect due to loading eccentricity is studied in detail. There are no available design recommendations for eccentric patch loading for corrugated web girders, therefore a numerical parametric study is conducted to determine the parameters which have influence on the patch loading resistance due to eccentric loading. The analyzed parameter range is coming from bridge design and having representative dimensions. Based on the numerical calculations and based on own experimental results conclusions for girders with trapezoidal corrugated webs are summarized and design recommendations are proposed concerning bridge launching in case of eccentric patch loading.

1.2.3. Interaction of shear and transverse forces

In practice the shear force diagram changes during launching of a bridge structure which is shown in Fig. 5. Before the launching truss reaches the pier, large shear and transverse force are introduced at the previous pier at the same time. It means that a large transverse force and

a large shear force are acting on the corrugated web in the same cross section, what should be considered in the design.

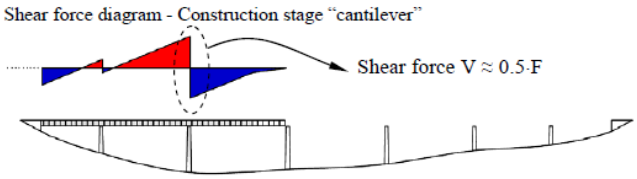

Figure 5: Shear force diagrams during launching, from [7].

In case of bridges, which are typically built with large web depths, the main part of the shear resistance comes from the contribution of the web. Bridges erected by incremental launching process have mostly thick webs and the applied loading length at the launching device is usually long. Therefore the main part of the patch loading resistance comes also from the web contribution. For corrugated web girders it is especially true, because due to the corrugation profile the lateral stiffness of the web increases which leads to the increase of the shear and patch loading resistance as well. It means that a larger part of the resistance comes from the web contribution. Due to the enlarged role of the web in both resistances, the interaction of shear and transverse forces is extensively investigated.

The interaction behaviour of steel girders subjected to combination of shear and transverse force was studied only scarcely by researchers in the past. Even for flat web girders there are only a limited number of investigations conducted in this topic till now and there is no standard design interaction formula in the current version of the EN1993-1-5 [4] neither for flat web nor for corrugated web girders. There is only one available investigation in the literature dealing with the interaction of transverse and shear force of corrugated web girders. No experiments on corrugated webs are conducted to analyze this effect and only some numerical calculations are available dealing with a relative small parameter range.

In the framework of a numerical parametric study the analyzed parameter range is extended for the typical bridge geometries. Typical corrugation profiles, longer loading lengths, and a larger range of web and fold ratios are investigated. Numerical parametric study is conducted to analyze the influence of each investigated parameters and tendencies are determined. Based on the numerical calculations design interaction equation is also developed.

1.3. Solution strategy

The aim of the research is fulfilled by the above listed general solution steps at each particular topic:

- literature overview,
- evaluation of the previous investigations and problem statement,
- numerical model development and model accuracy verification based on experiments,
- analysis of the structural behaviour,
- virtual experiments, extending the real experimental results if available,
- numerical parametric study to analyse the parameters which have influence on the load bearing capacity,
- development of design method proposals based on numerical and experimental results.

2. Determination of the patch loading resistance under centric loading

2.1. General

Patch loading of corrugated steel web girders is a research field where only a few investigations are conducted till now, however the local buckling of the thin steel web can occur under patch load during incremental launching. There is no standard design method in order to determine the patch loading resistance of corrugated web girders and only a few research recommendations can be found in the literature. A comprehensive study is executed in the frame of the current PhD thesis in this topic which is detailed in this chapter. The parameters which are used in the followings are noted in Fig. 6.

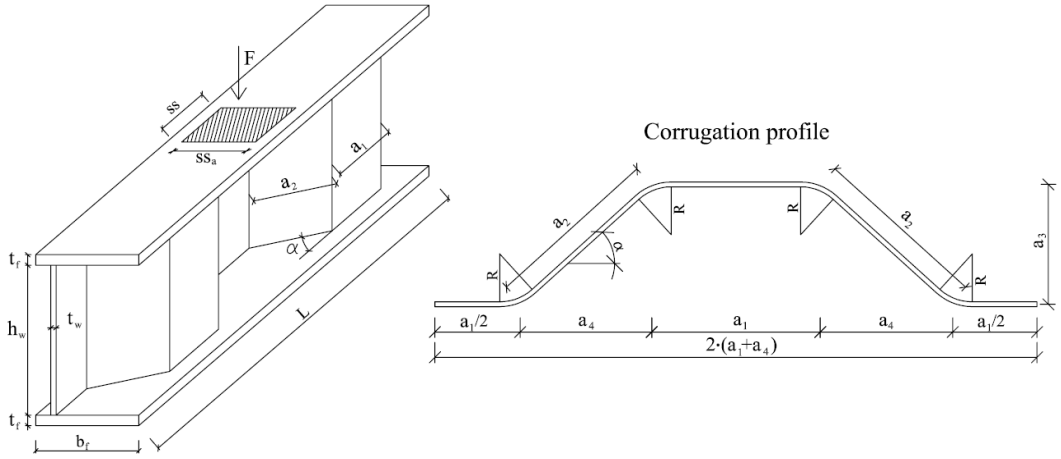

Figure 6: Used notations for trapezoidally corrugated girders.

2.2. Review of previous investigations

2.2.1. Experimental and numerical investigations

Experimental research on the patch loading resistance of girders with trapezoidally corrugated webs started in 1987 by Leiva-Aravena and Edlund [8]. A total of six specimens were tested in Sweden. Three parameters, namely the patch load width, the load location and the web thickness, were considered. The load was applied across the total width of the flange, as a 50 mm wide patch or as a line load at three different locations, namely, over a parallel or inclined fold, or at the fold line. Three different beam depths were analyzed in the frame of the experimental investigations. In 1988, Kähönen made six tests on different I-girders, where the web crippling was analysed under patch loading [5]. The influence of web thickness, web depth and span were examined. In all experiments, the girder was preloaded with two independent concentrated loads, covering the additional shear stress and bending moment for the structure. Based on the experiments Kähönen made the conclusion that the difference between girders with corrugated webs and traditional I-beams is not only in the patch loading resistance, but these I-beams have a special character, which is called by him as „snap-through-phenomenon". Its essence is that the failure of the girder appears very quickly after reaching the ultimate load. Elgaaly and Seshadri made five tests in 1997 [9]. The tests were performed on a simply supported beam by varying the position of the applied load. All tests focused on typical building structures, where the load is transferred from the purlins to the roof girder, and therefore the loading length is usually very short. In all cases, the failure was due to vertical bending of the flange and crippling of the web under the load. The vertical bending of the flange, when the load was applied over a parallel fold, was accompanied by twisting.

Numerical investigations were made by Elgaaly and Seshadri based on their experiments [9] and a finite element model was developed to analyse the patch loading failure. The finite element model was used thereafter to conduct parametric studies to examine the influence of the thickness and yield strength of the flange and web, the width and location of the applied load, the web panel aspect ratio, and the corrugation profile on the behaviour. Ultimate strength of girders with corrugated webs are determined and investigated under in plane compressive patch loading.

Further numerical investigations were conducted by Luo and Edlund in 1996 [10]. The ultimate strength of steel plate girders with trapezoidally corrugated webs under patch loading was studied using non-linear finite element analysis. The following factors were investigated: elasto-plastic strain-hardening material models; initial imperfections (global and local); variation of yield stress and strain-hardening degree at the corrugation corners due to cold-forming („corner effect"); loading position; load distribution length; variation of geometric parameters.

2.2.2. Theoretical investigations

Based on the experimental and numerical investigations design models were already developed and are available in the literature. The first design model for patch loading resistance of girders with corrugated webs was recommended by Kähönen in 1988 [5]. This design formula is based on the four plastic hinge failure mechanism (Fig. 7) developed by Rockey and Roberts for flat web girders [11].

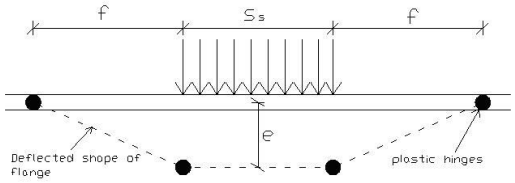

Figure 7: Flange mechanism under patch loading failure, from [5].

The resistance calculation method of Rockey and Roberts according to Eq. (1) can be subdivided into two parts, the first is the contribution of the flange, and the second is the contribution of the web [11].

$$F_R = \sqrt{4 \cdot M_{pl.f} \cdot t_w \cdot f_{yw}} + f_{yw} \cdot t_w \cdot (ss + f) \tag{1}$$

where: $M_{pl.f}$ plastic moment resistance calculated from the flange plate by Eq. (2),

$$M_{pl.f} = \frac{b_f \cdot t_f^{\,2}}{4} \cdot f_{yf}\,, \tag{2}$$

f_{yf} yield stress of the flange,
f_{yw} yield stress of the web,
t_w web thickness,
t_f flange thickness,
ss loading length,
f deflected shape length next to the applied load.

Kähönen modified this formula for corrugated web girders. The design method is calibrated to the experimental results with several factors. To include the possible interaction of bending moment and shear force and supplemented the formula with a third part, concerning the influence of the normal force in the flange plates.

Elgaaly and Seshadri also developed a design method on the basis of their experimental and numerical investigations [9]. Two distinct failure modes were observed, web crippling and

web yielding for which separate equations were proposed. The ultimate load for web crippling consists of two components. One represents the contribution of the flange which can be determined from the flange collapse mechanism, and the other represents the contribution from the web, which can be calculated on the basis of an empirical equation developed for flat web girders. The ultimate load of web yielding can be calculated based on yielding of the web. The smaller of the two calculated resistances is governing.

In 1996, Luo and Edlund [10] proposed an empirical design formula based on a simple design model for flat webs. According to their investigations the most influential parameters are the loading length and the corrugation angle. Recommendations for the influence of those parameters were developed, and they were taken into account in the resistance formula.

The EN1993-1-5 Annex D [4] deals with members with corrugated webs, but there is no standard design method for patch loading of girders with trapezoidally corrugated webs.

2.2.3. Summary of previous investigations and research aims

The parameter range of the previously executed tests and numerical calculations is shown in Fig. 8, depending on the loading length and web panel ratio. The grey area illustrates the considered parameter range used in bridges. The majority of the executed experiments until now deal with very short loading lengths where the loads are applied only along one fold. For bridges, built with incremental launching process, the launching device at the pier corresponds to the location of load introduction and its length is usually not limited to one fold, but it can be significantly longer. By the up to now built bridges the loading length varies in general between 40-80% of the web depth (ss/h_w = 0.4 to 0.8).

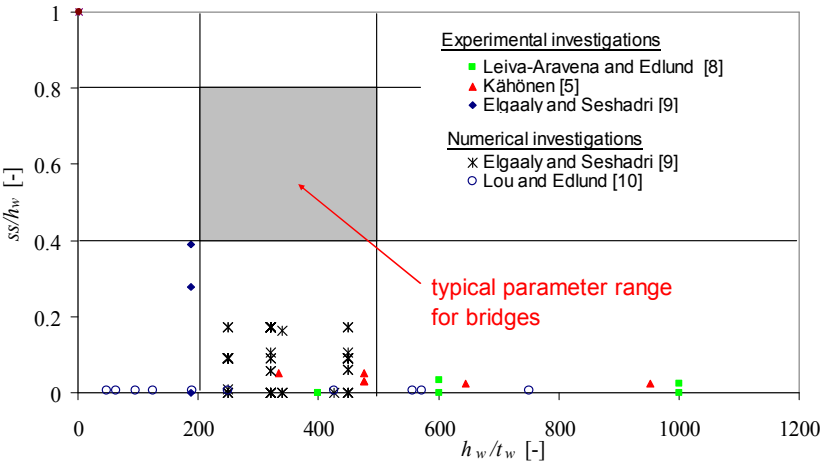

Figure 8: Parameter range of experimental and numerical investigations.

The other important difference is that in most of the tests the global web ratio (h_w/t_w) was higher than usually used in bridges. In bridges with trapezoidally corrugated webs this ratio is typically between h_w/t_w=250 - 500. Figure 8 shows that most of the executed tests are far from this typical parameter range, therefore an extended analysis is executed in the framework of a numerical parametric study and a numerical database is developed for patch loading resistance of girders with trapezoidally corrugated webs covering a large parameter range. Structural behaviour is analysed and all geometric parameters having influence on the patch loading resistance are determined and tendencies are clarified. All the previous theoretical investigations are based on limited number of test results or numerical calculations. The applicability of the previously developed design methods are studied and evaluated for bridge design. Based on the numerical database developed in this thesis, influences of all geometric parameters are established and tendencies are implemented in the design method developed by Braun and Kuhlmann [3], [12].

2.3. Verification of the numerical model

2.3.1. Geometrical model

Experiments of Elgaaly and Seshadri [9] are the nearest to the parameter range used in bridges (Fig. 8). Therefore a numerical model is developed on the basis of their tests using finite element software Ansys v10.0 [13]. Figure 9 shows the geometry of the test specimens and the developed numerical model is presented in Fig. 10.

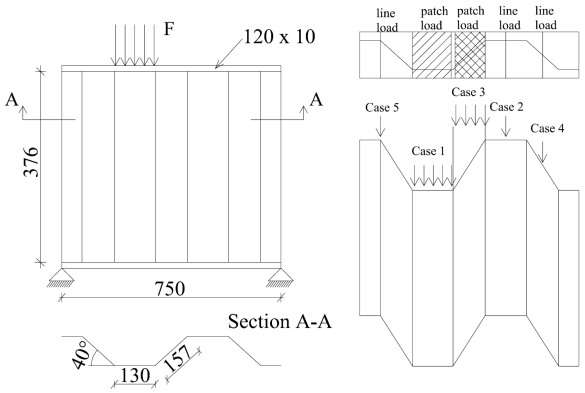

Figure 9: Test specimen of Elgaaly and Seshadri, from [9].

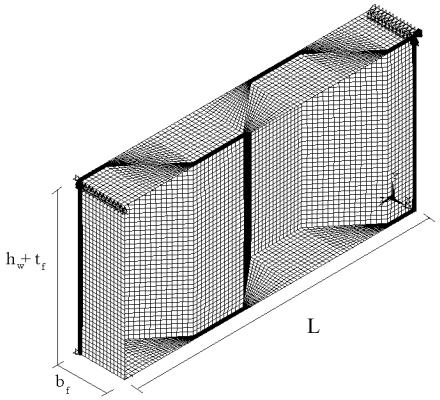

Figure 10: Geometry and finite element mesh of the developed model.

Geometric parameters of the specimens and material properties are published in [10]. The web thickness and web height of the analyzed girders are 2 mm and 376 mm, respectively. Both flanges are made from a 119.9 mm wide and 10 mm thick steel plate. Corrugation profile can be seen in Fig. 9. The corrugation angle takes 40°, a_1 and a_2 lengths are equal to 129.7 mm and 157.2 mm, respectively. All tests comprised a simply supported beam by varying the position of the applied load. The patch load was applied through a 25.4 mm thick loading plate (cases 1 and 3), and the line loads were applied using a 76.2 mm diameter steel rod (cases 2, 4 and 5).

Modelling is based on a full shell model. The applied finite element is the Shell181 element [13] of the Ansys program (Fig. 11).

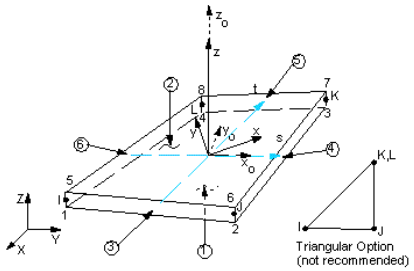

Figure 11: Applied finite element, from [13].

It is a four-node thin shell element, which has 6 degrees of freedom at each node, translations in the nodal x, y, and z directions and rotations about the nodal x, y, and z-axis. This element has both bending and membrane capabilities, so both in-plane and normal loads are permitted. Large strain and large deflection capabilities are also included. Well-suited for linear or nonlinear applications, geometrical and material nonlinearities can be also taken into consideration.

2.3.2. Material model

The applied material model is linear elastic - hardening plastic using multilinear isotropic hardening rule with von Mises yield criterion. The material is assumed to behave linear-elastic until reaching the yield strength by a Young's modulus of 210000 MPa. After it the material is assumed to follow linear hardening with a reduced hardening modulus E_r equal to 0.01·E=210 MPa. The material is modelled perfectly plastic when it reaches the ultimate strength. In the experiments of Elgaaly the yield and the ultimate strengths of the flange material were provided by the girder manufacturer, and they are 389 MPa and 563 MPa, respectively. The yield and ultimate stresses of the web were determined from test coupons to be 379 MPa and 413 MPa, respectively. The measured material properties are used for the model verification, and for the numerical parametric studies standard steel grades are used (S235, S355) with the characteristic values of the yield and ultimate strengths.

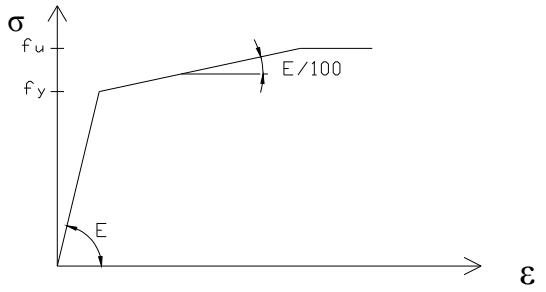

Figure 12: Linear elastic - hardening plastic material model.

2.3.3. Imperfections

For the nonlinear simulations global and local geometric imperfections are used, and the material nonlinearities are taken also into consideration. EC3 permits to use standard geometric imperfection patterns or eigenmode imperfections from a bifurcation analysis. Both imperfection types are used for the model verification. As global equivalent imperfection a sinusoidal curved shape over the web height is applied. The magnitude of this imperfection is $h_w/200$ for welded structures with a double symmetrical cross-section according to EN1993-1-5 [4]. This imperfection type is presented in Fig. 13.

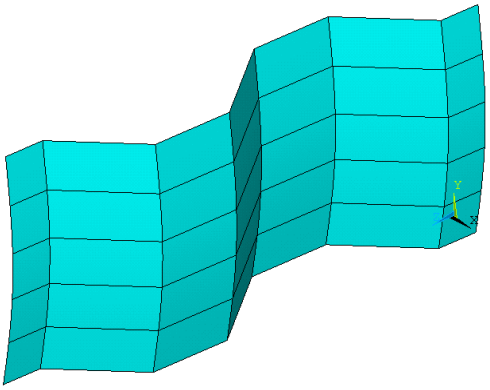

Figure 13: Global imperfection form.

In the bifurcation analysis no global eigenmode is found in the first 150 eigenmodes for the most of the models. Therefore as global imperfection only standard geometric imperfection pattern (Fig. 13) is applied.

As local imperfection, two different types of imperfection forms are studied. The first is, what the EN1993-1-5 Annex C [4] recommends in case of long, narrow plates. This imperfection form comprises a sinusoidal shaped wave in vertical direction, and in longitudinal direction it has also a sinusoidal form along the fold width (Fig. 14). The largest magnitude of it is $a_i/200$.

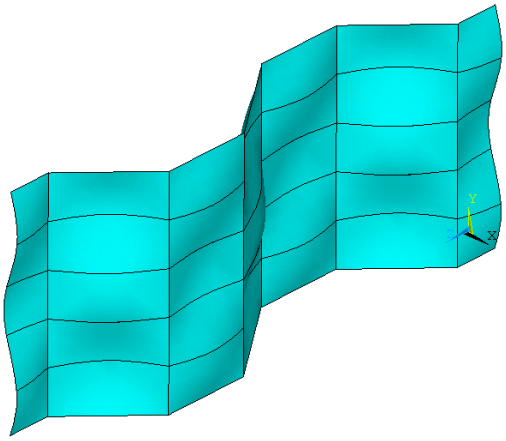

Figure 14. Local imperfection shape - type I.

The second version is closer to the local web crippling eigenmode of the girder. This shape can be determined by the function of $y = e^{-x} \cdot sin(x)$ in longitudinal direction and along the fold width it has a sinusoidal form (Fig. 15). The largest applied magnitude is $a_i/200$.

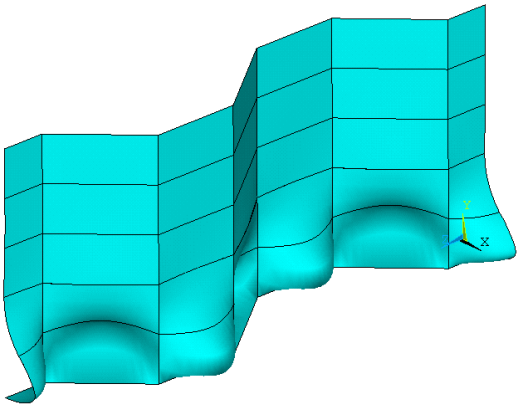

Figure 15: Local imperfection shape - type II.

As local equivalent geometric imperfection, eigenmodes can be also used. A typical eigenmode imperfection shape for patch loading analysis is presented in Fig. 16.

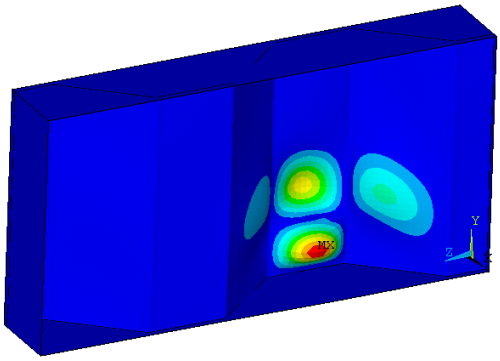

Figure 16: Local imperfection shape - type III.

2.3.4. Analysis and calculation results

Model verification is executed by simulation of all tests of Elgaaly and Seshadri [9]. The ultimate loads are determined by geometrical and material nonlinear analysis using imperfections. The Newton-Raphson approach is used in the nonlinear analysis. The convergence of the solution is checked on the basis of the Euclidean norm of unbalanced force vector by applying a tolerance of 0,1%. In the geometric nonlinear analysis large displacements and strains are considered. Automatic load stepping is used which cut a load step size in half whenever equilibrium iterations fail to converge and automatically restart from the last converged sub step. If the halved load step again fails to converge, bisection will again cut the load step size and restart, continuing the process until convergence is achieved or until the minimum load step size is reached.

The influence of the imperfection shapes and directions is analyzed. The standard local and global imperfection patterns made it possible to combine the imperfection shapes and directions in each folds. 16 different cases are analyzed. Eight from these belongs to the $y = e^{-x} \cdot sin(x)$ shaped imperfection form, and eight to the $y = sin(x)$ shaped form. The applied load on the structure is the experimental load carrying capacity of the structure according to Elgaaly's test report ($F_{R,exp}$=131.275kN). The ratio between the numerical and experimental results is studied and summarized in Table 1.

Table 1: Comparison of imperfections $F_{R,num}/F_{R,exp}$

Imperfection form: $e^{-x} \cdot sin(x)$							
+1+1+1	+1-1+1	+1+1-1	+1-1-1	-1+1+1	-1-1+1	-1+1-1	-1-1-1
0.96661	0.94987	0.93551	0.94994	0.97662	0.95469	0.94429	0.95469

Imperfection form: $sin(x)$							
+1+1+1	+1-1+1	+1+1-1	+1-1-1	-1+1+1	-1-1+1	-1+1-1	-1-1-1
0.9581	0.95337	0.94858	0.95928	0.9664	0.96084	0.9604	0.96361

The first number shows the direction of the global imperfection, the second one means the direction of the local imperfection of the parallel folds, and the third one means the direction of the local imperfection in the inclined folds. Where two signs are corresponding, the imperfection has the same direction. The definition of the signs is illustrated in Fig. 17. For example the imperfection code +1+1-1 means that the global imperfection form is in the positive direction (Fig. 17) and the local imperfection forms are in all folds in the opposite directions.

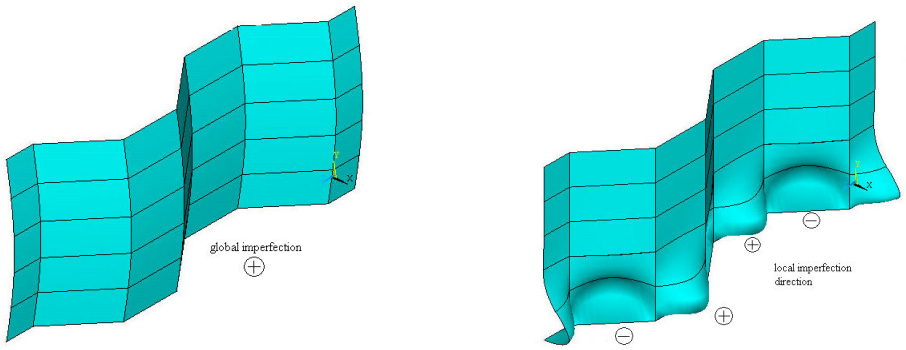

Figure 17: Illustration of imperfection directions.

It can be seen that the 93.5-97.7% of the experimental load carrying capacity is reached by the simulation by varying of the imperfection form. Results applying the sinus wave imperfection form give in all cases higher patch loading capacities than the other local imperfection shape. Case #5 gives the nearest resistance to the experiment, and case #3 resulted in the smallest

load carrying capacity (0.935·131.3=122.8kN), where the global and local imperfection of the parallel folds are in the same direction, and the local imperfection of the inclined folds are in the opposite direction. Calculations showed that the load carrying capacity is the smallest if the local imperfections of the neighbouring folds are in opposite directions. Reason for this is the ultimate buckling shape where buckling of the neighbouring folds is every time in opposite directions.

Patch loading resistance with eigenmode imperfections is also investigated. The load carrying capacity is $F_{R,num}$=126.04 kN, which is the 96.0% of the experimental value. This is higher than most of the results with standard imperfection forms. But it can be stated that the imperfection form and direction has not a significant influence on the patch loading capacity. Imperfection sensitivity showed that the influence is lower than 10%, if the applied imperfection magnitude is not larger than a_i/50.

After the detailed study of imperfection shapes and magnitudes all the test specimens of Elgaaly and Seshadri are recalculated. Table 2 shows the ultimate loads according to the experiments ($F_{R,exp}$) and numerical calculations ($F_{R,num}$). It is shown that the numerically calculated results give a good approach of the test results. Differences in cases 1-4 are between 2% - 9% and they are always on the safe side. In case #5 the experimental failure load is lower than the numerical, which may be due to the fact that this test was conducted last and after performing two tests on each flange, resulting in permanent deformations in the specimen as it was stated by Elgaaly and Seshadri in [9].

Table 2: Comparison between experimental and numerical results

Case	Location of load	Loading length, *ss* (mm)	$F_{R,exp}$ [kN]	$F_{R,num}$ [kN]	$F_{R,num}/F_{R,exp}$
Case 1	Parallel fold	146.05	131.275	122.81	0.935
Case 2	Parallel fold	≈ 0	82.325	79.737	0.969
Case 3	Inclined fold	104.14	102.35	99.79125	0.975
Case 4	Inclined fold	≈ 0	95.675	87.354	0.913
Case 5	Junction between a parallel and an inclined fold	≈ 0	73.425	100.73	1.372

The finite element model exhibited the same structural behaviour which could be observed during the tests and is published in [9]. A typical failure mode can be seen in Fig. 18/a showing not only pure web crippling, but also interaction of web and flange buckling.

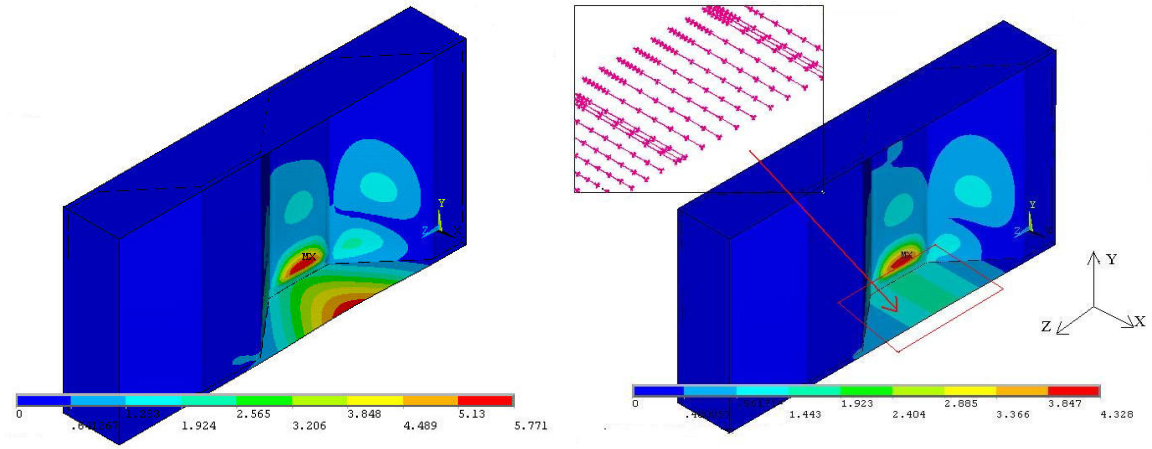

Figure 18: Typical failure mode by the numerical analysis.

In case of bridge launching the local lateral flange buckling cannot occur, because the launching device is usually stiff enough in both lateral and longitudinal directions to avoid this failure mode. Therefore in the numerical calculations the applied load is a uniformly distributed displacement load to model the load introduction through a rigid plate. This modelling approach is nearer to the real stiffness relationships in bridges as a flexible loading situation. In this way the stiffening effect of the launching device is taken into account and the failure mode is only web crippling (Fig. 18/b). The further results in the thesis are valid using this assumption.

Accomplished convergence study showed that the maximal adequate element side length is 20-40 mm depending on the fold length (a_1) of the developed model. It means that one fold should be modelled by minimum 8-10 elements along the fold length to determine the local web crippling resistance with adequate reliability. In the forgoing numerical parametric study this principle is used and the models are characterised by an element number between 9000 to 20000 depending on the span and corrugation profile.

2.4. Numerical parametric study

2.4.1. Structural behaviour

Based on the verified model a comprehensive parametric study is executed in order to analyse the patch loading resistance in the typical parameter range used in bridges. The analysed parameters, which have influence on the load carrying capacity are varied between the following values:

- web ratio: h_w/t_w=200 - 300 - 400 - 500
- fold ratio: a_i/t_w=12.5 - 25 - 50 -75 - 100 - 116.7 (in all cases a_1=a_2)
- loading length: s_s/h_w=0.4 - 0.6 - 0.8
- corrugation angle: α=15° - 30° - 45° - 65°
- flange width: b_f=150 - 300- 400 - 500mm
- flange thickness: t_f=20 - 40 - 60 - 80 - 100mm

Depending on the web and fold ratios and loading length the collapse modes can be different. For small web and high fold ratios the failure mode is mainly local buckling of the fold. For a short loading length the local buckling occurs only in one fold, for longer loading length in more folds. For small fold ratios buckling mode can change to global buckling of the whole web panel. Failure mode is mainly depending on the corrugation profile, web and fold ratios and loading length. Different failure modes are shown in Fig. 19.

local buckling in one fold → local buckling in more folds → global buckling

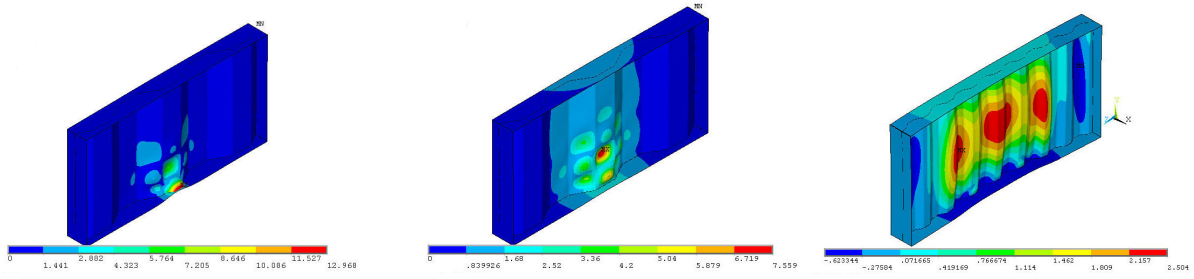

Figure 19: Different failure modes.

Figure 20 shows that for high fold ratios local buckling occurs. With decreasing local fold ratio, i.e. smaller fold widths, the global buckling becomes decisive which is dependent on the web ratio. The failure mode of girders with high web ratio is mainly global buckling, and the failure mode of girders with high local fold ratio is mainly local buckling.

Generally, it can be concluded that the failure mode of the analysed girders used in bridges are rather in the local buckling domain, and the global buckling occurs only at the limits of the analysed parameter range. In case of global buckling a further decrease in fold width only leads to a small or no increase in the ultimate load.

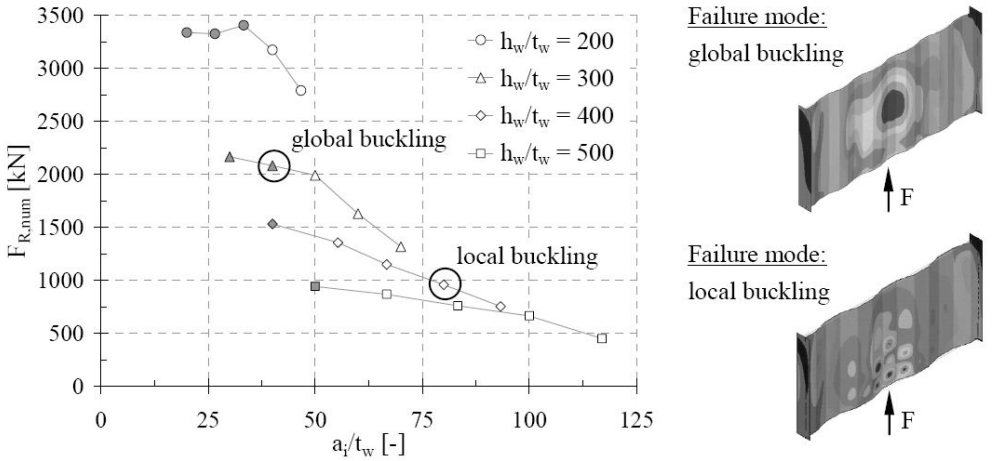

Figure 20: Change from local to global buckling.

This PhD thesis focuses only on the local web crippling in one or more folds. Numerical simulations show that the change from local and global buckling is related to web (h_w/t_w) and fold (a_i/t_w) ratios and corrugation angle. Based on the numerical database created in this study a limit function is determined by Braun [12] for the minimum fold length a_i in order to ensure local buckling.

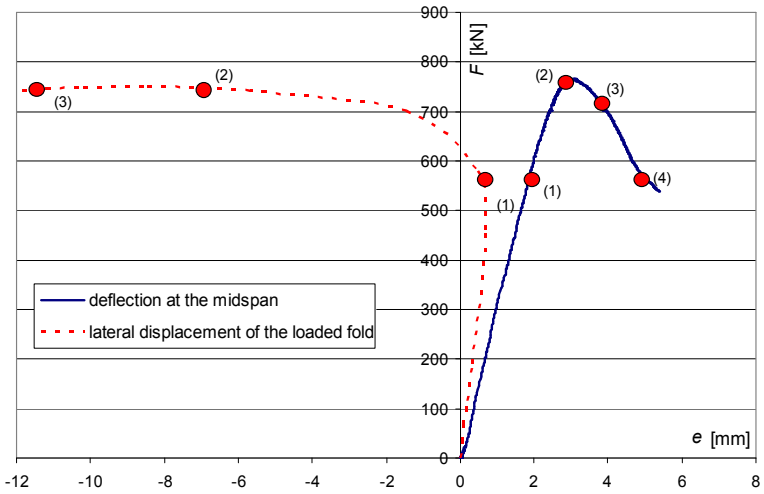

Figure 21: Typical load-displacement curves.

A typical load-displacement curve under patch loading is presented in Fig. 21. Characteristic points of the structural behaviour are signed by points. Linear part of the diagram finishes at point (1) which means the first yielding in the flange or in the web depending on the web and flange geometries and imperfection size (Fig. 22/a). Between points (1) and (2) the flange and web plates are yielding simultaneously (Fig. 22/b). Ultimate load is reached after reaching point (2) if two plastic hinges in the flange and a continuous yield line in the web are completely developed (Fig. 22/c). In the post ultimate range of the load displacement curve the third and fourth plastic hinges begin to develop at point (3) in the flange which leads to the failure mechanism of the girder. Point (4) shows the situation if all four plastic hinges are completely developed (Fig. 22/d).

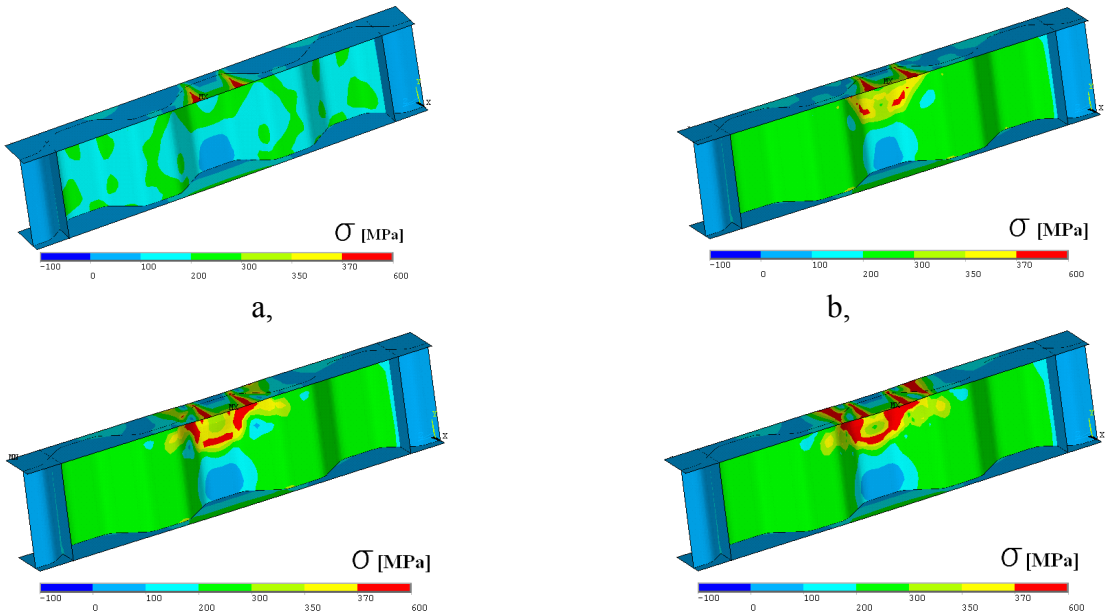

Figure 22: Yield patterns in different load steps.

2.4.2. Effect of the loading length

Increasing loading length results a nearly linear increase in the load carrying capacity. The increase is due to the activation of more web folds in case of long loading lengths. Figure 23 represents the load carrying capacity in the function of the loading length. Results show a nearly linear relationship. Numerical parametric study proved that the web ratio and the other geometric parameters have no influence on this linear tendency.

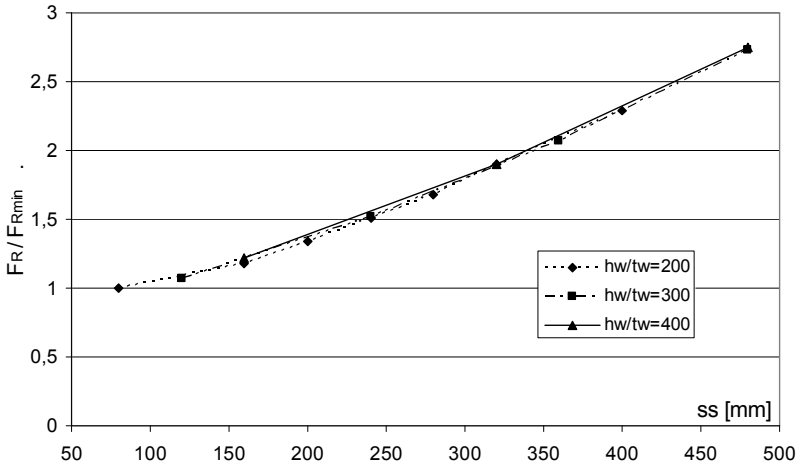

Figure 23: Effect of loading length.

2.4.3. Effect of the local fold and global web ratios

Fold width, web thickness and web height define the (local) fold and (global) web ratios (a_i/t_w and h_w/t_w). Influence of the fold ratio on the buckling resistance is analysed for different corrugation angles (20°, 35°, 45°, 65°). The relationship between buckling resistance and fold ratio is shown in Fig. 24. On the vertical axis of the diagram the patch loading resistance is divided by the loading length. The relationship shows a part of the typical reduction curve for all corrugation angles, i.e. the load carrying capacity decreases with higher fold ratios if the failure mode is local buckling.

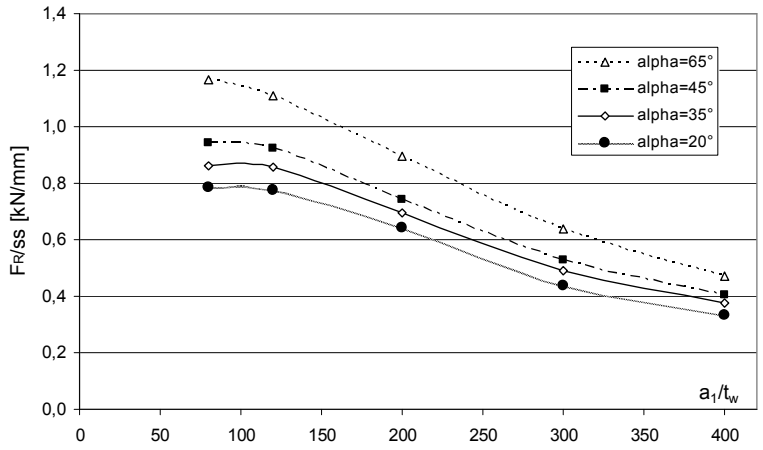

Figure 24: Influence of fold slenderness.

The global web ratio has a quite low influence on the patch loading resistance if failure mode is local buckling. If the failure mode is global buckling, the web ratio has an important effect and the reduction of the global ratio results in decrease in the load carrying capacity.

2.4.4. Effect of the corrugation angle

The corrugation angle has a significant influence on the patch loading resistance. For higher corrugation angles the patch loading resistance increases. The character of the relationship between corrugation angle and patch loading resistance can be hardly studied. If the loading length is kept constant and the corrugation angle is changed, the number of the loaded folds changes as well. If one more fold is under the applied load, the patch loading resistance increases and the relationship has a stepped character as observed before in my diploma thesis [14]. But the linear increase of the corrugation angle does not result in an increase with stepped character in the patch loading resistance; therefore the investigation mode is changed and further developed. The applied load is always placed at the mid span of the girder linked to the middle of a parallel fold and the loading length is always chosen as the multiple of the corrugation wavelength as shown in Fig. 25.

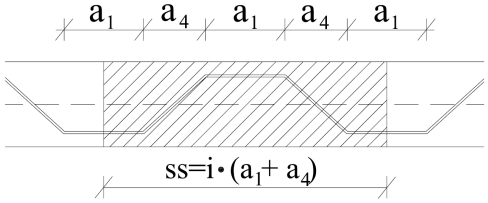

Figure 25: Load position linked to the middle parallel fold.

In this case the loading length changes with the corrugation angle. It is already known that the loading length has a significant influence on the patch loading resistance; therefore the evaluation of the results is possible only if the load carrying capacity is specified on the loading length (F_R/ss). Numerical calculations showed that the character of the relationship between corrugation angle α and relative patch loading resistance (F_R/ss) has no more a stepped character, as it is shown in Fig. 26 for different web thicknesses.

The following observations can be drawn on the results:

1, On the loading length specified load carrying capacity increases with increasing corrugation angle continuously.

2, Evaluating the various curves, the increase of the corrugation angle leads to the same increase in the load carrying capacity (39-45%) between $20° \leq \alpha \leq 65°$. Therefore the influence of the corrugation angle does not depend on the fold or web ratios.

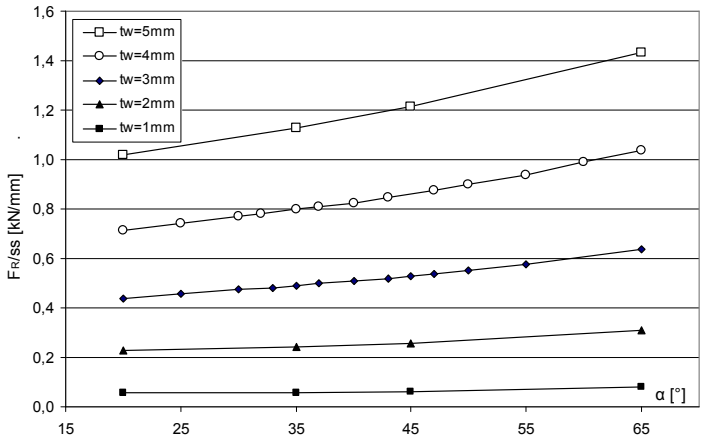

Figure 26: Influence of the corrugation angle.

2.4.5. Effect of the flange size

The flange size has a significant influence on the patch loading resistance of corrugated web girders. The flange thickness and flange width are also investigated in the frame of numerical parametric study. Figure 27 shows the resistance increasing tendency in the function of the flange thickness. Results showed that the relationship between the flange thickness and the load carrying capacity is nearly linear.

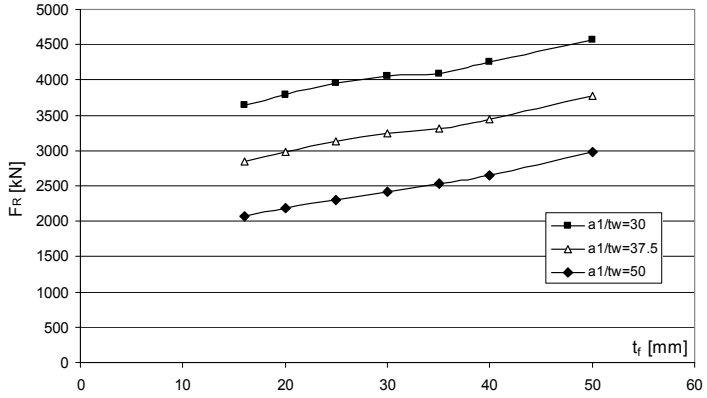

Figure 27: Influence of the flange thickness.

Effect of the flange width on the patch loading resistance can be seen in Fig. 28. The diagram shows that the relationship has a square root function. The analysed parameter range is limited to avoid the flange local buckling, because this failure mode is not part of this PhD thesis.

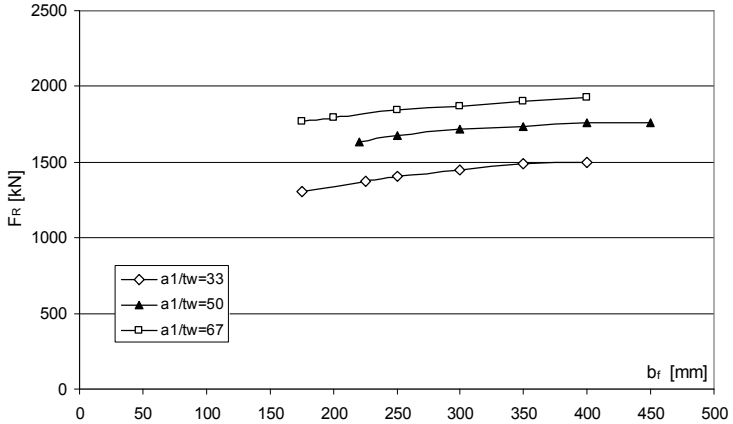

Figure 28: Influence of the flange thickness.

2.5. Design method development

2.5.1. Evaluation of the previous design methods

Regarding the conditions during bridge launching, the calculated resistances of the different design proposals (introduced in Section 2.2.2.) are compared to the results of the developed numerical database and to the results obtained from literature. This evaluation is illustrated in Fig. 29. The vertical axis of the diagrams shows the resistances according to the numerical calculations and experimental studies. The horizontal axis presents the patch loading resistances according to four different design proposals that are the followings:

1. resistance model of the EN1993-1-5 for flat web girders,
2. resistance model of Kähönen [5] for corrugated web girders,
3. resistance model of Elgaaly and Seshadri [9] for corrugated web girders,
4. resistance model of Luo and Edlund [10] for corrugated web girders.

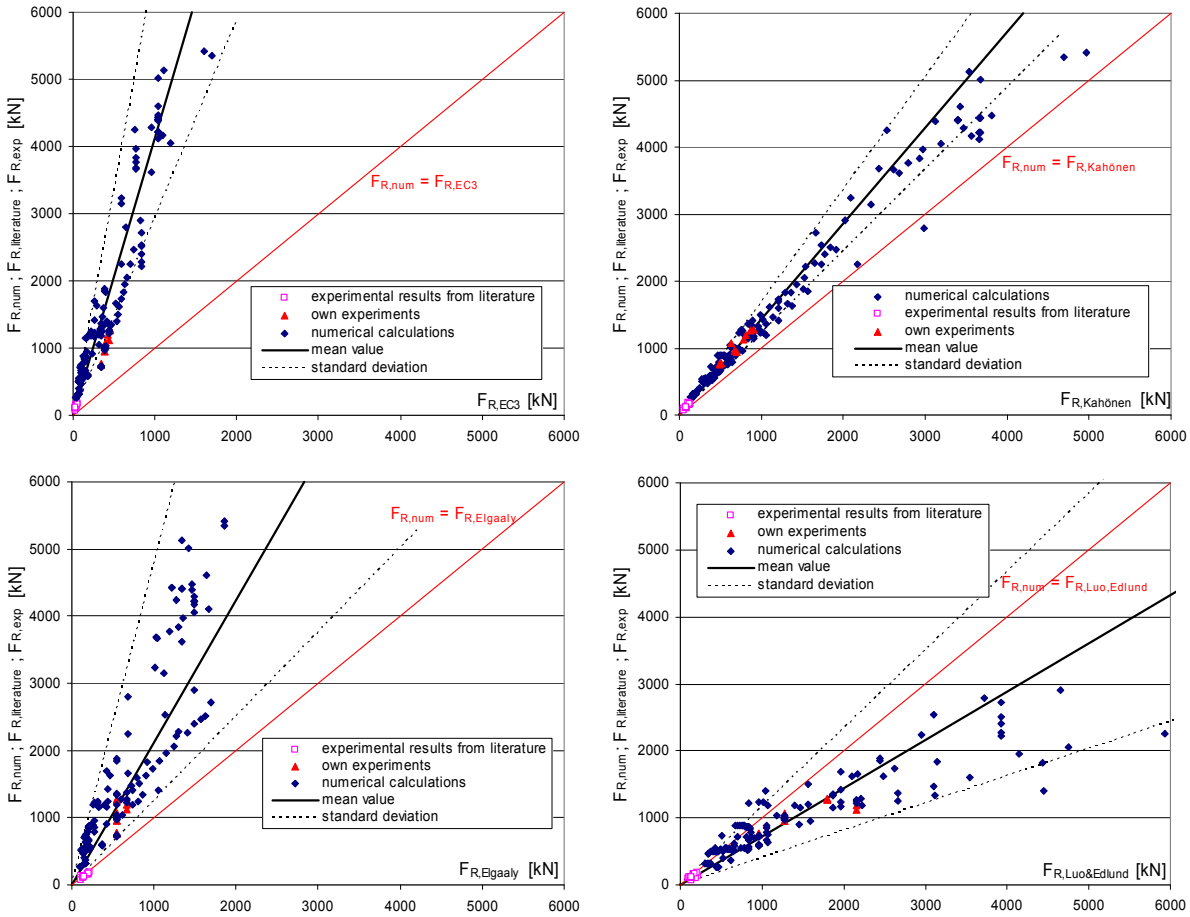

Figure 29: Comparison of the design methods to the experimental/numerical resistances.

The statistical evaluation of the resistances are summarized and presented in Table 3. Mean values and standard deviations of the $F_{R,design\_method} / F_{R,num}$; $F_{R,exp}$ ratios are calculated. If this ratio is equal to 1 the design method leads to the same resistance than numerically calculated or measured in the experiments. This case is shown by the red line on the diagrams. If this ratio is greater than 1 the design method leads to larger resistance than the real value and it means that the design method is not on the safe side. If the ratio is less than 1 the design proposal results smaller patch loading resistance than the calculated or measured values and it means that the design method is on the safe side.

Comparison shows that the resistance model for flat web girders according to EN1993-1-5 [4] leads to conservative results for corrugated web girders and it provides only a lower bound solution for the determination of the patch loading resistance of corrugated web girders.

The design proposal of Kähönen [5] leads to appropriate resistance for the existing experimental and numerical results in the parameter range used in bridges. This is due to the introduction of an effective web thickness which is able to cope with the number of loaded folds as long as local buckling occurs. Statistical evaluation showed that the design method of Kähönen underestimates the patch loading resistance of the corrugated web girders with about 30% in average and the standard deviation of the results are relative small.

The design proposal of Elgaaly and Seshadri [9] gives a good prediction of the main experimental results from literature. Since the chosen formulas for the resistance calculation are not able to account for loading of several folds appropriately, therefore the results of this design method shows larger differences for longer loading lengths which are used in bridges. This design method is recommended rather for building structures and not for bridges.

The design model of Luo and Edlund [10] generally overestimates the resistance. This originates from the calibration of the empirical factors, which is based only on a limited number of numerical calculations. In the extended analyzed parameter range this design method is not on the safe side and the scatter of the calculation results are also relative large.

Table 3: Statistical evaluation of different design methods ($F_{R,design\ method}$ / $F_{R.Num}$; $F_{R.Exp}$)

Design method:	EC1993-1-5	Kähönen	Elgaaly and Seshadri	Luo and Edlund
Mean value:	0.242	0.701	0.471	1.386
Standard deviation:	0.092	0.092	0.262	0.414

The comparison shows that the design method of Kähönen leads to the nearest resistance to the existing experimental and numerical results in the whole extended parameter range therefore it is used for further development of the patch loading resistance model. This design method does not contains the effect of the corrugation angle which has a significant effect as shown based on the numerical parametric study (Section 2.4.4.) and it does not follow the general format of the Eurocode 3 in case of stability analysis (reduction factor based design). Therefore a new modified design proposal is developed by Braun and Kuhlmann [3], [12] based on the presented numerical calculations completed by myself.

2.5.2. Design method of Braun and Kuhlmann

Based on the numerical database developed by myself an enhanced design method is developed at the Institute of Structural Design of the University of Stuttgart by Braun and Kuhlmann [3]. This section does not contain my work but a short review about this design method is definitely needed to understand the further research results of mine because they are partly claimed to this design method.

The design method is based on the four plastic hinge failure mechanism according to the patch loading theory of Rockey and Roberts [11] which was evolved for flat web girders. The design method was calibrated for corrugated web girders by Kähönen [5], and further investigated and modified by Braun and Kuhlmann for a larger parameter range based on my numerical calculations published in [14]. Equation (3) gives the value of the patch loading resistance.

$$F_R = \left(k_\alpha \cdot F_{R,w} + F_{R,fl}\right) \cdot k_0 \qquad \text{for} \qquad a_i \geq \left(\frac{h_w}{t_w} + 260\right) \cdot \frac{t_w}{11.5} \tag{3}$$

The first part of this equation refers to the resistance of the web and the second part to the resistance of the flange. The web resistance can be calculated by Eq. (4).

$$F_{R,w} = \chi \cdot t_w \cdot f_{yw} \cdot ss \cdot k_w \tag{4}$$

χ should be calculated from Eqs. (5) and (6):

$$\chi = \frac{1.9}{\bar{\lambda}_p} - \frac{0.798}{\bar{\lambda}_p^2} \qquad \text{if } \bar{\lambda}_p > 1.273 \tag{5}$$

$$\chi = 1.00 \qquad \text{if } \bar{\lambda}_p \le 1.273 \tag{6}$$

where:

$$\bar{\lambda}_p = \sqrt{\frac{f_{yw}}{\sigma_{cr}}} \quad , \quad \sigma_{cr} = \frac{k_\sigma \cdot \pi^2}{12 \cdot (1-\upsilon^2)} \cdot E \cdot \left(\frac{t_w}{a_i}\right)^2 \quad , \quad k_\sigma = 1.11 \tag{7), (8), (9)}$$

f_{yw}: yield strength of the web,
t_w: web thickness,
a_i: loaded fold length (if more fold are loaded, the maximum fold length)
ss: loading length,
k_w: modification factor due to shear and transverse force interaction.

Recommendation for the flange resistance is in Eq. (10) according to [3].

$$F_{R,fl} = 2 \cdot \sqrt{4 \cdot M_{pl.f} \cdot \chi \cdot t_w \cdot f_{yw} \cdot k_f \cdot k_w} - 0.07 \cdot \sigma_f \cdot b_f \cdot t_f \tag{10}$$

where: $$M_{pl.f} = \frac{b_f \cdot t_f^{\,2}}{4} \cdot f_{yf} \tag{11}$$

f_{yf}: yield strength of the flange,
k_f: modification factor due to bending and patch loading interaction,
b_f: flange width,
t_f: flange thickness,
σ_f: normal stress in the flange,
τ_w: shear stress in the web plate.

The design method takes the influence of the shear and bending interactions by several modification factors into account. These are the followings:

$$k_0 = 1{,}63 \cdot \frac{\sigma_f}{f_{yf}} \cdot \frac{\tau_w \cdot \sqrt{3}}{f_{yw}} + 0{,}63 \qquad \text{if } \frac{\sigma_f}{f_{yf}} \cdot \frac{\tau_w \cdot \sqrt{3}}{f_{yw}} < 0{,}23 \quad , \tag{12}$$

$$k_0 = 1{,}0 \qquad \text{if } \frac{\sigma_f}{f_{yf}} \cdot \frac{\tau_w \cdot \sqrt{3}}{f_{yw}} \ge 0{,}23 \quad , \tag{13}$$

$$k_w = \sqrt{1 - \left(\frac{\tau_w}{0{,}5 \cdot f_{yw}}\right)^2} \quad , \tag{14}$$

$$k_f = 1 - \left(\frac{\sigma_f}{f_{yf}}\right)^2 \quad . \tag{15}$$

The new non-dimensional slenderness curve (λ_p-χ) was derived from the formula of Kähönen [5] and it can be applied for the patch loading resistance of corrugated web girders. The recommendation is shown in Fig. 30. Curve ① is the proposal of EN1993-1-5 [4] for patch loading of flat web girders, points show the results calculated from tests, curve ② shows the

proposal derived from the formula of Kähönen, and curve ③ is the recommended enhanced non-dimensional slenderness curve for local buckling of corrugated web girders by Braun and Kuhlmann [3].

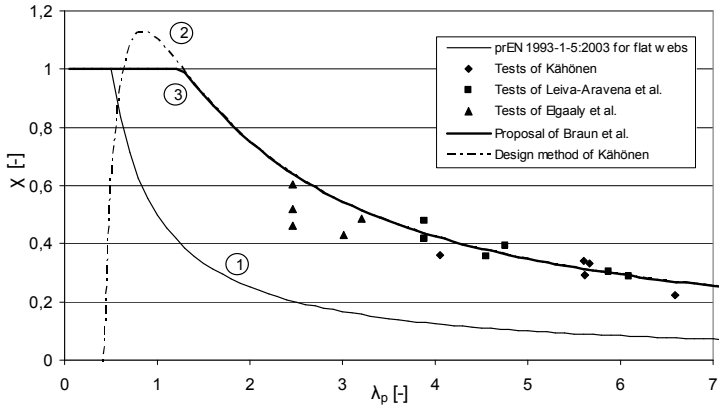

Figure 30: Non-dimensional slenderness and reduction factor relationship.

Numerical results showed that the corrugation angle has a significant influence on the patch loading resistance. Luo and Edlund [10] developed an empirical design formula which considers the influence of the corrugation angle. Parametric study shows that this curve does not follow the numerical results calculated by myself in case of larger corrugation angles ($\alpha > 40°$). According to the numerical parametric study the character of the increasing patch loading resistance can be described sufficiently well by referring the real length of the folded web to the projected loading length. Therefore it is proposed by Braun and Kuhlmann to improve the design method by the factor k_α, which can be calculated from Eq. (16) developed in [12].

$$k_\alpha = \frac{a_1 + a_2}{a_1 + a_4} \tag{16}$$

The points in Fig. 31 show the results of the numerical calculations. The proposal of Luo and Edlund is illustrated by curve ①, and the proposal of Braun and Kuhlmann is shown by curve ②, which follows the numerical results well and in the whole analyzed parameter range it is on the safe side. The applicability of the developed k_α is proved by me based on the numerical calculations.

The developed design method is valid for corrugation angles $15° \leq \alpha \leq 65°$, for loading lengths in the range between $ss/h_w = 0.4$ and 0.8, if inclined and parallel folds have the same length ($a_1 = a_2$). This design formula can be used between the web h_w/t_w= 200 to 500 and fold ratios a_1/t_w= 15 to 100. This parameter range is relevant for bridges.

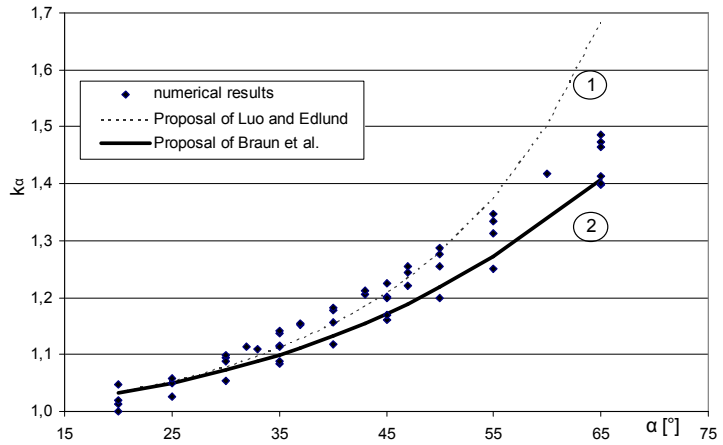

Figure 31: Influence of the corrugation angle.

2.6. Summary and conclusions

All the presented results are directly applied in a German research project (FOSTA Project No. P 645) aiming (among others) to analyze the patch loading resistance of corrugated web girders. The project is introduced in [3].

On the basis of the till now executed experiments a numerical model is developed with the finite element program Ansys 10.0. On this model a nonlinear calculation is conducted with geometrical and material nonlinearities. A model verification is executed by the comparison of the ultimate loads and failure modes observed in the tests and in the numerical calculations. In the frame of the numerical simulations different imperfection forms and magnitudes are also studied. After the model verification a large number of numerical simulations (virtual tests) are carried out. The influences of all geometric parameters are analyzed and the following conclusions are drawn:

- increase of loading length → linear increase of the patch loading resistance,
- increase of fold ratio → decrease of the load carrying capacity if failure mode is local buckling,
  this has no effect if the failure mode is global buckling,
- increase of web ratio → decrease of the load carrying capacity in the global buckling domain,
  this has no effect if the failure mode is local buckling,
- increase of corrugation angle → patch loading resistance increases continuously,
- increase of flange thickness → linear increase of the patch loading resistance,
- increase of flange width → increase of the patch loading resistance.

Numerical calculations are used for the design method development which may be applied for the practical design of corrugated web girders. An enhanced design method is developed by Braun and Kuhlmann for patch loading of corrugated web girders in [3], [12]. A new formulation of the corrugation angle influence is developed and its applicability in a large parameter range is proved.

3. Experimental investigations

3.1. Aim of the tests

Patch loading tests are conducted on 12 simply supported girders. The aim of the tests is to determine the patch loading resistance of corrugated web girders with a typical corrugation profile of a real bridge girder by tests. Ultimate loads are determined and structural behaviours and failure modes are analysed and described. Based on the test results the previously developed design method is verified and improved.

3.2. Test program

3.2.1. Test specimens and test arrangement

A total of 12 one span simply supported girders are tested under patch load at the Department of Structural Engineering of the Budapest University of Technology and Economics in 2009. Test arrangement and specimen may be seen in Fig. 32.

Figure 32: Test arrangement.

The girders have a 6 mm thick and 500 mm depth web, made of cold formed steel plates. The flange width is 225 mm and the thickness of the flange varies between 20 and 30 mm. The span is 1875 mm if a parallel fold and 1500 mm if an inclined fold is loaded. To analyze the bending moment and transverse force influence one test is carried out on a very short span girder (L=1140 mm). Bearing stiffeners at both ends of the girders are made from the same steel plate as the flanges with 20 mm thickness. The corrugation profile is the same for all specimens, the geometry is shown in Fig. 33. The fold lengths are a_1=210 mm, a_2=212 mm and the projected lengths of the inclined folds are a_3=133 mm and a_4=165 mm. The corrugation angle is 39° for all specimens. The corrugation amplitude is 66.5 mm and the wavelength is 844 mm. The measured average yield and ultimate strengths of the flange material are 379 MPa and 517 MPa, and for the 6 mm thick web plate 373 MPa and 542 MPa, respectively. The measured yield and ultimate strengths and the ultimate elongations are summarized in Table 4.

The load is applied along the total width of the flange by a 50 mm thick loading plate. Four different loading lengths are used (90, 200, 300 and 380 mm). In two cases the load eccentricity is analyzed, therefore only a part of the flange along the width (80 mm) is loaded at the first time by a centric load and than with 30 mm eccentricity. In these two cases the load is applied through a 300x80x50 mm loading plate. The geometry for all specimens and the loading positions are given in Table 5.

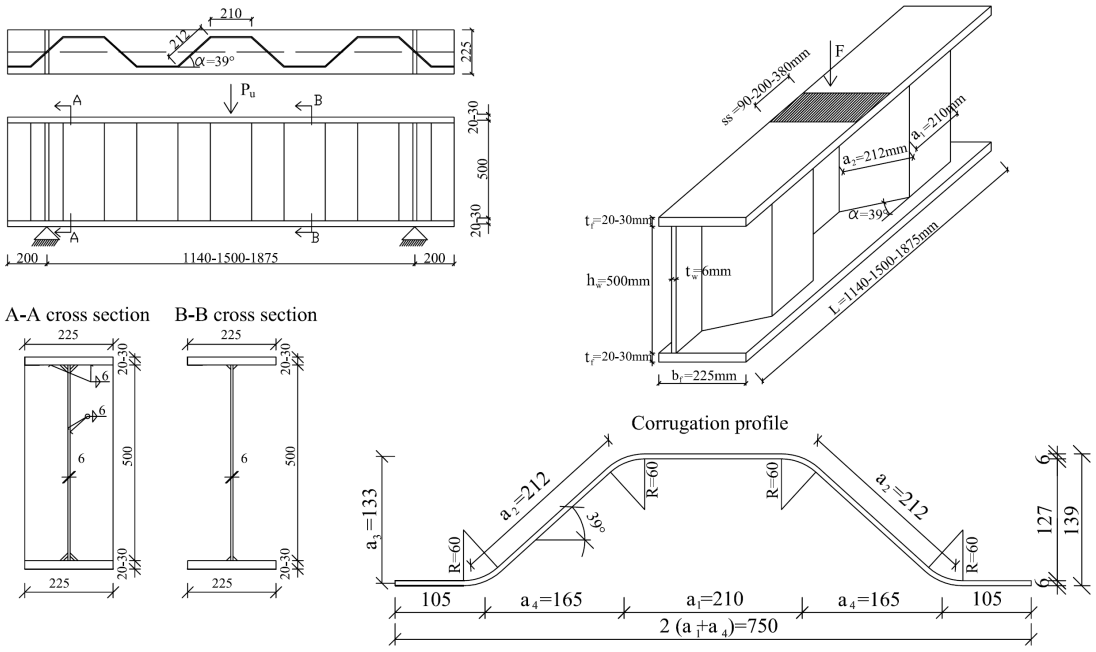

Figure 33: Test specimen.

Table 4: Measured material properties

Specimen number	Specimen		Yield strength	Ultimate strength	Ultimate elongation
	thickness	width			
			f_y	f_u	A
	mm		N/mm^2		%
BME94/1	5,99	20,2	374	541	27,0
BME94/2	5,99	20,2	374	544	26,0
BME94/3	5,99	20,2	370	541	29,5
BME94/4	19,74	15,5	367	510	26,5
BME94/5	20,32	15,4	410	535	25,5
BME94/6	20,01	15,5	360	507	27,0

Table 5: Geometry of test specimens and loading positions

specimen	t_f [mm]	L [mm]	ss [mm]	loaded fold
1	*20*	*1500*	*90*	inclined
2	*20*	*1500*	*200*	inclined
3	*20*	*1875*	*90*	parallel
4	*20*	*1875*	*200*	parallel
5	*30*	*1875*	*200*	parallel
6	*30*	*1500*	*200*	inclined
7	*20*	*1140*	*200*	parallel
8	*20*	*1500*	*380*	inclined
9	*30*	*1500*	*300x80*	inclined (centric loading)
10	*30*	*1500*	*300x80*	inclined (eccentric loading)
11	*20*	*1875*	*380*	parallel
12	*20*	*1500*	*90*	corner area

3.2.2. Measurement system

Applied loading press is a VEB 276/3 hydraulic press which has a loading capacity of 6000 kN. During the tests the applied force and displacements are measured on different positions. Load is determined using a load cell connected to the hydraulic jack. Inductive displacement transducers are used to measure the vertical and horizontal displacements of the specimens. In case of specimens 1-4 two inductive transducers (T1 and T2) and in case of specimens 5-12 three inductive transducers are applied (T1-T3). Location of the transducers is identical in all test sets and the arrangement is shown in Fig. 34.

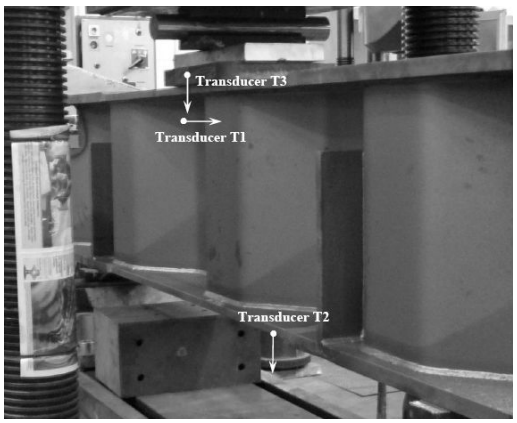

Figure 34: Measurement system.

Measuring goals:

- Transducer 1 (T1) is placed on the web in 50 mm distance from the upper flange. This transducer measures the horizontal displacement of the loaded fold and therefore it is placed near to the zone where web crippling is expected.
- Transducer 2 (T2) measures the vertical displacement of the tested girder at the mid span under the lower (unloaded) flange.
- Transducer 3 (T3) measures the vertical displacement of the upper (loaded) flange under the loading plate.

The measured data of the inductive transducers and load cell are recorded at 1 Hz frequency by a HBM Spider8 amplifier connected to a Laptop PC running the HBM CatmanEasy software. During a real-time data visualization the load is increased continuously by a constant loading velocity.

3.3. Experimental program and test results

The aim of the tests is to determine the patch loading resistance by different geometrical arrangements, loading lengths and positions. These tests give verification background for the finite element model development and for the design method presented in Section 2.5.2. In the frame of the tests the following parameters are varied:

- loading length (90 mm; 200 mm; 380 mm),
- loaded fold (inclined, parallel fold or corner area),
- flange thickness (20 mm; 30 mm),
- span (1140 mm; 1500 mm; 1875 mm),
- load eccentricity in transverse direction.

Two different failure modes are observed during the tests. If the loading length is short the web buckling is limited mainly in one fold, and the wavelength of the buckled shape along the web depth is relatively short. If buckling occurs in the neighbouring folds as well, all buckling waves have the same direction as presented in Fig. 35/a. This failure mode is called web crippling in the following. If the loading length is longer, more folds take part in the load

carrying and therefore web buckling appears in all loaded folds at the same time. The buckling zone extends on more folds and it is longer compared to the previous one as illustrated in Fig. 35/b. In this failure mode bucking waves in the neighbouring folds have every time alternating direction. This failure is called local web buckling. These two failure modes are compared in Fig. 35. A sharp limit between them cannot be determined, it is mainly depending on the loading length, corrugation profile and on the fold ratio. In the case of all tested girders one of these two failure types occurred.

a, web crippling *b, local web buckling*

Figure 35: Observed failure modes.

During the tests the applied force, the deflection of the upper and lower flange, and the lateral displacement of the loaded fold are measured and presented in diagrams for all test specimens. The corresponding failure modes are shortly described and presented in the following figures.

Specimen 1:

In case of specimen #1 the inclined fold is loaded with a relatively short (*ss*=90 mm) loading length. The span of the girder is 1500 mm and the flange thickness is 20 mm. Only one fold is loaded and therefore the extension of the buckled zone is quite small and mainly limited on the loaded fold. The neighbouring folds are only partly buckled and plastic deformations in the flange plate can also be observed. This failure mode is the typical web crippling. The measured ultimate load during the experiment is 754.2 kN and the recorded load-displacement curves are presented in Fig. 36. The red thin curve on the diagram shows the lateral displacement of the inclined web fold under the applied load. The diagram has a characteristic point at the load level of 630 kN. Horizontal deformations are relatively small under this load level; this means that buckling of the web developed only after reaching this load level. The linear part of the load-displacement curve finishes here and the first yielding appears near to this point. On higher load levels until reaching the ultimate load and in the post ultimate behaviour the plastic deformations of the web panel are relatively large. The blue bold curve shows the vertical deflection of the lower flange at the midspan. The linear part of this diagram is relative long and after the first yielding the ultimate load is reached quite quickly. It means that the girder has only a small plastic reserve and the failure comes relatively quickly after the first yielding. The post ultimate range of the load-displacement curve shows a typical buckling failure where after reaching the ultimate load the load carrying capacity falls down quickly.

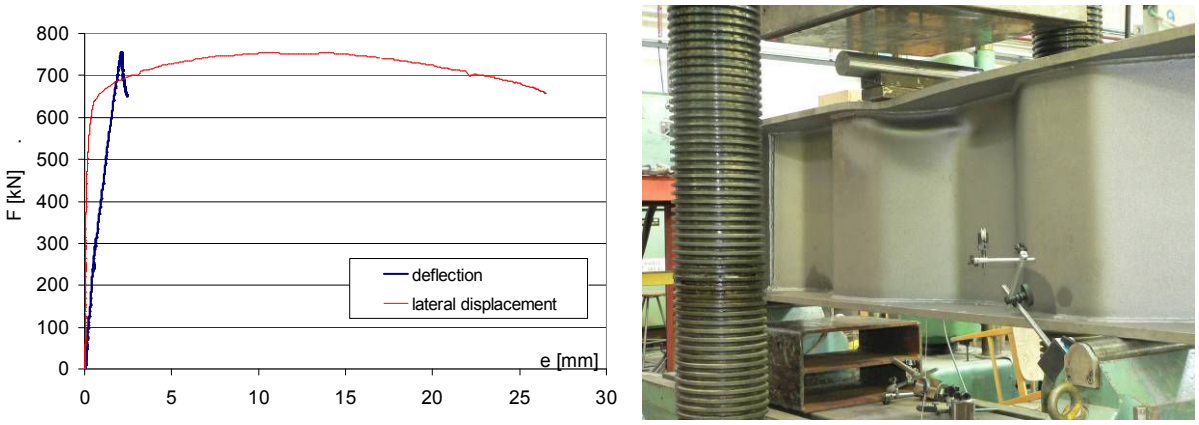

Figure 36: Failure mode of test specimen #1.

Specimen 2:

Specimen #2 is loaded by a 200 mm long loading plate above an inclined fold. The span of the girder is 1500 mm and the flange thickness is 20 mm. Neighbouring folds have buckling waves with alternating directions and the extension of the buckled zone is larger than by the first test and not limited to one fold. This failure mode is the local web buckling. First yielding appears at the load level of 820 kN and the ultimate load is reached at 956.5 kN. The load-deflection curve shows the same character as in case of specimen #1. The load - lateral displacement diagram has an interesting tendency. It starts in the negative direction and after reaching a higher load level buckling occurs in the opposite direction. The same structural behaviour can be observed in case of some other specimens as well and this phenomenon is dominant if a parallel fold is loaded. It can be explained by the imperfection direction. If the initial geometric imperfection is in the opposite direction than the final buckling shape the horizontal displacement diagram has a tendency as presented in Fig. 37. This effect is much larger in case of specimens where a parallel fold is loaded, because the loaded cross-section is unsymmetrical. In case of specimens #1 and #2 this effect is relatively small and in case of specimens #3 and #4 where parallel folds are loaded it is dominant.

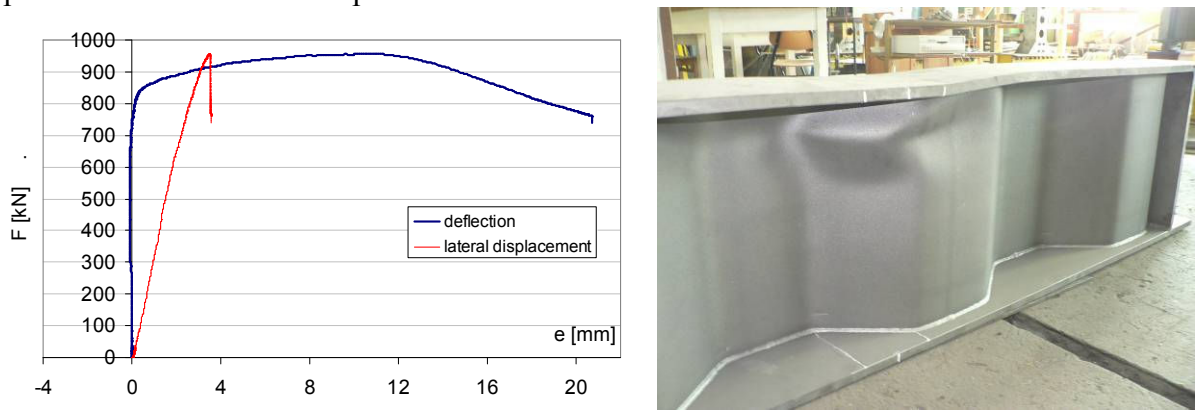

Figure 37: Failure mode of test specimen #2.

Specimen 3:

A parallel fold is loaded in case of specimen #3, and the loading length is 90 mm. The failure mode of the girder is web crippling and the buckled shape has in all folds the same direction. The ultimate load is reached by 764.8 kN. Load and horizontal displacement diagram in Fig. 38 shows that the initial imperfection has the opposite direction as the final buckling shape.

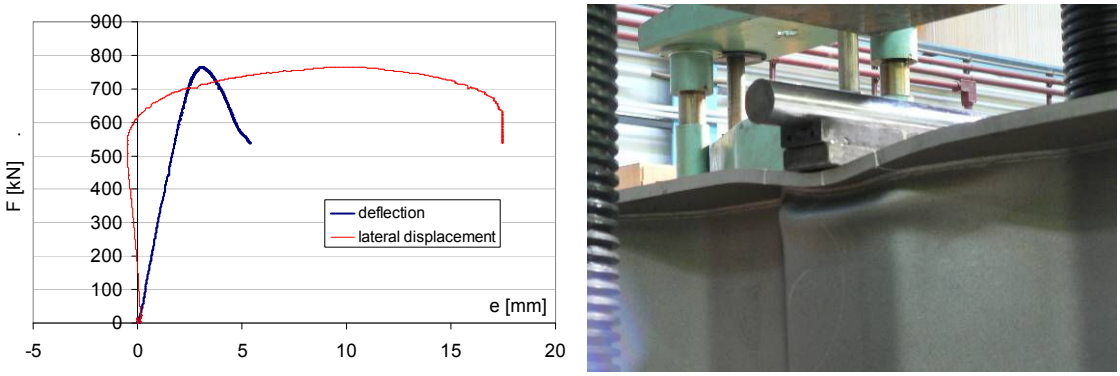

Figure 38: Failure mode of test specimen #3.

Specimen 4:

In case of specimen #4 a parallel fold is loaded with a loading length of 200 mm. The flange thickness is 20 mm and the span of the girder is 1875 mm. The failure mode is typical local web buckling and ultimate load is reached at 949.0 kN. The structural behaviour is the same as described previously and the initial geometric imperfection has the same direction as the final buckling shape.

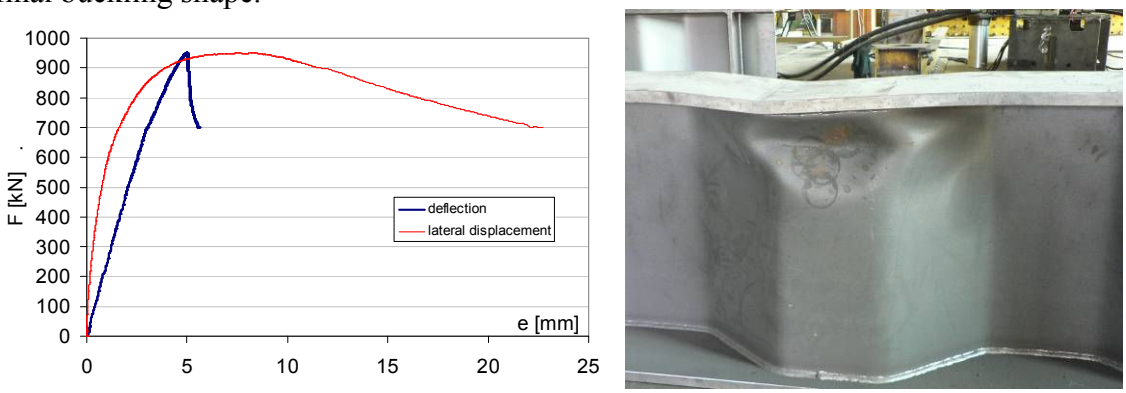

Figure 39: Failure mode of test specimen #4.

Specimen 5:

The failure mode of the specimen #5 is local web buckling. The buckled shape in all folds have alternating directions and the buckling is dominant in several folds. The loaded fold is a parallel fold, and the loading length is 200 mm. The flange thickness is 30 mm and the span of the girder is 1875 mm. The linear part of the load-deflection diagram finishes at the load level of about 970 kN and the measured ultimate load is reached by 1192.0 kN. This specimen has a larger plastic deflection and plastic reserve compared to the previous tests. It can be interpreted by the thicker flange, because flange contribution in the patch loading resistance is more dominant in this case and the flange failure mechanism has a larger plastic reserve than the web buckling.

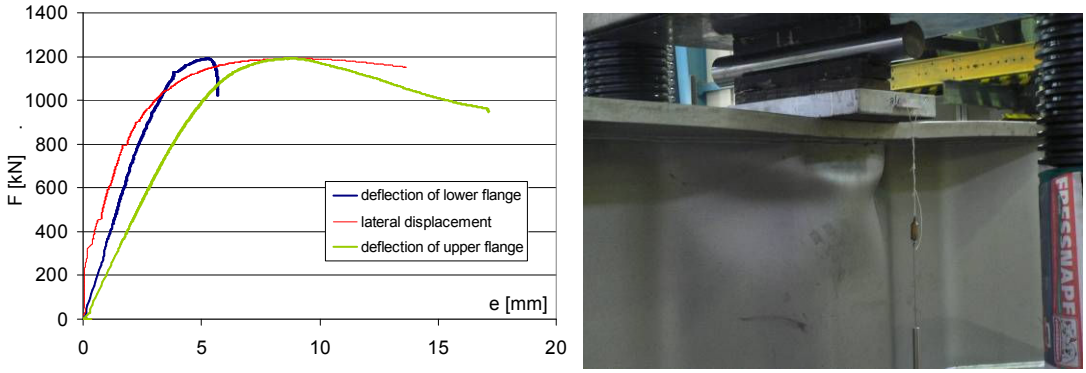

Figure 40: Failure mode of test specimen #5.

Specimen 6:

Failure mode of the specimen #6 is the same local web buckling as previously. The loaded fold is an inclined fold, and the loading length is 200 mm. The flange thickness is 30 mm and the span of the girder is 1500 mm. First yielding occurred at the load level of 810 kN and the ultimate load is measured at 1119.3 kN. The horizontal displacement is until reaching the first yielding almost negligible as typical if an inclined fold is loaded.

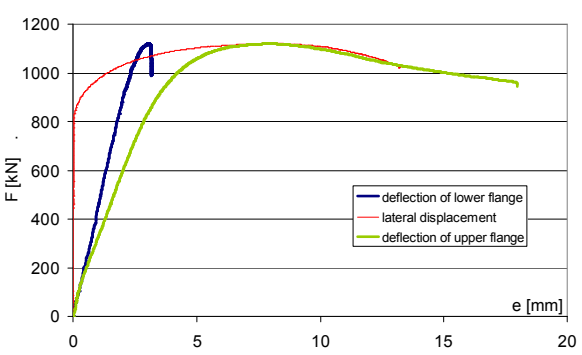

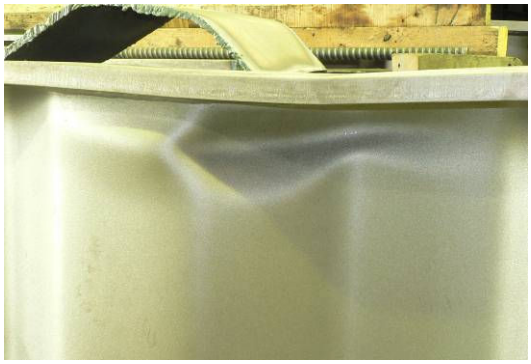

Figure 41: Failure mode of test specimen #6.

Specimen 7:

In case of specimen #7 the span is 1140 mm and the flange thickness is 20 mm. The loaded fold is a parallel fold, and the loading length is 200 mm. The very short span does not indicated any change in the failure mode. The measured patch loading resistance is 1077.7 kN which is 12% higher than in case of specimen #4 with the same loading conditions and with the span of 1875 mm. It means that the effect of the bending moment cannot be neglected during the patch loading resistance determination.

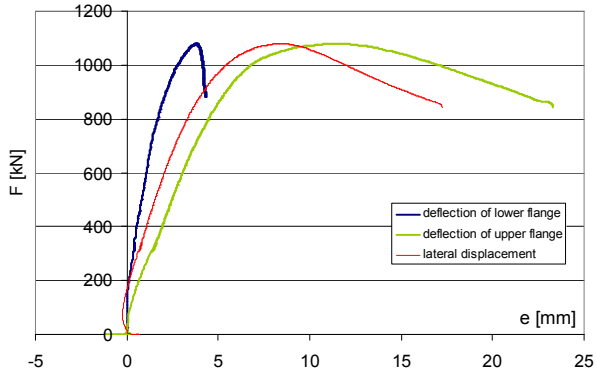

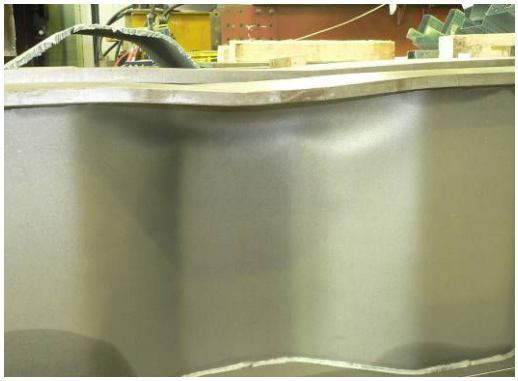

Figure 42: Failure mode of test specimen #7.

Specimen 8:

Loading position of the specimen #8 is a parallel fold, and the loading length is 380 mm. The span is 1500 mm and the flange thickness is 20 mm.

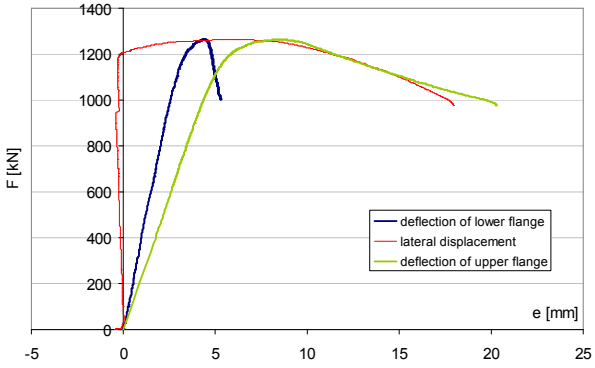

Figure 43: Failure mode of test specimen #8.

The failure mode of the specimen is local web buckling. By this test specimen the patch loading resistance under longer loading length is investigated. The failure mode does not change compared to the previous tests and the ultimate load is increased to 1263.94 kN.

Specimen 9:

In case of specimen #9 the applied load is introduced through a 80 mm wide and 300 mm long loading plate. The flange thickness is 30 mm and the span of the girder is 1500 mm. Aim of this test is to execute a reference experiment for the next research step to analyze the effect of the loading width and eccentricity. The failure mode does not change due to the effect of the loading width and the girder failed by local web buckling. Ultimate load is reached at 1220.48 kN.

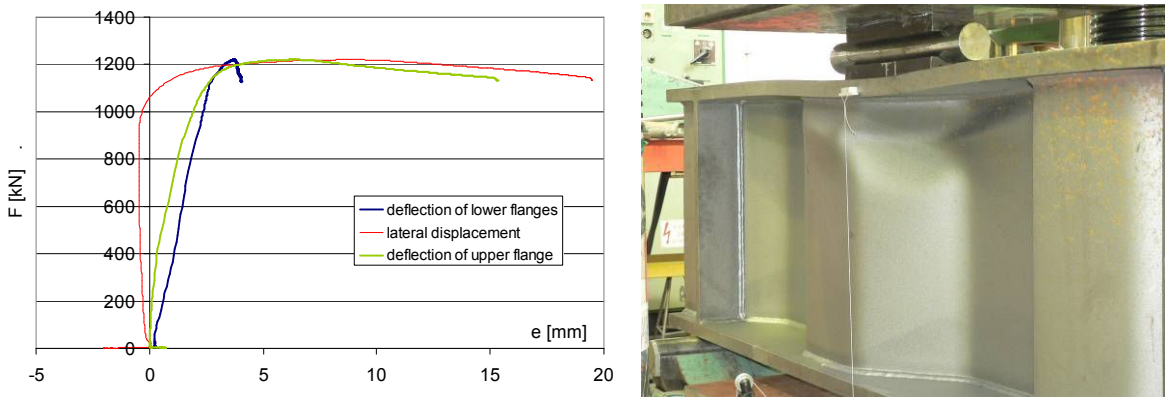

Figure 44: Failure mode of test specimen #9.

Specimen 10:

Specimen #10 is loaded under eccentric patch loading. Girder geometry, span, loaded fold and the loading plate is the same as in the previous tests, only the loading position is modified and the applied load is introduced with a 30 mm eccentricity. This test is a calibration test to analyze the effect of the loading eccentricity, which is investigated in details and presented in Chapter 5. The numerical model is developed based on this test specimen and the effect of the loading eccentricity is studied by numerical calculations. The experiment showed that the failure mode does not change due to the loading eccentricity and the girder failed by local web buckling. The displacements are not measured on this specimen because of the global buckling danger of the whole specimen. The ultimate load is reached at 1090.2 kN, which is 10.69% lower than the ultimate load in the reference test (specimen #9). This result showed that the load eccentricity has a significant effect on the patch loading resistance which should be investigated further.

Figure 45: Failure mode of test specimen #10.

Specimen 11:

In case of specimen #11 the flange thickness is 20 mm. A parallel fold is loaded therefore the span of the girder is 1875 mm. The load is applied through a 380 mm long loading plate to

analyze longer loading lengths. The failure mode is local web buckling and the area of the buckled zone is relatively large due to the long loading length. Ultimate load is reached at 1280.99 kN which is approximately the same as in the case of specimen #8, which had the same geometry only the span and the loaded fold differed. The experiments showed that the loaded fold and the load position has not a significant influence on the patch loading resistance of corrugated web girders.

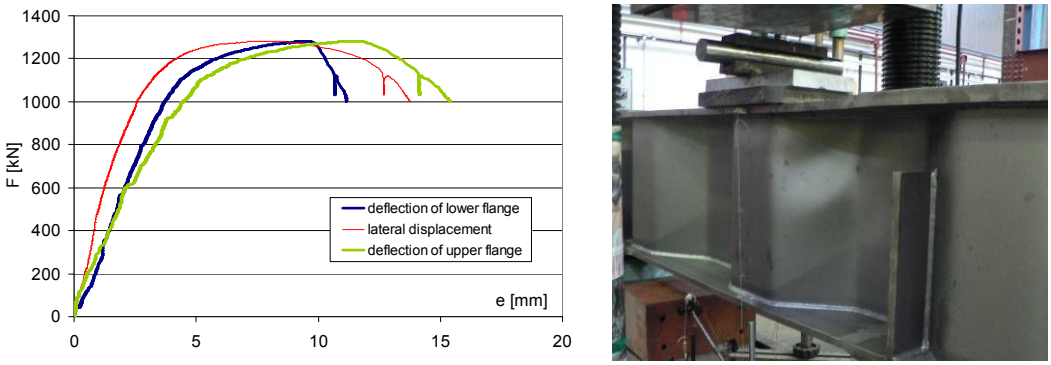

Figure 46: Failure mode of test specimen #11.

Specimen 12:

In case of specimen #12 the span is 1500 mm and the flange thickness is 20 mm. The girder is loaded through a 90 mm long loading plate. The load is introduced at the corner area of two neighbouring folds. Buckling occured in both folds against the short loading length and the failure mode is local web buckling. Ultimate load is reached at 772.39 kN. In comparison with the other specimens which are loaded by a 90 mm loading plate the difference between load carrying capacities are under 2.5%. This result proved that the loading position has not a significant influence on the patch loading resistance.

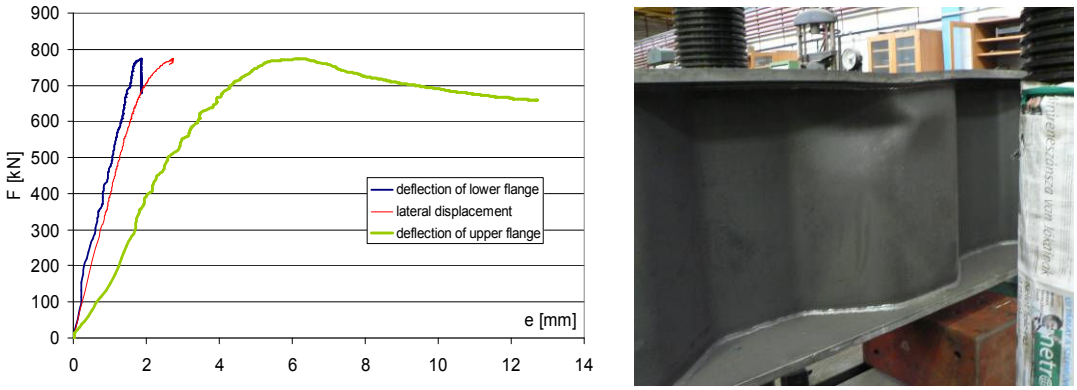

Figure 47: Failure mode of test specimen #12.

3.4. Verification and modification of the developed design method

Based on the executed experiments and numerical database the design method developed by Braun and Kuhlmann is refined. The aim of the further investigations is to determine the pure patch loading resistance without interacting shear force and bending moment. Possible interaction of patch loading, bending and shear is separatly investigated later and an interaction equation is developed in Chapter 7.

Eq. (17) gives the pure patch loading resistance without any interaction consideration.

$$F_R = \left(F_{R,w} + F_{R,fl}\right) \tag{17}$$

The formulation of this modified design method is the same as developed by Braun and Kuhlmann in [3], only the interactions are not considered. The first part of the equation gives

the resistance of the web and the second one gives the resistance of the flange. The web resistance can be calculated by Eq. (18).

$$F_{R,w} = \chi \cdot t_w \cdot f_{yw} \cdot ss \cdot k_\alpha \tag{18}$$

Recommendation for the flange resistance gives the Eq. (19).

$$F_{R,fl} = 2 \cdot \sqrt{n \cdot M_{pl.f} \cdot \chi \cdot t_w \cdot f_{yw}} \tag{19}$$

Notations are the same as explained in Section 2.5.2. A newly introduced parameter is the factor n, which depends on the t_f/t_w ratio. If the t_f/t_w ratio is lower than 4, the complete yield lines in the web and all four plastic hinges in the flange can be evolved during the failure mechanism. If the flange is more dominant (t_f/t_w>4) the web failure mechanism is activated earlier and all 4 plastic hinges cannot be developed, therefore the patch loading resistance is smaller. This resistance decrease can be taken into account in the number of the considered flange plastic hinges and *n* can be determined by the Table 6.

Table 6: Number of the considered flange plastic hinges

t_f/t_w	*n*
t_f/t_w <4	4
$4 \le t_f/t_w \le 7$	3
$7 < t_f/t_w$	2

Experimental patch loading resistances are compared to the modified design method and results are summarised in Table 7.

Table 7: Comparison between test results and design method

Specimen	t_f [mm]	L [mm]	ss [mm]	loaded fold	$F_{R,exp}$ *[kN]*	$F_{R,design\_method}$ *[kN]*	difference [%]
1	20	1500	90	inclined	754.2	737.0	-2.34
2	20	1500	200	inclined	956.5	991.0	3.48
3	20	1875	90	parallel	764.8	739.7	-3.39
4	20	1875	200	parallel	949.0	995.2	4.64
5	30	1875	200	parallel	1192.0	1153.9	-3.31
6	30	1500	200	inclined	1119.3	1149.3	2.60
7	20	1140	200	parallel	1077.7	995.2	-8.29
8	20	1500	380	inclined	1263.9	1406.7	10.15
11	20	1875	380	parallel	1281.0	1413.2	9.36
12	20	1500	90	fold edge	772.4	737.0	-4.80

In column 6 and 7 of Table 7 the measured ultimate loads of the tests $F_{R,exp}$ and the patch loading resistance calculated by the proposed design method $F_{R,design\_method}$ are presented. Differences between the calculated and measured values are under 10% in all cases. The correlation shows that the modified design method gives a good approach for the patch loading resistance of girders with corrugated webs if the failure mode is local web buckling or web crippling.

Finally the new design proposal is compared to the results of the numerical database in Fig. 48. The vertical axis of the diagram shows the numerical or the experimental results. The horizontal axis shows the calculated results based on the proposed design method. Data shows a good correlation between the design method and the numerical as well as experimental results.

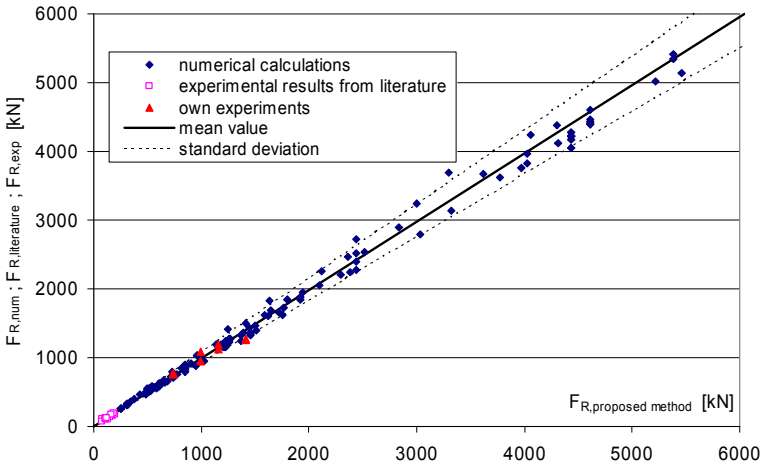

Figure 48: Comparison of numerical results to the design method.

The mean value of the ratio of the experimental or numerical results and the design method is 1.008. It means that the difference between the calculated and measured resistances are 0,8% in average and the standard deviation is 0.06.

Calculation results are presented in the function of the t_f/t_w ratio in Fig. 49. The horizontal axis shows the t_f/t_w ratio and the vertical axis the ratio of the numerical or experimental results divided by the patch loading resistance calculated by the proposed design method. The pink points show the calculation results if $n = 4$ is used in the design method independent of the t_f/t_w ratio. Blue points present the calculation results if the calculation is executed according to Table 6. It can be concluded that the patch loading resistance reduction in function of the t_f/t_w ratio is necessary and applicable.

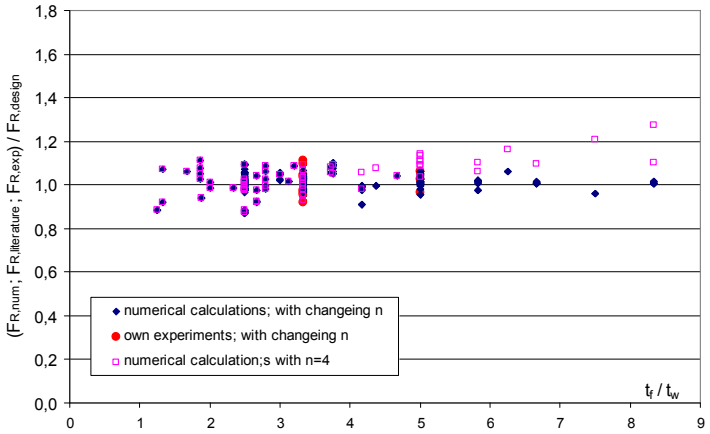

Figure 49: Comparison of calculation results in function of t_f/t_w ratio.

3.5. Summary

12 large scale tests are executed at the Department of Structural Engineering of the Budapest University of Technology and Economics on simply supported short span girders under partial compressive patch loading. The aim of the experiments is the determination of the pure patch loading resistance by different geometrical arrangements, loading lengths and loading positions. Ultimate loads are determined for all test specimens. Different failure modes and structural behaviour are analysed and described in function of the investigated parameters.

Based on the test results the design method developed by Braun and Kuhlmann is studied and the necessary modifications are executed. All interaction formulas are taken away from the design method and investigated separately in frame of further numerical calculations which are presented in Chapter 7. Separate interaction equation is developed to handle the

interaction of transverse and shear forces. The interaction between patch loading and bending is a future research topic. This chapter focuses only on the determination of the pure patch loading resistance. The design method of Braun and Kuhlmann is modified according to the test results and numerical calculations. The resistance influencing effect of the t_f/t_w ratio is determined and built in the design method.

Finally the result of the design proposal is compared to the own laboratory tests and numerical database. Ultimate loads measured during the tests and the calculated values show a good correlation, therefore the design method is verified and it may be used for girders within the parameter range detailed in Chapter 2 which is relevant for bridges.

4. Development of FEM based design method for patch loading of corrugated web girders

4.1. General

Based on the executed tests presented in Chapter 3 recommendations are formulated for finite element simulation based design method. The aim of the finite element calculations is the direct determination of the design value of the patch loading resistance. In the design by finite element simulation the consideration of the equivalent geometric imperfection has a major importance as proved by several researchers in the past [15], [16], [17], [18], [19], [20], [21] and [22]. Since there are no standardized imperfection shapes and scaling factors for corrugated webs in the EN1993-1-5 [4], this chapter emphasizes the development of applicable imperfection shapes and scaling factors for patch loading resistance calculation of corrugated web girders.

Based on the executed experiments a numerical model is developed, and the patch loading resistance is determined by nonlinear analysis using geometric imperfections and material nonlinearities. Failure modes, load carrying capacities and post-ultimate behaviour are determined and studied. The imperfection shape and scaling factor used in the nonlinear analysis are investigated and its influence on the structural behaviour is determined. Based on the experiments and numerical investigations, recommendations are formulated for applicable equivalent geometric imperfection shapes and scaling factors.

4.2. Numerical model development and structural behaviour

Based on the experimental background numerical model is developed for all test specimens using finite element program Ansys v10.0 [13]. The aim of the numerical investigations is to determine the design value of the patch loading resistance for corrugated web girders by nonlinear finite element simulations. The analyzed girders are modelled using four node thin shell elements. Numerical models have the same geometry and dimensions as the test girders presented in Chapter 3. Figure 50 shows the finite element mesh of the developed numerical model.

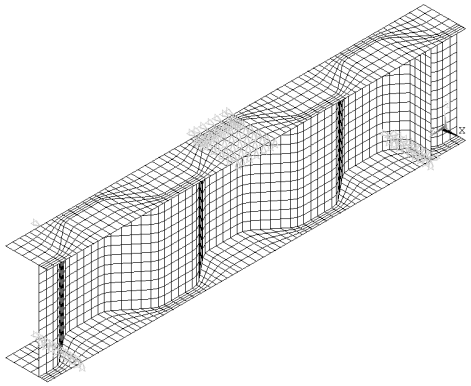

Figure 50: Developed numerical model.

The applied linear elastic - hardening plastic material model is a four-linear approach of the real material measured in the experiments using isotropic hardening rule with von Mises yield criterion. The material is linear elastic until reaching the yield strength by a Young modulus of 210000 MPa. The yield plateau is modelled to 1% strains without hardening. From the yield stress the material model follows linear hardening with a reduced modulus until reaching the ultimate strength by 15%. The material is perfectly plastic when it reaches the ultimate strength.

The ultimate loads are determined by geometrical and material nonlinear analysis using different imperfection shapes. The finite element model exhibited the same structural behaviour and the same failure modes which are observed during the tests. The measured patch loading resistances are compared to the numerical calculations, the experimental failure modes to the numerical failure modes and the measured load displacement curves to the equilibrium paths of the numerical analyses.

Convergence study gave the same result as established in Chapter 2. One fold should be modelled minimum of 8-10 elements along the fold length to determine the patch loading resistance with adequate reliability. In the forgoing studies this principle is taken into account and the models are characterised by an element number between 10000 to 15000 depending on the span and corrugation profile.

Figures 51 to 55 show the comparison of the experimental and numerical failure modes for five specimens. On the left side of the figures the experimental failure modes and on the right side the result of the finite element calculations are presented.

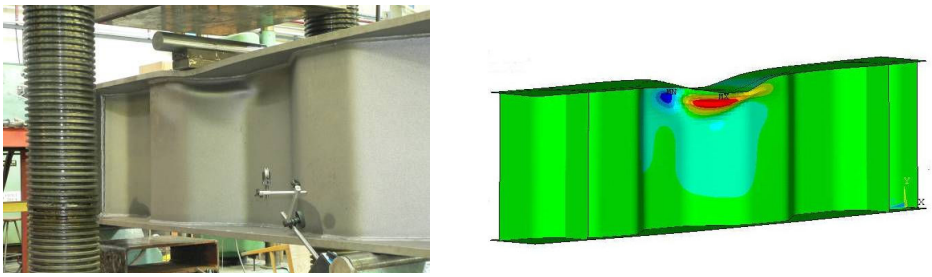

Figure 51: Experimental and numerical failure modes - specimen #2.

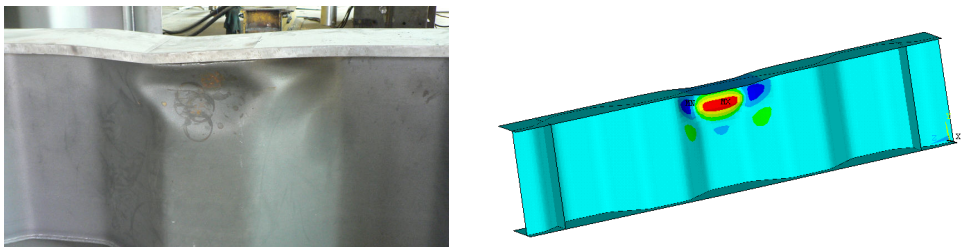

Figure 52: Experimental and numerical failure modes - specimen #4.

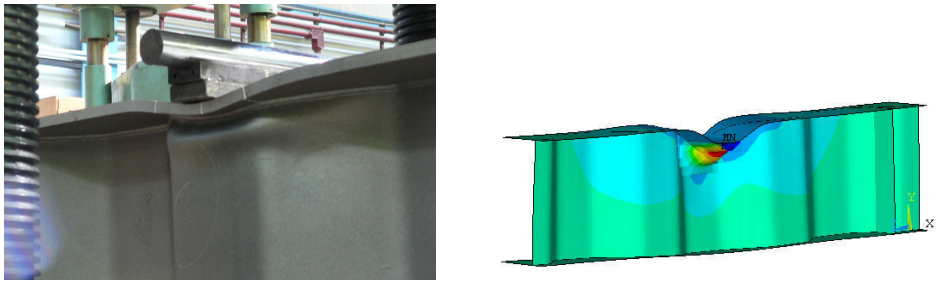

Figure 53: Experimental and numerical failure modes - specimen #5.

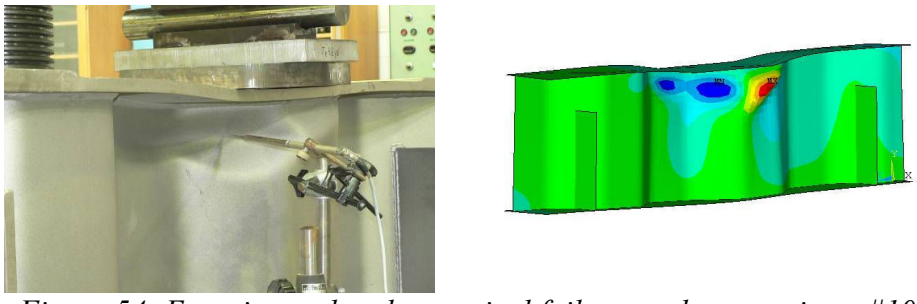

Figure 54: Experimental and numerical failure modes - specimen #10.

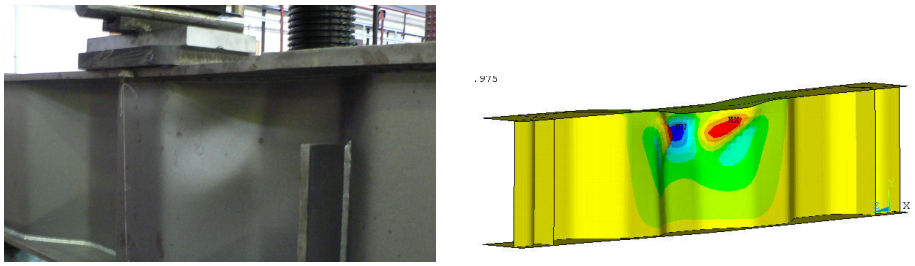

Figure 55: Experimental and numerical failure modes - specimen #14.

The comparison is made for all test specimens and presented here for five girders. It proves that the structural behaviour of the tested girders and the numerical models show good agreement.

The measured and calculated load-deflection curves are also compared and the analysis showed differences in the post-ultimate behaviour. All measured load-deflection curves are investigated and compared to each other and differences are observed in the descending branch. Figure 56 shows four different and typical measured curves. Specimens #1, #2 and #4 have the same post-ultimate branch, but in case of specimen #3 the curve shows a different tendency, despite the failure modes are in all cases the same.

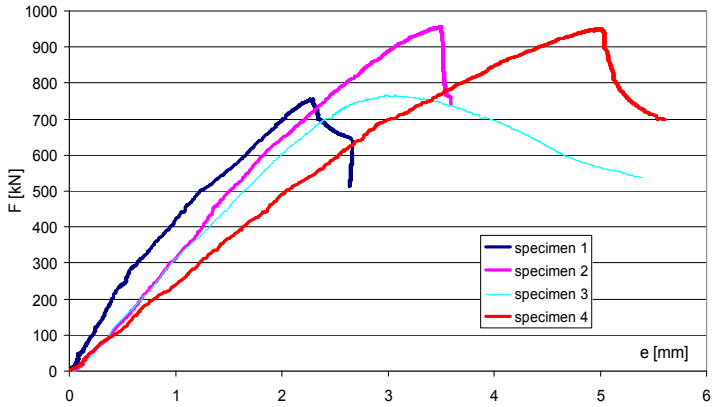

Figure 56: Measured load - deflection curves.

To get the reason of this difference the parameters of the numerical model are studied. The investigations showed that the reason is the applied imperfection shape and magnitude. Figure 57 shows the results of the completed numerical simulations applying different imperfection magnitudes. Differences in the load carrying capacities are relatively small but the post-ultimate branch changes rapidly by increasing imperfection magnitudes.

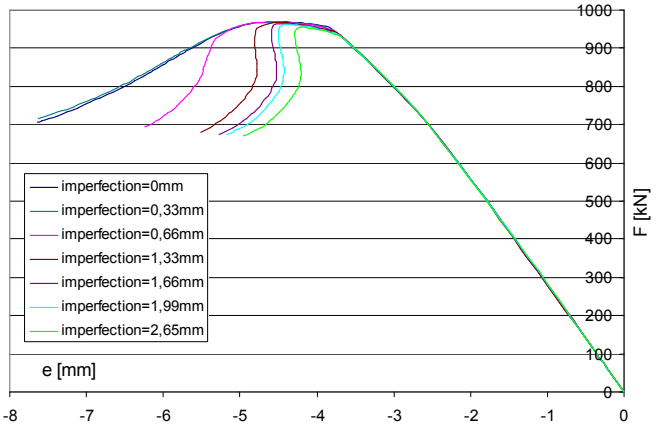

Figure 57: Calculated load - deflection curves by different imperfection sizes.

Figure 58 presents the typical points of two load - deflection diagrams. The solid blue curve shows a simulation conducted without imperfection and the dotted red line with a relatively large imperfection magnitude. The applied imperfection shape is the first buckling mode. Point #1 shows the first yielding in the flange if no imperfection is applied (Fig. 22a). In the same load step a simultaneous yielding in the flange and web appears if the applied imperfection is relatively large. The phenomenon is illustrated in Fig. 22b. The difference between the two structural behaviours is the appearing time of the first yielding in the web. If the imperfection size is 0, it appears at point #2 and if a large imperfection is applied it appears at point #1. Points #3 and #4 show the load levels when 2 plastic hinges are completely developed in the flange, as it is illustrated in Fig. 22c, and points #5 and #6 mean the load levels when all 4 plastic hinges are developed (Fig. 22d).

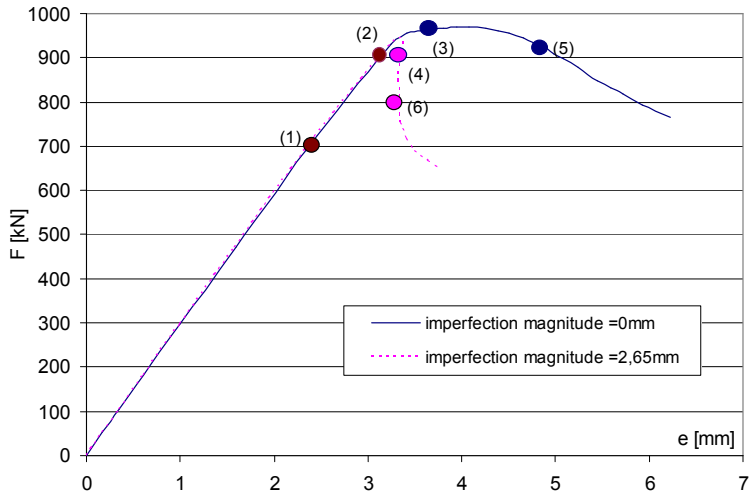

Figure 58: Analysis of imperfection size.

Experiments and numerical investigations showed that the imperfection has an important effect on the structural behaviour in the descending branch. Using an adequate imperfection shape and magnitude the numerical simulation leads to the same load carrying capacity and to the same structural behaviour as the tested girders. The comparison of the measured and calculated load - displacement curves are illustrated in the case of five specimens (Figs. 59-63). The two solid lines always show the deflection and the lateral displacement measured in the tests and the dotted lines represent the results of the numerical simulations.

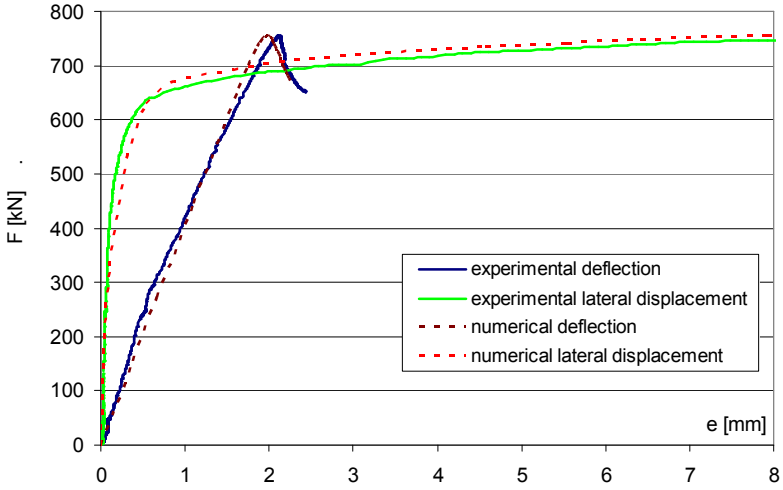

Figure 59: Experimental and numerical load - displacement curves, specimen #1.

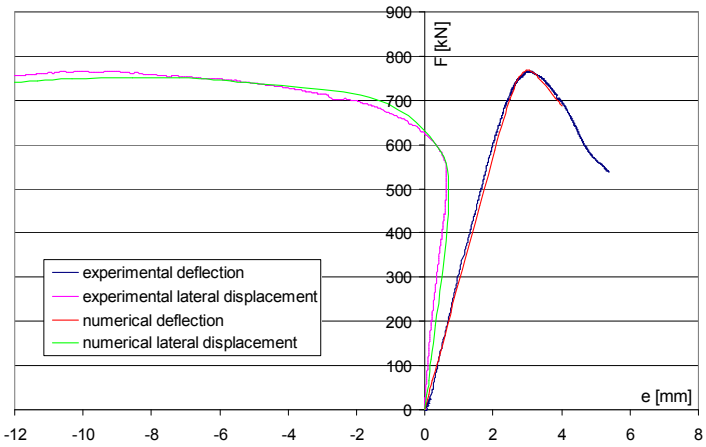

Figure 60: Experimental and numerical load - displacement curves, specimen #3.

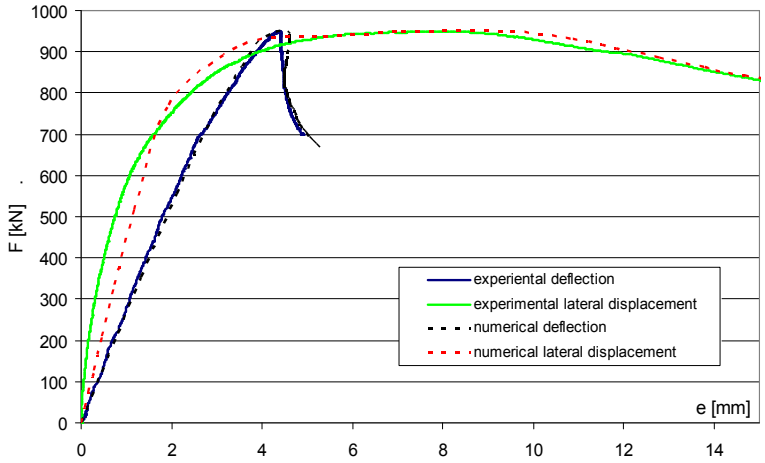

Figure 61: Experimental and numerical load - displacement curves, specimen #4.

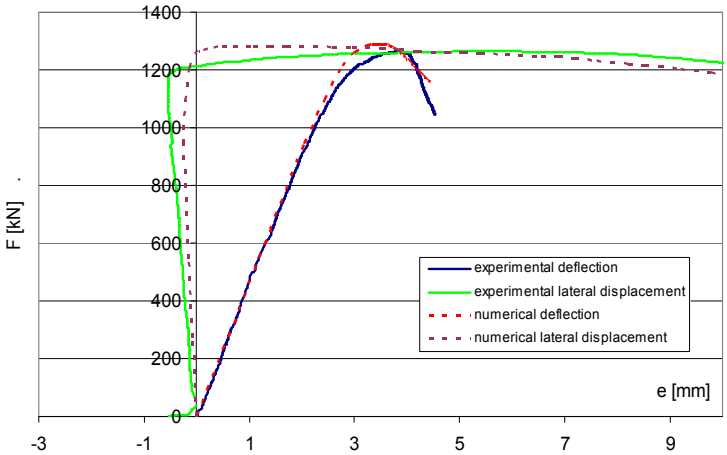

Figure 62: Experimental and numerical load - displacement curves, specimen #8.

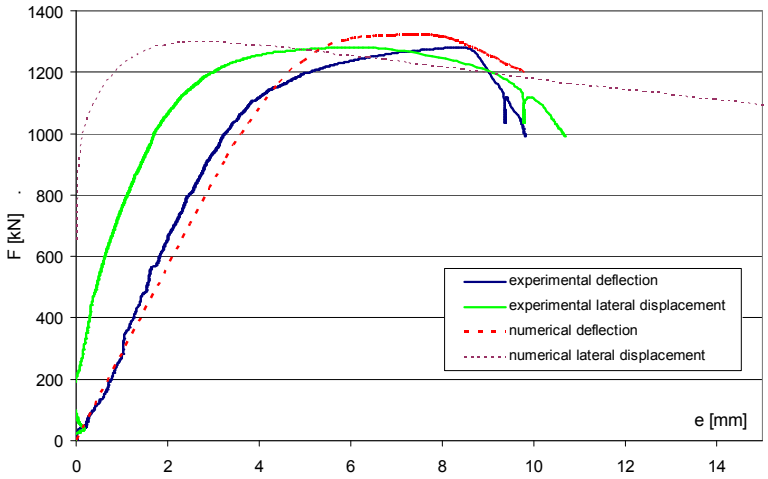

Figure 63: Experimental and numerical load - displacement curves, specimen #11.

The measured and calculated results are very close to each other if the adequate imperfection shape and scaling factor is known. Therefore to find the adequate geometric imperfection different shapes and magnitudes are studied in the followings.

4.3. Analysis and development of equivalent geometric imperfection shapes

4.3.1. Investigated imperfection shapes

Investigations showed that the imperfection has major importance on the structural behaviour in case of girders with corrugated webs. In the finite element simulations the consideration of the equivalent geometric imperfection is always the critical point and there are no recommendations in the EN1993-1-5 [4] for corrugated webs. In this chapter different imperfection shapes and scaling factors are investigated based on the executed experiments and numerical analyses, and recommendations are developed for the practical application of equivalent geometric imperfection shapes and adequate magnitudes for girders with corrugated webs.

The studied imperfection shapes are presented in Figs. 64 to 66. EC3 allows the use of the critical buckling modes as imperfection shape therefore the first buckling mode is examined. The second used shape is the sine wave shape based on the EC3 subpanel model. The third one is the ultimate shape as a possible imperfection, which represents a previously analysed loaded shape of the girder. The ultimate shape is taken from the highest point of the load - deflection curve calculated without initial imperfections.

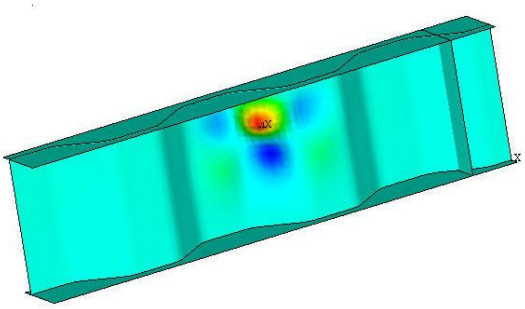

Figure 64: Eigenmode imperfection shape.

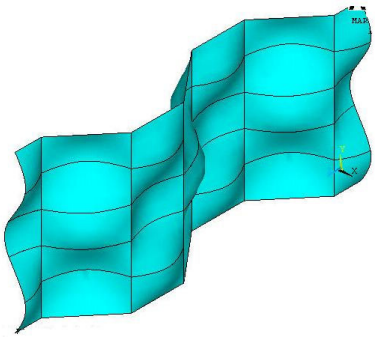

Figure 65: Sinus wave imperfection shape.

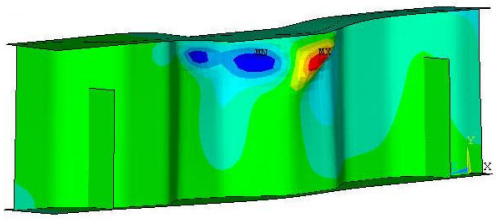

Figure 66: Ultimate shape imperfection.

4.3.2. Development of a new modified imperfection shape

A modified sine wave imperfection shape is developed which is an approach of the first buckling mode of corrugated web girders under eccentric patch load. The aim of the modified sine wave imperfection shape is to give the equivalent geometric imperfection in a closed form to be applied for patch loading of corrugated webs. This function can be described by the multiplication of a sine and an exponential function, as expressed in Eq. (20). The cross-section of the shape along the fold length is illustrated in Fig. 67. In the lateral direction it has a sine wave form.

$$f(x) = e^{-\frac{1}{L \cdot m} \cdot x} \cdot \sin\left(\frac{1}{L} \cdot k \cdot \pi \cdot x\right) \tag{20}$$

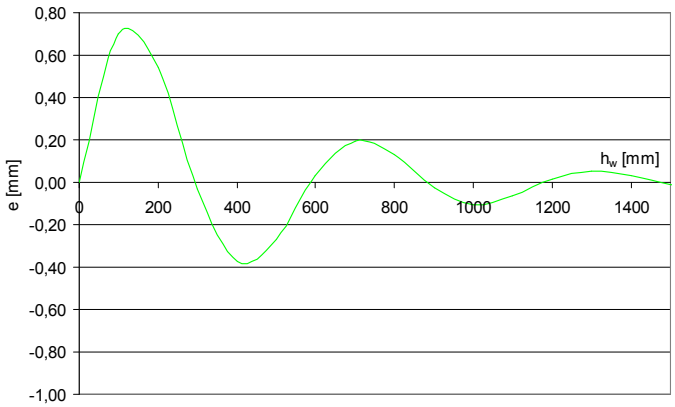

Figure 67: Recommended imperfection shape.

This function can be described by two parameters, m and k. The parameter m gives the falloff rate, which represents the decreasing tendency of the function. The parameter k is representing the number of waves in one fold; therefore it adjusts the wavelength of the function. In the frame of a numerical parametric study all geometric parameters are investigated to find the relationship of them with the wavelength and falloff rate (m and k). Calculations showed that both parameters are depending on the web depth, fold length and loading length. All the other investigated parameters have minor influence on the first buckling mode, if the first buckling mode is local buckling or web crippling.

Parameter k can be calculated by Eq. (21). It gives the number of waves in one fold. The expected value of it is the ratio of the web depth and fold length if the load is applied along one fold. It means that the wavelength of the buckling shape is equal to the fold length.

$$k = \frac{h_w}{a_i} \cdot c \tag{21}$$

where: h_w web depth,
a_i loaded fold length,
c modification factor due to loading length, it can be calculated by Eq. (22).

Calculations showed that if the applied loading length is smaller, the wavelength of the buckling mode is also shorter than one fold length, and if the loading length is larger, the wavelength is also larger, as it is illustrated in Fig. 68.

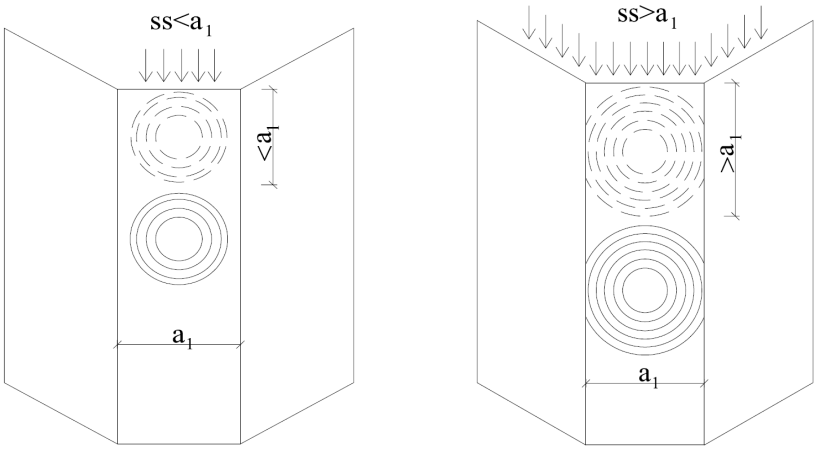

Figure 68: Buckling wavelengths in case of short and long loading lengths.

According to this observation *k* should be modified according to the ratio of the loading length and fold length. The modification factor can be read from the diagram in Fig 69, or it can be calculated by Eq. (22).

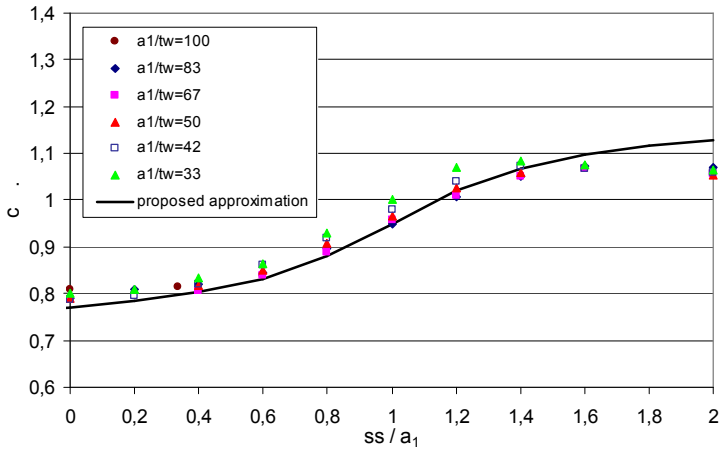

Figure 69: Modification factor c.

$$c = \arctan\left[2{,}5 \cdot \left(\frac{ss}{a_1} - 1\right)\right] \cdot 0{,}15 + 0{,}95 \qquad (22)$$

The falloff rate depends also on the same three parameters as the wavelength. If the ratio of the web depth and fold length is known, the ratio of the minimum and maximum values (which are denoted by *d*) can be read from the diagram of Fig. 70, or it can be calculated by Eqs. (23) and (24). The ratio of the minimum and maximum values leads to 1, if the web depth is much longer than the fold length. If the web depth is smaller, the falloff rate of the buckling mode will be more dominant and the relationship can be expressed by Eqs. (23) and (24).

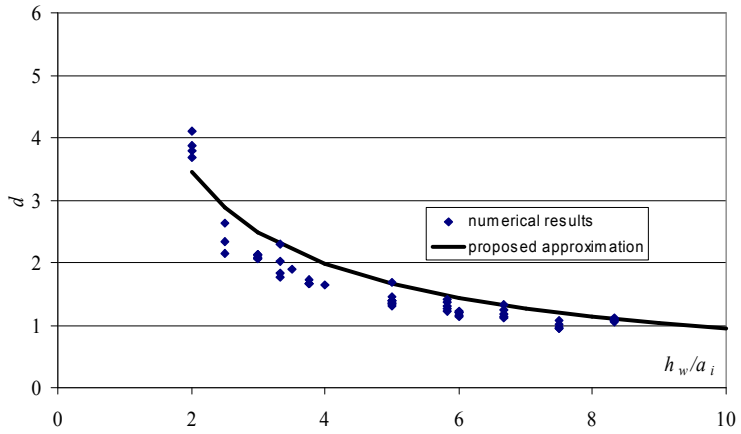

Figure 70: Ratio of the maximum and minimum magnitudes (d).

$$d = 6 \cdot \left(\frac{h_w}{a_i} \right)^{-0,8} \qquad \text{if ss>a}_1 \tag{23}$$

$$d = 6 \cdot \left(\frac{h_w}{a_i} \right)^{-0,8} \cdot \left(2,0 - \frac{ss}{a_1} \right) \qquad \text{if ss}\leq\text{a}_1 \tag{24}$$

If the loading length is smaller than the fold length the wavelength decreases as noted before, and at the same time the falloff rate increases. The ratio of loading length and fold length has an increasing effect on the falloff rate which can be taken into account by Eq. (28). Parameter *m* depends on the *d* and on *k* and can be taken from the diagram in Fig. 71. The value of *m* can be interpolated between the given curves in dependence on *k*.

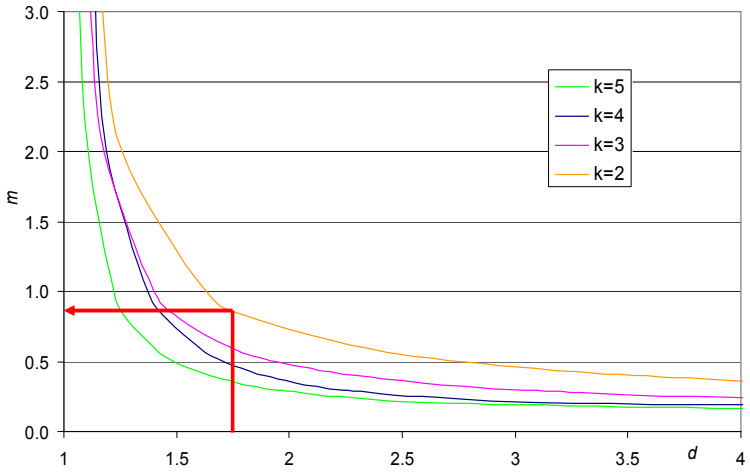

Figure 71: Determination of parameter m.

If *m* and *k* are determined, the recommended imperfection shape can be built in any finite element program. This modified sine wave may be applied in all loaded folds and also in the two neighbouring folds, while unloaded folds remain flat. The directions of the waves are also of importance, they should be oriented in each neighbouring folds in opposite direction.

This imperfection shape is equivalent with the first buckling mode imperfection in the analysed parameter range, and it can be used as an equivalent geometric imperfection for patch loading of corrugated web girders. The investigations are executed in the following - in practically applied - parameter ranges: h_w = 500-2000 mm; t_w = 3-16 mm; t_f = 10-100 mm; b_f = 200-500 mm; L = 1500-4125 mm; ss = 0-960 mm; α = 15-60°; a_1=a_2=150-600 mm.

4.4. Analysis and development of equivalent geometric imperfection magnitudes

4.4.1. Imperfection sensitivity analysis

Based on the executed tests recommendations are developed for the adequate imperfection magnitude in the case of all analysed imperfection shapes. Imperfection sensitivity is studied for all test specimens and numerical calculations are compared to the measured patch loading resistances. From the intersection points of the calculated and measured resistances the necessary imperfection magnitudes are determined. The results of the imperfection sensitivity analysis are shown in the case of two tested girders in Figs. 72 and 73.

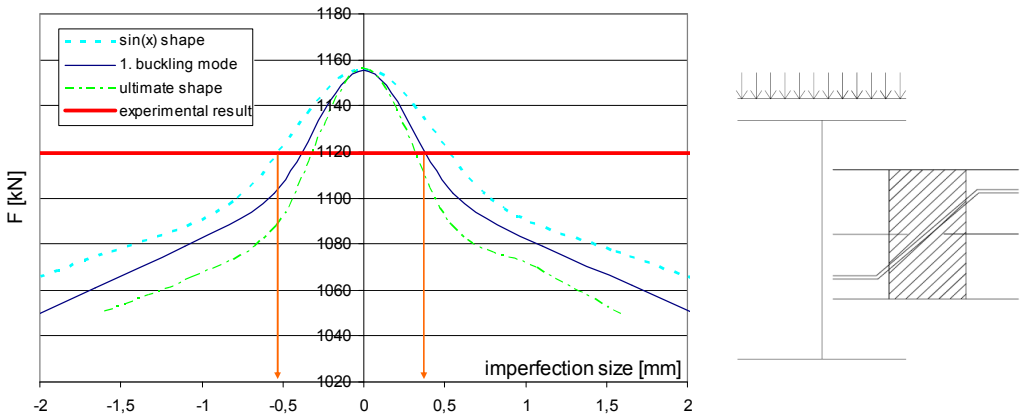

Figure 72: Imperfection sensitivity diagram - symmetrical case (inclined fold loaded).

Figure 72 shows the imperfection sensitivity analysis if the loaded fold is an inclined one. In this case the loaded cross-section is symmetric; therefore the imperfection sensitivity diagram is also symmetrical. The light blue dotted curve shows the imperfection sensitivity if sine wave shape is used as equivalent geometric imperfection, the dark blue solid curve belongs to the first buckling mode and the green dotted one to the ultimate shape imperfection. The diagram shows that the ultimate shape imperfection gives the lowest and the sine wave shape the largest resistance. The red horizontal line means the measured resistance during the test. From the intersection points the necessary imperfection magnitude can be determined. According to this diagram the largest imperfection is needed in the case of the sine wave shape imperfection and the smallest by the ultimate shape imperfection.

If the parallel fold is loaded the pertinent cross-section is asymmetrical, therefore the imperfection sensitivity diagram is also asymmetrical. The reason of this is the imperfection direction.

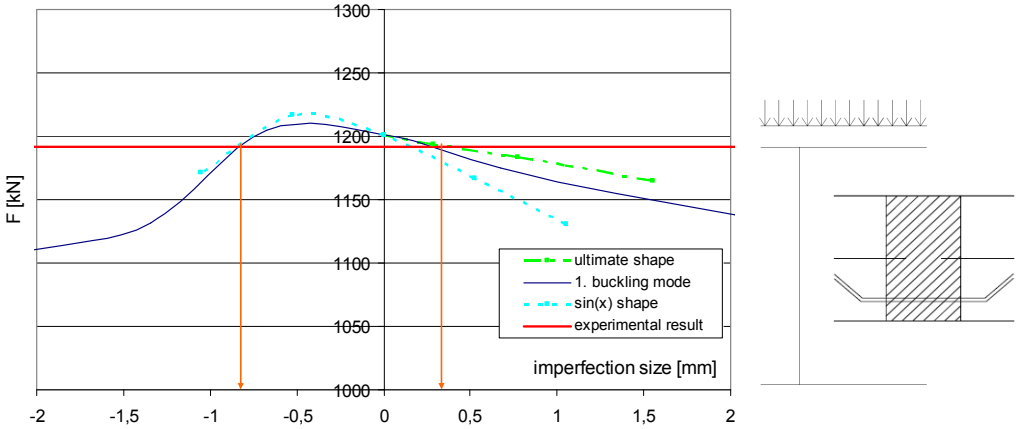

Figure 73: Imperfection sensitivity diagram - asymmetrical case (parallel fold loaded).

If the applied imperfection goes in the opposite direction as the final failure shape, a small imperfection can lead to patch loading resistance increase. The asymmetrical imperfection sensitivity diagram is shown in Fig. 73.

The imperfection magnitude is expressed by the ratio of the loaded fold length and the adequate scaling factor ($e=a_i/sf$). In the cases of the first buckling mode and sine wave shapes both the positive and negative scaling factor can be applied. In the case of the ultimate shape the negative value has no sense. Therefore in some cases the necessary imperfection size can be read from the positive side of the diagram for the ultimate shape and from the negative side for the other two shapes. Due to this difference the scaling factors (*sf*) are not always comparable to each other, but the applicable imperfection magnitudes can be determined for all shape types.

4.4.2. Determination of the necessary imperfection magnitudes

The sensitivity analysis is completed for all 12 test specimens and necessary scaling factors are determined. The results of the investigations are summarized in Fig. 74.

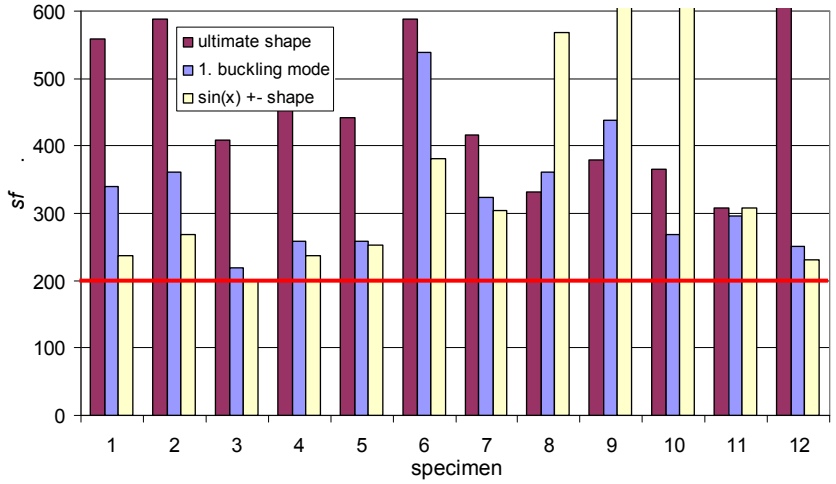

Figure 74: Determined scaling factors (sf).

The horizontal axis of the diagram shows the number of the specimens. On the vertical axis the necessary imperfection scaling factor is presented. The first column for each specimens belongs to the ultimate shape imperfection, the second one to the first buckling mode and the third one to the sine wave shape. In most cases the ultimate shape imperfection leads to the lowest resistance, therefore the smallest imperfection is needed for this imperfection type. The sine wave shape imperfection results in the largest resistance; therefore the largest imperfection is needed for that.

The research study showed that an imperfection scaling factor equal to the fold length divided by 200 (a_i/200**)** can be used for the first buckling mode, for the sine wave shape and for the modified sine wave shape imperfections as well. In the case of the modified sine wave shape imperfection the scaling factor a_i/200 can be applied in the loaded folds and one quarter of this value in the neighbouring folds. Unloaded folds remain flat. In the present study only these cases are considered when parallel and inclined folds are equal.

4.4.3. Evaluations of the ultimate shape imperfection

The above study showed that if the ultimate shape is applied as equivalent geometric imperfection a smaller magnitude may be sufficient, but in three cases (specimens #8, 9 and 10) some contradictions are observed. For these specimens the ultimate shape imperfection led to the largest resistance and the sine wave shape to the smallest, therefore these three specimens are investigated in detail. This unexpected result can be explained by two reasons.

The first one is illustrated in Fig. 75, and explained as follows. Buckling occurs in more folds and in more waves in the case of the critical buckling shape (Fig. 75a) and only in one wave in the ultimate shape (Fig. 75b). It can be the first reason that the critical buckling shape imperfection leads to lower resistance than the ultimate shape imperfection.

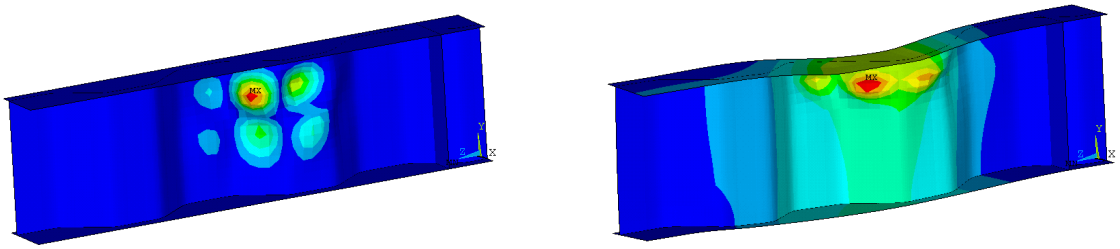

Figure 75: Imperfection shapes: (a) buckling shape (b) ultimate shape.

The second observation is that the load step from which the ultimate shape is taken has a major importance. Figure 77 shows two different ultimate shapes. The first one is taken from the ultimate load step of the load - deflection curve (Fig. 76 point #1), and the second one from the post-ultimate branch (Fig. 76 point #2). The results show that in some cases the total buckling pattern is developed only in the descending branch, therefore if the ultimate shape is taken from point #1 it can give larger load carrying capacities.

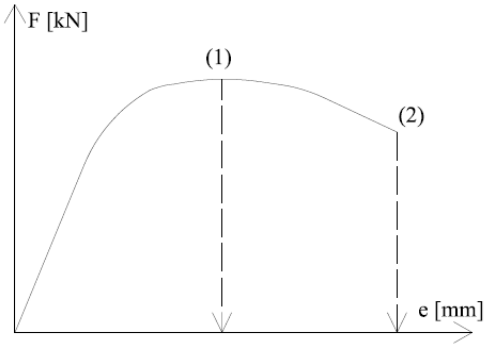

Figure 76: Different ultimate shape imperfections.

Ultimate shape in point #1 Ultimate shape in point #2

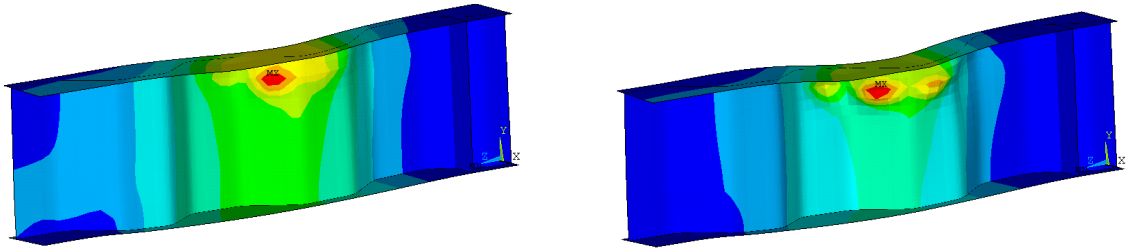

Figure 77: Different ultimate shape imperfections.

4.5. Application of the results

The investigated and developed imperfection shapes and the determined scaling factor can be applied directly in the patch loading design of girders with corrugated webs. The investigated and evolved imperfections permits to determine the patch loading resistance of corrugated web girders by finite element simulation with adequate accuracy and safety.

The determination method of the equivalent imperfection magnitude based on experimental background (comparison of numerical calculations and experimental results) can also be applied to analyze other structural details.

4.6. Summary

The focus of the research work is the determination of the patch loading resistance of corrugated web girders by nonlinear finite element simulation. Based on the experimental investigations presented in Chapter 3 an FE based design method is developed. The numerical model is built for all test girders and the load carrying capacities are determined by geometrical and material nonlinear analysis using imperfections. Verification of the numerical model is executed by the comparison of failure modes, patch loading resistances and load - deflection curves measured in the experiments and calculated in the numerical simulations.

Comparison of the measured and calculated load - deflection curves showed differences in the post-ultimate behaviour. Detailed investigations showed that the reason of this is the imperfection magnitude. In the FE based design method the consideration of the equivalent geometric imperfection has a major importance and there are no recommendations in EN1994-1-5 [4] for corrugated web girders. In the completed research work applicable equivalent geometric imperfection shapes and appropriate scaling factors are developed.

Four imperfection shapes are analysed. The first critical buckling mode, the ultimate shape and the sine wave imperfection form are investigated, and a modified sine wave imperfection is also developed to predict the first buckling mode.

The imperfection sensitivity is studied for all types of imperfection shape and based on the experiments applicable imperfection magnitudes are developed. Calculations showed that the applicable imperfection magnitude is the fold length divided by 200, if the first buckling mode, the sine wave shape or the modified sine wave shape is used as equivalent geometric imperfection.

5. Patch loading resistance considering the loading width and eccentricities

5.1. General

Eccentric patch loading is a research field where only a few investigations are conducted till now, however during launching of the bridge structure eccentricities in the patch load are unavoidable in practice. There is no standard design method to determine the resistance reduction due to eccentricities and only a few investigations and research recommendations can be found in the literature dealing with this topic even for flat web girders. There are no available investigations dealing with corrugated web girders therefore a comprehensive parametric study is executed in the frame of this thesis what is detailed in this Chapter. The eccentric loading and the used notations are shown in Fig. 78.

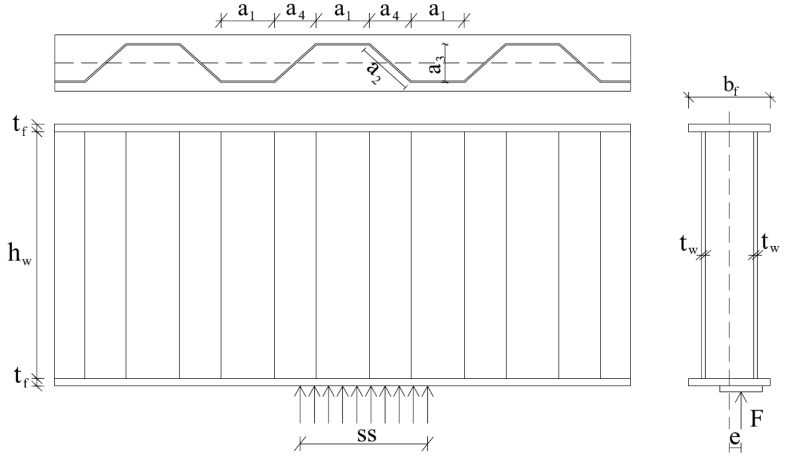

Figure 78: Eccentric patch loading of corrugated web girders.

5.2. Review of previous investigations and research aims

In the last decades researchers investigated only scarcely this research field. All the previous investigations are conducted on steel girders with flat webs and there are no available investigations dealing with corrugated web girders. This Chapter gives a short overview about the available research studies and their results. The applicability of these results is studied from the point of view of bridge structures and corrugated web girders.

a. Research at the University of Stuttgart (1979)

Experimental research in the field of eccentric patch loading was started by Oxfort and Weber in 1979 [23]. 6 tests were conducted on flat web I-girders and the effect of the eccentric patch loading was studied. In the experiments the flange rotated along its longitudinal axis, and therefore it ensured a softer support for the web plate. Due to the softer support conditions the web buckled at a lower ultimate load level. Experiments showed that the resistance decrease did not depend significantly on the flange size and the longitudinal web stiffener had a much smaller efficiency in case of eccentric loading.

b. Research at the University of Maine (1988-1990)

Elgaaly and his team conducted a comprehensive experimental program on 35 steel I-girders with flat webs under eccentric patch loading between 1988 and 1990 [24]-[26]. The investigated parameters in the experiments are the loading mode (loading plate or loading rod), the t_f/t_w, L/h_w and e/b_f ratios. Based on the experimental results the following conclusions are published. If the load was applied through a loading plate (Fig. 79/a.), the failure mode was in all cases web crippling and the eccentricity issued a relatively small effect on the load carrying capacity. If the load was introduced through a loading rod, where the loading width

is much smaller (Fig. 79/b), the failure was the combination of web crippling and transverse flange buckling. In this case eccentricity had a relatively large effect on the patch loading resistance reduction [24]. In 1989 Elgaaly and Sturgis showed that the patch loading resistance decreases with increasing eccentricity (e/b_f) and the decreasing tendency is depending on the t_f/t_w ratio [25]. They appointed that the web panel aspect ratio L/h_w did not cause any definite changes in the load carrying capacity.

Figure 79: Loading modes for eccentric loading.

Based on the test results Elgaaly and Salkar established in 1990 that the efficiency of the longitudinal web stiffener is much smaller in the case of eccentric loading and tests proved that the resistance decreasing tendency depends on the t_f/t_w and e/b_f ratios [26]. A numerical model is developed to determine the patch loading resistance and a numerical parametric study is conducted to analyze the patch loading resistance reduction due to eccentricities. Based on the test results and numerical calculations design model is developed in the form of Eq. 25 which can be applied in the parameter range between $1<t_f/t_w<4$ and $e/b_f<1/6$ [26]. Value of F_R represents the patch loading resistance under centric loading and F_R^{red} under eccentric loading.

$$\frac{F_R^{red}}{F_R} = \left[-0.45 \cdot \left(\frac{t_f}{t_w} \right)^2 + 4.45 \cdot \left(\frac{t_f}{t_w} \right) - 12.75 \right] \cdot \left(\frac{e}{b_f} \right) + \left[1.15 - 0.025 \cdot \left(\frac{t_f}{t_w} \right) \right] \tag{25}$$

c. Research activity at the Academy of Sciences of the Czech Republic (1991)

Drdacky investigated 6 unstiffened I-girders under eccentric patch load [27]. All girders were loaded by a steel rod. Tests showed that the flange deflection and loading eccentricity has a nearly linear relationship. Drdacky established that due to flange deflection an additional longitudinal stress appears in the loaded flange which can be calculated by Eq. (26).

$$\Delta\sigma = e \cdot \frac{F \cdot t_w \cdot L}{0.75 \cdot I_{tf} \cdot h_w}, \tag{26}$$

where: I_{tf} torsion inertia of the flange.

d. Research at LCPC in France (1991)

In 1991 at the LCPC in Paris two ½ scale specimen of a bridge girder were tested under eccentric patch load [28]. Transverse flange bending did not occurred which can be explain by the relative large t_f/t_w=6,7 ratio. Due to this large flange to web thickness ratio the reduction of the resistance coming from eccentricities was negligible.

e. Research at the University of Montenegro (2001/2002 and 2008/2009)

Altogether 125 specimens are tested by Sćepanović and co-researchers between 2001 and 2009 to analyze the eccentric patch loading resistance of flat web girders [29]-[32]. The main aim of the tests and numerical modeling was to enlarge the previously analyzed parameter range. Experiments showed that the effect of the eccentricity can be neglected for large t_f/t_w ratios, but the resistance reduction can be significant by smaller t_f/t_w ratios. The analyzed parameter range is: t_f/t_w=1-4; h_w/t_w=70-233; b_f/t_f=12.5-50; ss=50mm; e/b_f=0-0.167. Based on

the test results numerical model was developed and the design method of Elgaaly et al. [26] was further investigated and enhanced in the form of Eq. (27).

$$\frac{F_R^{red}}{F_R} = \left[-0.32 \cdot \left(\frac{t_f}{t_w} \right)^2 + 3.60 \cdot \left(\frac{t_f}{t_w} \right) - 7.67 \right] \cdot \left(\frac{e}{b_f} \right) + \left[1.00 - 0.0025 \cdot \left(\frac{t_f}{t_w} \right) \right] \tag{27}$$

f. Evaluation of the previous studies and research aims

Previous studies showed if the transverse load is applied through a wide loading plate the eccentricity has a negligible effect. If the loading width is small the eccentricity can lead to a significant reduction of the patch loading resistance due to the flange torsion along its longitudinal axis in case of I-girders with flat webs. Experiments showed that the effect of the eccentricity by smaller t_f/t_w ratio is much larger than by larger t_f/t_w ratio. Taken this effect into account Elgaaly et al. [26] developed an empirical design formula based on numerous test results and numerical calculations. This design proposal was further investigated and improved by Sćepanović et al. [32] based on a large number of test results. A comprehensive literature overview in this topic can be found in [33].

Evaluating the previous studies considering the corrugated web girders the following conclusions can be drawn. Only girders with flat webs were studied till now and there are no available investigations dealing with corrugated web girders, therefore the main aim of the current research activity is the extension of the research for corrugated web girders. In most of the previous tests only short loading length was analyzed, however in case of bridges longer loading lengths are usually applied.

Before analyzing the eccentricity the effect of the loading width is investigated. It should be smaller than the flange width if eccentric load is introduced. Reduced loading width indicates a reduction in the patch loading resistance as well, what should be considered in the design. No investigations are available dealing with the effect of the loading width in the literature, therefore a numerical parametric study is completed in this topic. Based on the numerical calculations the parameters which have influence on the patch loading resistance are separately investigated, tendencies of the results are determined and design proposal is developed.

In the frame of a second numerical parametric study the patch loading reduction due to loading eccentricities is analyzed. Based on the numerical calculations the structural behaviour of corrugated web girders is studied. Observations and conclusions of the numerical parametric study are summarized and a design method is proposed to determine the patch loading resistance under eccentric loading.

5.3. Numerical modelling and structural behaviour

Calculations are executed on the same numerical model which are introduced in Chapter 4. The applied finite element, the used material model and support conditions are the same as detailed previously.

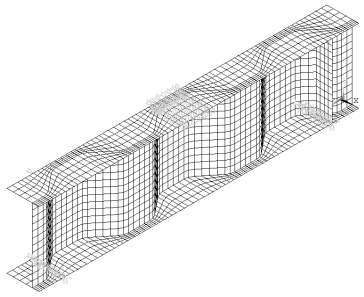

Figure 80: Finite element model.

The applied finite element mesh has the same density as in the case of the previous models which are verified based on the experimental background. The applied equivalent geometric imperfection in the nonlinear simulation is the recently determined (Sections 4.3. and 4.4.) eigenform imperfection shape and magnitude. The finite element mesh of the numerical model is shown in Fig. 80.

The structural behaviour and failure mechanism are studied under three different loading conditions. These are centric patch loading along the whole flange width, along a smaller loading width and under eccentric loading. Load-deflection and load-horizontal displacement diagrams are studied and compared in the three analyzed cases in Fig. 81. Left side of the diagram shows the load-deflection and the right side the load and horizontal displacement relationships measured at the parallel web fold 100 mm below the load introduction place.

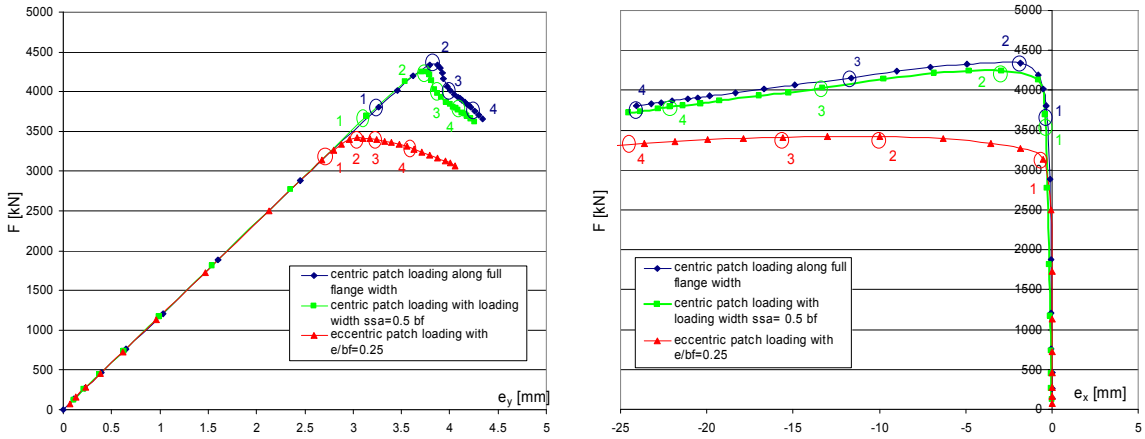

load – deflection diagram load – lateral displacement diagram

Figure 81: Comparison of the different loading conditions.

The blue thick curves represent the structural behaviour under centric patch load introduced along the whole flange width. This is the previously investigated and determined structural behaviour presented and detailed in Sections 2.4.1. ; 3.3. and 4.2. The marked points have the same meaning as presented before. Point #1 means first yielding in the flange or in the web. Point #2 presents the situation where 2 plastic hinges in the flange and a continuous yield line in the web is developed. Point #3 is the starting point of the 3. and 4. plastic hinge developments in the flange, and they are completely developed at Point #4.

The thick green curves show the structural behaviour if the applied loading width is smaller than the flange width. The presented diagram and the observed failure modes proved that there are no significant differences in the failure mechanism if the applied loading width is shorter. The tendency of the two curves are the same only the first yielding in the flange and web plates and the plastic hinge developments evolve at lower load levels. It can be explained by the fact that if the loading width is narrower the applied load is more concentrated and it leads to earlier yielding. Ultimate load decreasing degree depends on the degree of concentricity (ss_a/b_f)

The red curves show the structural behaviour under eccentric loading. It has a different character than the another two curves. The linear part of the diagram has the same gradient, it means that there are no differences in the elastic behaviour but the first yielding occurs at a lower load level, the load carrying capacity is also smaller and the post-ultimate behaviour changes as well. The gradient of the post-ultimate branch is smaller than in the first two cases. To get the reason for it the structural behaviour of the post-ultimate branch is investigated in details. In the descending branch the 3. and 4. plastic hinges develop and yielding extends to a large web area. No differences are found in the yield pattern or yield extension in the web

between the different loading modes, but the development of the plastic hinges in the flange are completely different in the case of eccentric loading as presented in Figs. 82 to 83.

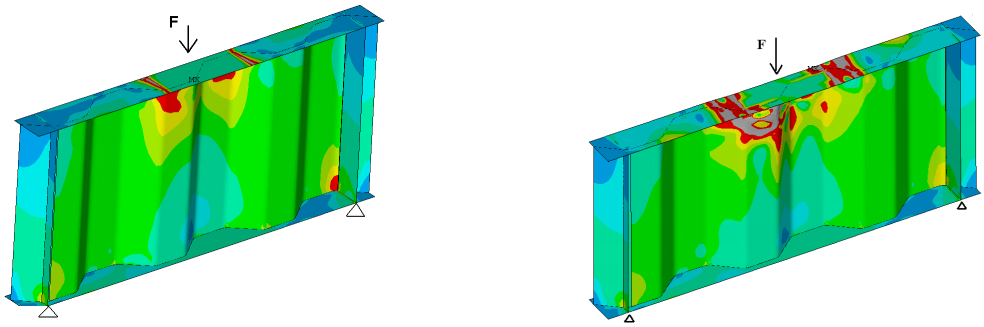

2 plastic hinges in the flange 4 plastic hinges in the flange

Figure 82: Plastic yield lines under centric loading.

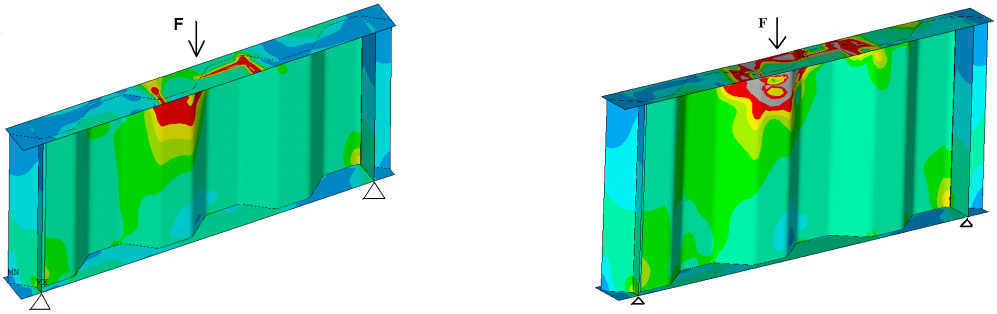

2 plastic hinges in the flange 4 plastic hinges + extra yield line in the flange

Figure 83: Plastic yield lines under eccentric loading.

Along the loading plate in longitudinal direction between the 2. and 3. plastic hinges an extra yield line develops. If the first two plastic hinges are completely developed the ultimate load is reached. In the case of centric loading after the ultimate load the 3. and 4. plastic hinges develops and the load carrying capacity of the girder is quickly lost. In the case of eccentric loading after reaching the ultimate load an extra yield line develops what gives extra resistance for the girder and the load carrying capacity does not fall as quickly as in the centric case.

5.4. Resistance reduction effect due to loading width

5.4.1. Numerical parametric study

Loading width has a major importance on the patch loading resistance. In the experimental program - introduced in Chapter 3 - one reference test (specimen #9) is conducted to analyze the effect of the loading width. Based on this test result the numerical model is verified. A numerical parametric study is conducted and the patch loading resistance for more loading widths are calculated. Results showed that the resistance decreases by reduced loading width and its tendency is presented in Fig. 84. On the diagram if $ss_a=b_f$ (225 mm), the whole flange is loaded. This case is analyzed in the previous chapters and the patch loading resistance (F_R) can be determined according to Section 3.5. If the loading width reduces the patch loading resistance reduces as well. The red point shows the experimental results where the loading width is 80 mm and the flange thickness is 225 mm. Blue points show the results of the numerical calculations and the thick green line presents the proposed model for the contribution of the resistance reduction.

The character of this model can be described by two parameters, the first one is the breaking point and the second one is the decreasing tendency. The main aim of the parametric study is to determine the parameters which have influence on these two values.

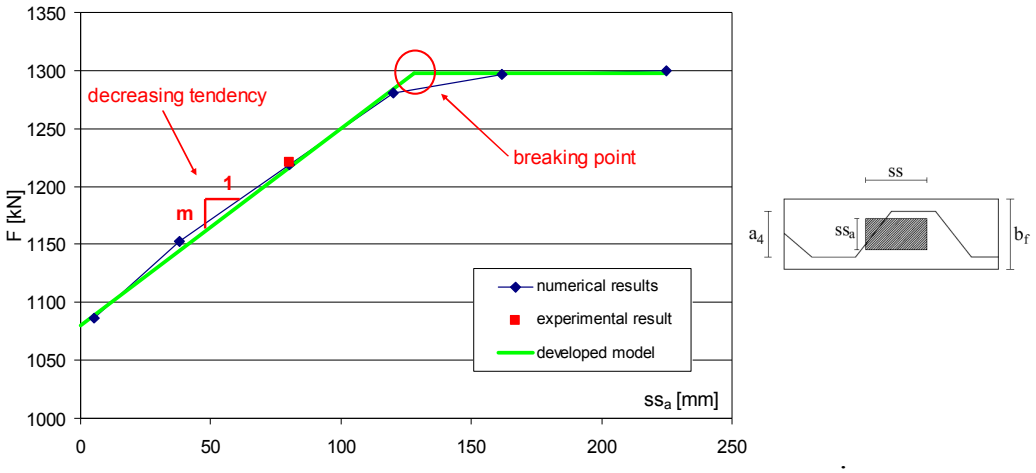

Figure 84: Effect of the loading width.

The following parameters are studied in the range of:

- loading length (*ss*): 200 – 1200 mm (in 100 mm steps),
- flange thickness (t_f): 20 – 25 – 30 – 35 – 40 – 45 – 50 – 60mm,
- flange width (b_f): 225 – 250 – 300 – 350 – 400mm,
- web ratio (h_w/t_w): 83 – 100 – 125 – 150 – 175 – 200 – 250 – 300 – 375 ,
- corrugation angle (α): 20° – 30° – 40° – 50° – 60° ,
- fold ratio (a_1/t_w): 25 – 30 – 40 – 45 – 50 – 67 – 70 (in all cases $a_1=a_2$) .

The first studied parameter is the loading length. Results showed that this parameter has influence on the breaking point as well as on the decreasing tendency, as presented in Fig. 85. In case of short loading lengths ($ss<a_1+a_2 \cdot cos(\alpha)$) the breaking point is always located at $a_3=a_2 \cdot cos(\alpha)$. It means if the loading width is larger than the corrugation height (a_3) loading width has no influence on the load carrying capacity. If loading width is smaller the patch loading resistance is also smaller. The reason of this phenomenon is that the applied load is transferred from the flange to the web and if the loading width is large enough the whole applied load can be introduced in the web without any resistance decrease. If the loading width is smaller than a_3, the applied load is more concentrated and the flange cannot transfer the whole load to the web. In the case of long loading lengths ($ss>a_1+a_2 \cdot cos(\alpha)$) the breaking point shifts to the left and reduction begins at smaller loading widths but with increased reduction intensity. It can be explained by the fact that in case of long loading lengths more folds take part in the load carrying what results a more uniform load distribution, therefore the applied load can be transferred to the web by smaller loading width as well.

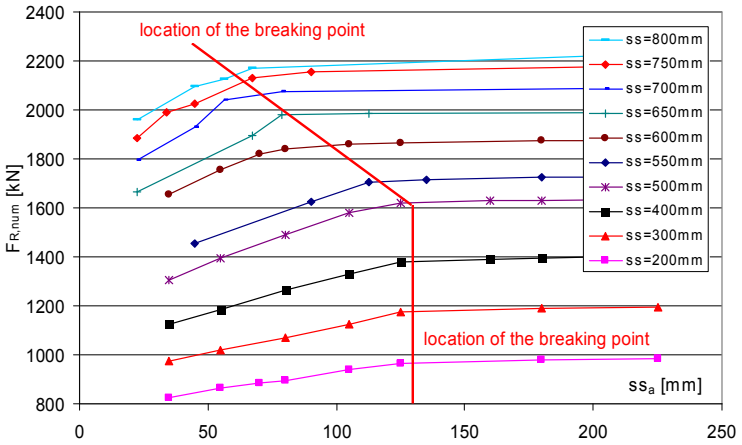

Figure 85: Effect of the loading width for different loading lengths.

Based on these observations the studied problem can be divided into two parts, as illustrated in Fig. 86.

1. short loading length $ss < a_1 + a_2 \cdot \cos(\alpha)$,
2. long loading length $ss \geq a_1 + a_2 \cdot \cos(\alpha)$.

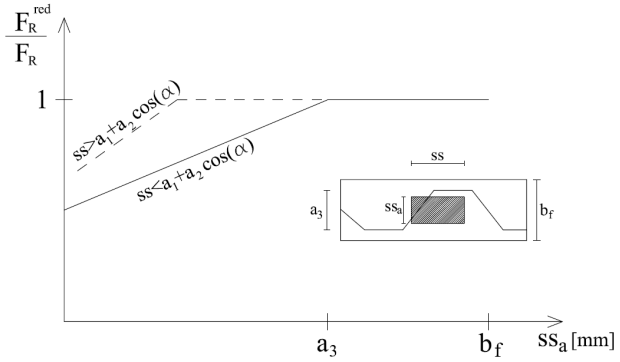

Figure 86: Effect of the loading width.

Tendencies for short loading lengths

The flange thickness has effect on the decreasing tendency, as shown in Fig. 87. If the flange thickness is larger, the patch loading resistance reduction is smaller because a more rigid flange can distribute the applied load more efficiently to the web folds. A thinner flange cannot distribute the load as efficiently therefore there is a larger resistance decrease. The breaking point is at a_3 in case of short loading length. Numerical calculation showed that no further geometric parameters have influence on the breaking point location.

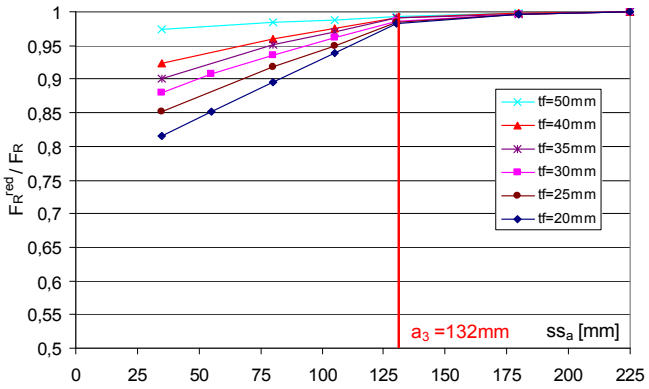

Figure 87: Effect of the loading width for different flange thicknesses.

The parametric study showed that the flange width and web thickness has only a minor influence on the breaking point as well as on the decreasing tendency. Figures 88 and 89 show the effect of the fold length and the corrugation angle.

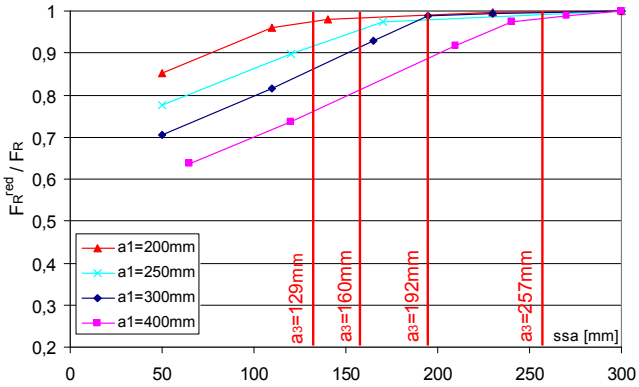

Figure 88: Effect of the loading width for different corrugation angles.

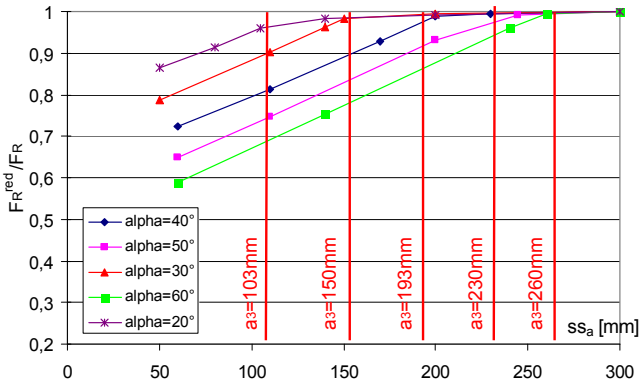

Figure 89: Effect of the loading width for different fold lengths.

The variation of the corrugation angle and the fold length result the same effect. Decreasing tendencies are independent from these two parameters, but the breaking points are moved. Reason of it is that due to changing of these parameters the a_3 length changes as well and the breaking point of the diagrams is located always at a_3. As a summary it can be concluded that the decreasing tendency depends mainly on the flange thickness and the breaking point is situated always at a_3 in the case of short loading lengths.

Another phenomenon should be also handled in the case of short loading lengths. If the loading width is small and it has also eccentricity, this two effects can result in an another failure type, what is the transverse flange bending, as shown in Fig. 90. The analysis of this failure mode is not part of this PhD thesis, because it can occur rarely in the praxis, therefore a minimal plate geometry of the launching device is determined and proposed to avoid this failure mode.

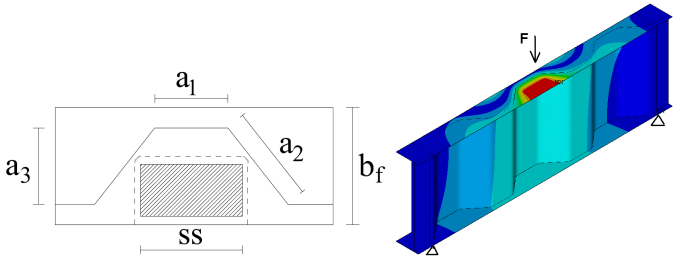

Figure 90: Transversal bending of the flange plate.

Minimal plate geometry of the launching device:

minimal plate width: $$ss_a > \frac{a_3 + b_f}{2} - t_f\,, \tag{28}$$

minimal plate length: $$ss > a_1 + a_2 \cdot \cos(\alpha)\,. \tag{29}$$

From this two criteria minimum one should be fulfilled. The launching plate should be wide enough, and it can be short at the same time, or it should be long enough and its width can be smaller at the same time, to avoid the transverse flange bending.

Tendencies for long loading lengths

In case of long loading length the breaking point is shifted to the left and the decreasing tendency changes as well. The first analyzed parameter is the flange thickness. It has influence on the breaking point as well as on the shifting ratio, as shown in Fig. 91.

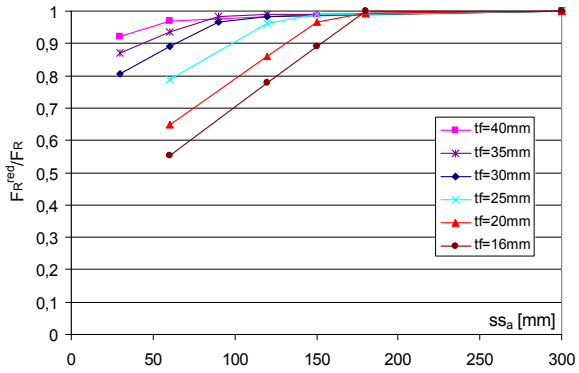

Figure 91: Effect of the loading width in the function of the flange thickness.

Larger flange thickness leads to smaller patch loading resistance decrease which is the same phenomenon as observed for short loading length. The breaking point depends on the flange and web thickness, the relationship can be described by the t_f/t_w ratio. The location of the breaking point shifts from a_3 to the left, the shifting ratio is called as b and its physical meaning is illustrated in Fig. 92. Numerical calculation showed that larger t_f/t_w leads to larger shifting ratio. It means that thicker flange distributes the load better and the reduction of the patch loading resistance is smaller, as it was discussed earlier.

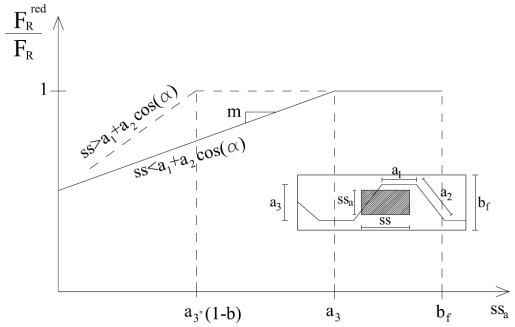

Figure 92: Characteristic of the diagram for long loading length.

The second parameter which has influence on the breaking point is the fold ratio (a_1/t_w). Larger fold ratio leads to larger resistance decrease. It can be explained by the fact that in the case of larger fold ratios the web cannot carry the load efficiently. If the fold ratio is low, the large rigidity of the web helps the load distribution therefore the resistance reduction is smaller. The decreasing tendency is independent from the fold ratio, as shown in Fig. 93.

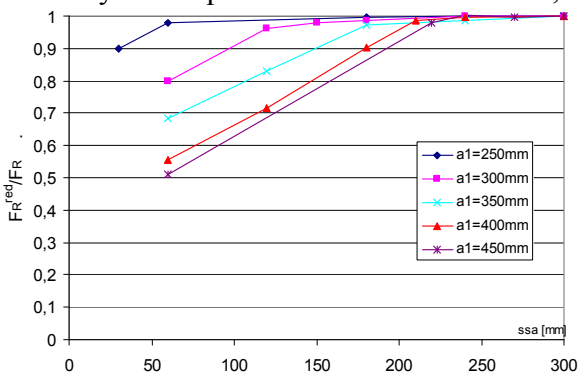

Figure 93: Effect of the loading width for more fold lengths.

It can be concluded that the decreasing tendency for long loading length is depending only on the flange thickness as in the case of short loading length. The shifting ratio of the breaking point from a_3 however depends on the t_f/t_w and a_1/t_w ratios. The relationship of b, t_f/t_w and a_1/t_w ratios is presented in Fig. 94.

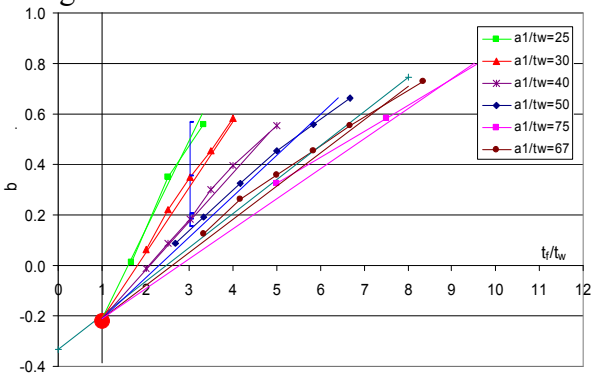

Figure 94: Shifting ratio in the function of fold and flange/web thickness ratio.

5.4.2. Design method development

Based on the results of 330 numerical simulations a design method is developed to consider the resistance decreasing effect due to reduced loading width. The basis of the design method is the model what is introduced in Fig. 92. The general form of the proposed design method is formulated in Eq. (30). The parameters b and m are determined separately for short and long loading lengths. The relationships between the two loading modes are determined and finally the parameters are combined in one design method.

$$F_R^{red} = F_{R.} \cdot \{1 - m[a_3 \cdot (1-b) - ss_a]\} \tag{30}$$

where: F_R : patch loading resistance if the full flange width is loaded, according to Section 3.5,
m: decreasing tendency,
a_3: projected fold length; wave height of the corrugation profile,
b: shifting ratio of the breaking point,
ss_a: loading width.

In the case of short loading length the breaking point is always located at a_3, therefore the shifting ratio is zero (b=0). The decreasing tendency for short loading length (m_1) is linearly depending on the flange thickness, as presented in Fig. 95/a and expressed in the form of Eq. (31).

$$m_1 = \left(2.8 - 0.05 \cdot t_f\right) \cdot 10^{-3} \qquad t_f \text{ is to be substituted in [mm].} \tag{31}$$

In the case of long loading length the breaking point is shifted to the left and numerical calculations showed that the shifting ratio depends on the t_f/t_w and a_1/t_w ratios. The results are presented in the diagram of Fig. 94. For different a_1/t_w ratios the effect of the t_f/t_w ratio is different. One line presented in Fig. 94. can be calculated by Eq. (32) in the function of c, what depends on the a_1/t_w ratio, as expressed in Eq. (33).

$$b = c \cdot \left(\frac{t_f}{t_w} - 1\right) - 0.2 \tag{32}$$

$$c = 8 \cdot \left(\frac{a_1}{t_w}\right)^{-1} \tag{33}$$

The decreasing tendency in the case of long loading length (m_2) depends only on the flange thickness as shown in Fig. 95/b and the relationship is expressed in Eq. (34).

$$m_2 = \left(5.3 - 0.08 \cdot t_f\right) \cdot 10^{-3} \qquad t_f \text{ is to be substituted in [mm].} \tag{34}$$

Eq. (30) for short loading length and Eqs. (31)-(33) for long loading length are different only in constants. Numerical results showed that b and m are in a linear relationship between the two equations, therefore the two formulas can be combined in one design method. The linear changing of the shifting ratio is shown in Fig. 85. The breaking point is constant for short loading length and for longer ones it is shifted almost linearly. The parameter b should be multiplied by a linear function, which results in 0 for $ss = a_1 + a_2 \cdot \cos(\alpha)$, and 1 for $ss = 1.5\,[a_1 + a_2 \cdot \cos(\alpha)]$. The value of b can be calculated according to Eq. (35).

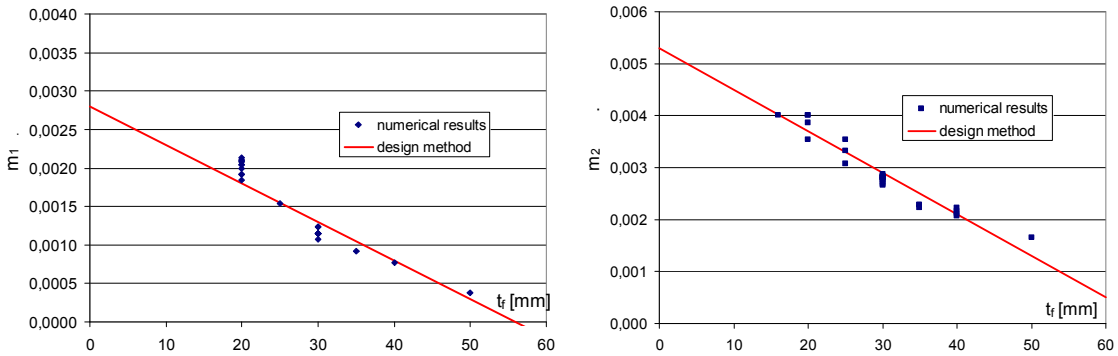

Figure 95: Decreasing tendency in the function of the flange thickness if $ss < a_1 + a_2 \cdot \cos(\alpha)$.

$$b = \left[c \cdot \left(\frac{t_f}{t_w} - 1 \right) - 0.2 \right] \cdot \left(2 \cdot \frac{ss}{a_1 + a_2 \cdot \cos(\alpha)} - 2 \right) \qquad \text{and } 0<b<1 \tag{35}$$

Decreasing tendency is depending only on the flange thickness, therefore Eqs. (30) - (34) is coupled in the function of the loading length, and it can be calculated by Eqs. (36) - (37).

$$m = \left(5 \cdot \beta - 2.2 - \left(0.06 \cdot \beta - 0.01\right) \cdot t_f\right) \cdot 10^{-3} \tag{36}$$

$$\text{where: } \beta = \frac{ss}{a_1 + a_2 \cdot \cos(\alpha)} \tag{37}$$

This expression gives for β=1 the Eq. (31) and for β=1.5 the Eq. (34). Results of the numerical calculations are compared to the developed design method in Fig. 96.

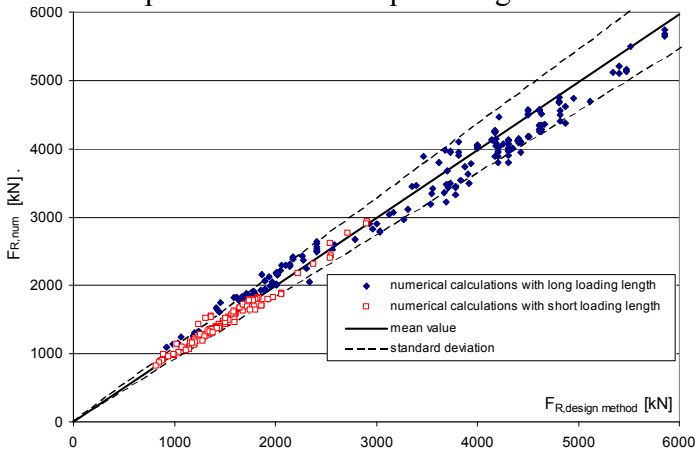

Figure 96: Comparison of the numerical calculations and the developed design method.

The blue points show the results with short loading length and the red hollow points present the results with long loading length. Results show a good correlation between the design proposal and numerical calculations. Mean value and standard deviation are also presented on the diagram in Fig. 96 and these are 0.995 and 0.063, respectively.

An enhanced design proposal is evolved to determine the decreasing tendency (m). It can be calculated by the ratio of x (maximal possible resistance decrease) and the breaking point ($a_3 \cdot (1\text{-}b)$). The illustration of the main idea is presented in Fig. 97.

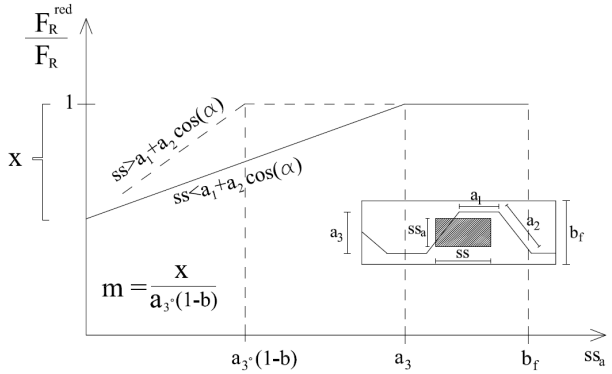

Figure 97: Illustration of the design method development.

The value of x depends on two factors, the first one is the decreasing tendency which is the function of the flange thickness and the second one is the breaking point which is the function of the t_f/t_w and a_1/t_w ratios. For all analyzed geometries the x values are determined from the numerical results. In the case of short loading lengths results for one fold length (a_3) is presented in Fig. 98/a. Depending on a_3 several parallel lines exist, this relationship can be found in Fig. 98/b. The value of x_1 for short loading length can be determined by Eq. (38).

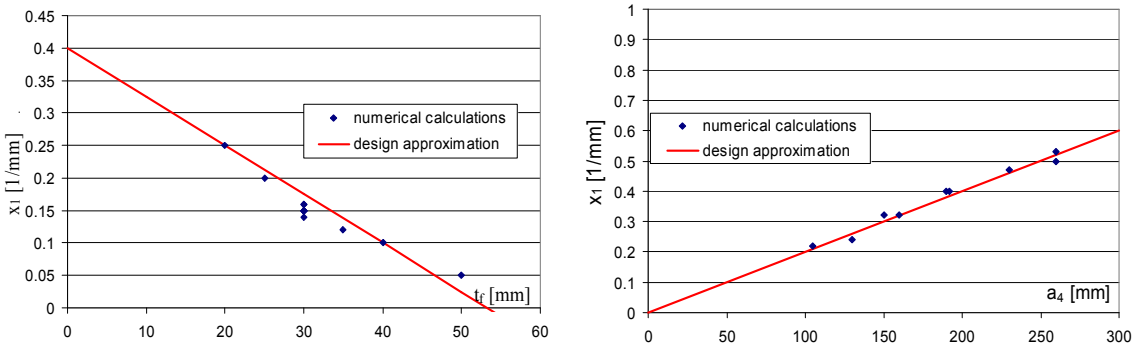

Figure 98: Determination of the x_1 in the function of a_3 and t_f.

$$x_1 = 0.1 + \frac{a_3}{500} - 0.0075 \cdot t_f \,. \tag{38}$$

The first two parts of Eq. (38) show the position of the breaking point and the third one shows the decreasing tendency. Based on these estimations m_1 can be determined by Eq. (39) in the case of short loading length.

$$m_1 = \frac{0.1 + \frac{a_3}{500} - 0.0075 \cdot t_f}{a_3} \,. \tag{39}$$

In the case of long loading length the same calculation is executed. The x_2 values are determined for all analyzed girder geometries and presented in the function of t_f and $a_3 \cdot (1\text{-}b)$ in Fig. 99. The same equations are derived for long loading lengths on the same basis as for short loading length in the form of Eq. (40).

$$x_2 = 0.4 + \frac{a_3 \cdot (1-b)}{350} - 0.013 \cdot t_f . \tag{40}$$

The breaking point is expressed by the first two members of Eq. (40) and decreasing tendency is determined by the third one. As x_2 is known the slope of the diagram can be calculated by Eq. (41).

$$m_2 = \frac{0.4 + \frac{a_3 \cdot (1-b)}{350} - 0.013 \cdot t_f}{a_3 \cdot (1-b)} . \tag{41}$$

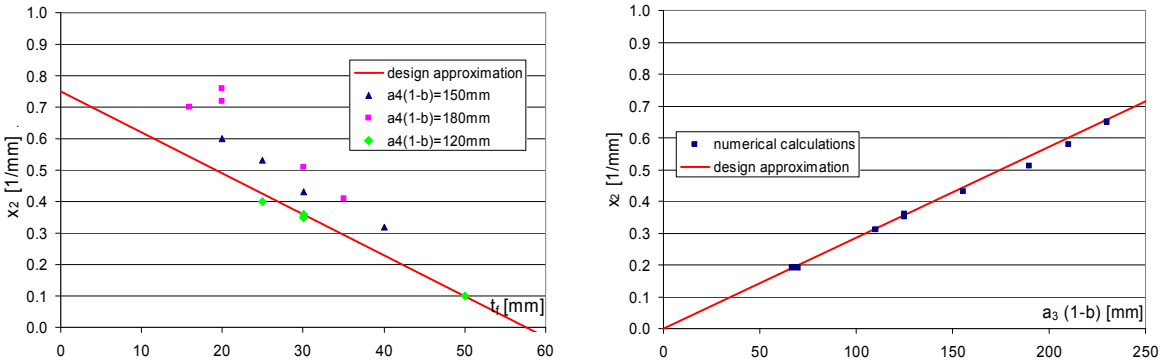

Figure 99: Determination of x_2 in the function of $a_3 \cdot (1\text{-}b)$ and t_f.

Values of m_1 and m_2 can be also coupled in the function of the loading length on the same way as detailed before because both equations have the same structure and only the constants are different. The slope of the decreasing tendency can be expressed by Eqs. (42)-(43).

$$m = \frac{0.6 \cdot \beta - 0.5 + \frac{a_3 \cdot (1-b)}{800 - 300 \cdot \beta} - (0.011 \cdot \beta - 0.0035) \cdot t_f}{a_3 \cdot (1-b)} \tag{42}$$

$$\text{where: } \beta = \frac{ss}{a_1 + a_2 \cdot \cos(\alpha)} \tag{43}$$

This expression gives for β=1 the Eq. (40) and for β=1.5 the Eq. (42). The value of the breaking point and the shifting ratio b can de determined by the previously developed expression Eq. (35). The modified design method is developed only for the decreasing tendency determination. Results of the numerical calculations are compared to the developed design method and the comparison is shown in Fig. 100. Diagram proves that this method is equivalent by the previously developed one and it can be also used for corrugated web girders with the same reliability. Mean value and standard deviation are 0.991 and 0.064, respectively.

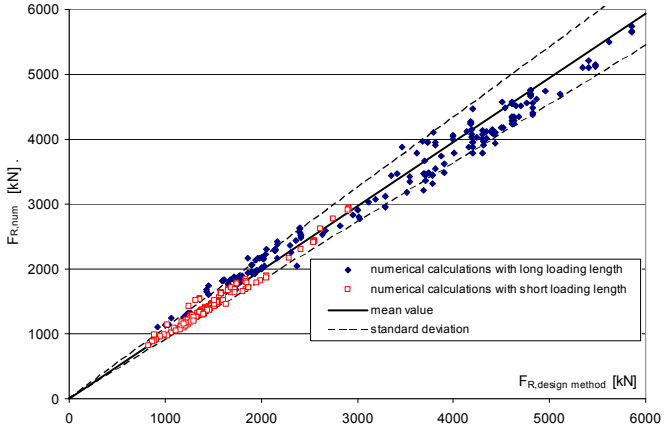

Figure 100: Comparison of the numerical results and the enhanced design method.

5.5. Resistance reduction due to loading eccentricity

5.5.1. Numerical parametric study

There are no available design recommendations for eccentric patch loading of corrugated web girders, therefore a comprehensive parametric study is executed in frame of this research to investigate the parameters which have influence on the patch loading resistance reduction due to loading eccentricities. This Section introduces the results of the numerical calculations, their evaluations and conclusions which are built in the design method.

Parameters which are studied in the numerical parametric study are the same as introduced in the last sections. The studied parameter ranges cover the typical used values of the praxis. The minimal loading plate size to avoid the transverse flange buckling gives a limit function for the analyzed loading widths and lengths. These limit functions are introduced in Eqs. (28)-(29). Investigation in the field of loading eccentricities is also separated into two parts based on the loading length. If the loading length is short ($ss < a_1 + a_2 \cdot cos(\alpha)$) the loading width should be larger than the limit function of Eq. (28). In this case the applied eccentricity can be small based on the assumption that the introduced load cannot slide down from the loaded girder. Numerical calculations showed that the resistance reduction due to eccentric loading remains under 5% in the analyzed parameter range. Conclusion can be drawn that the effect of the loading eccentricity can be neglected if the loading length is short ($ss < a_1 + a_2 \cdot cos(\alpha)$) and the loading width is larger than expressed in Eq. (28). These results are illustrated in Fig. 101.

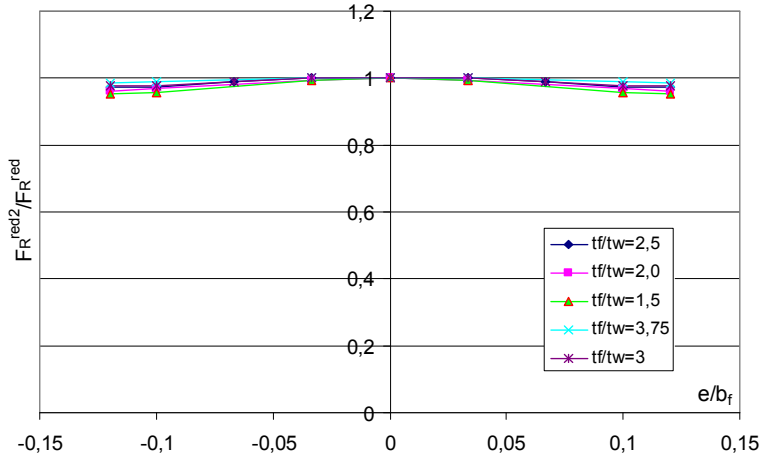

Figure 101: Effect of the eccentric patch loading in the case of short loading length.

The further results and conclusions are valid for long loading lengths ($ss > a_1 + a_2 \cdot cos(\alpha)$). Numerical results showed that the effect of the eccentric patch loading depends on three parameters in the case of corrugated web girders. The first one is the flange thickness. In the case of flat web girders the effect was depending on t_f/t_w ratio according to the literature, but in the case of corrugated web girders the t_w has much smaller effect on the load carrying capacity. The dominant parameter is the flange thickness. Figure 102 shows the resistance reduction in the function of t_f and t_w. The diagram shows that the effect of the eccentricity reduces with increasing flange thickness. The decreasing tendency is parabolic in the case of smaller flange thicknesses (t_f<20mm). Between 20<t_f<40mm the relationship is nearly linear and for larger flange thicknesses it has a square root function character. The same parametric study is executed for different web and flange thicknesses (t_w=6-8-10-12mm; t_f=12-18-20-24-30-36-40-48-50mm) and all calculation showed the same tendencies.

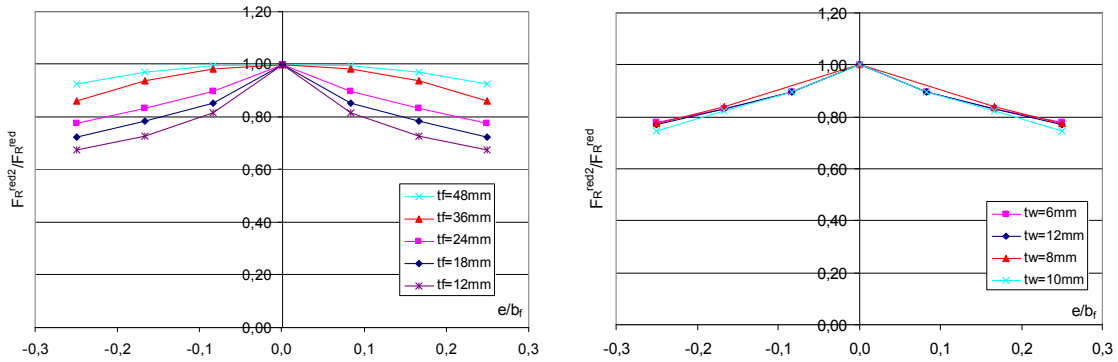

Figure 102: Effect of eccentric loading in the function of t_f and t_w.

Investigations showed that in the case of corrugated web girders the lateral stiffness of the web plate has also an important effect. The situation is the same for flat web girders, if the web thickness („lateral stiffness“) increases the resistance reduction due to eccentricities increases as well. This phenomenon has been observed by several researchers in the past for flat web girders. It is the same for corrugated web girders, but the lateral stiffness is mostly depending not on t_w but on the corrugation angle (α) and fold length (a_1). The effect of these two parameters is presented in Fig. 103. If the fold length (a_1) or the corrugation angle (α) increases the lateral stiffness of the corrugated web increases as well and it leads to a larger resistance reduction.

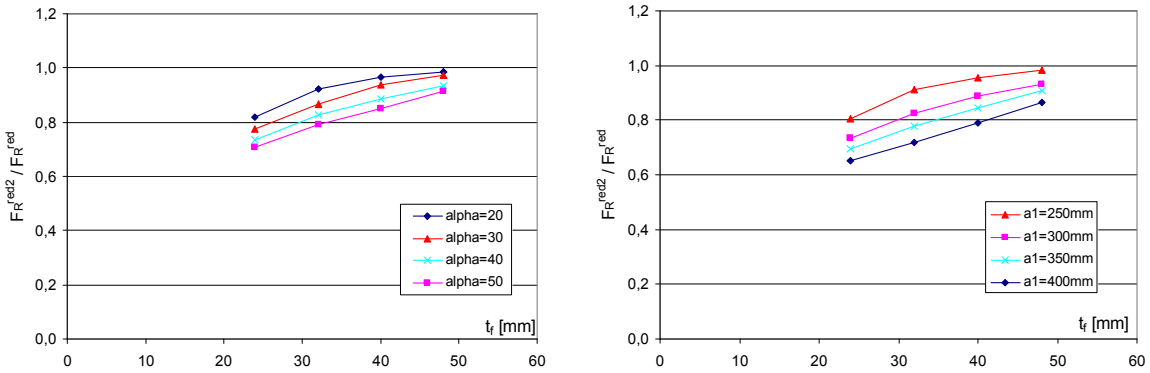

Figure 103: Effect of eccentric loading in the function of α and a_1.

These two parameters can be handled together using the parameter of a_3. Calculations showed that for different corrugation angles and for different fold lengths the results can be plotted in function of the wave height (a_3) of the corrugated web. Figure 104 shows, if the lateral stiffness of the web is higher, eccentric loading leads to a larger resistance reduction. This figure shows an another important information as well, that the effect of the flange thickness has the same character for all web corrugation geometry.

The phenomenon that the increase of the lateral stiffness leads to the increase of the resistance reduction due to eccentric loading is investigated in details. Four different cases, shown in Fig. 105 are studied to analyze the reason of it. Failure mechanism and stress distribution in the corrugated web plate are investigated with two different corrugation angles (α=20°, 60°) and two flange thicknesses (t_f=20mm, 70mm). Results showed that the effect of t_f and a_3 cannot be handled separately. The reason of it is the load distribution along the web folds. If a_3 is larger the distance between the parallel folds is larger therefore the lever arm increases but the balanced transverse bending moment is smaller if the flange is not able to carry the applied force from one side to the other one. The studied geometries and the force distribution in the parallel folds is illustrated by different flange thicknesses and a_3 distances in Fig. 106.

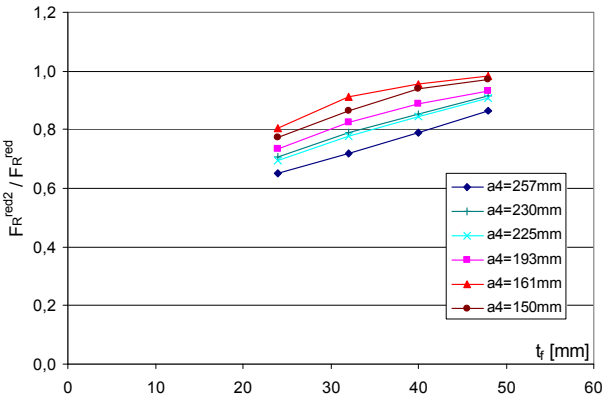

Figure 104: Resistance reduction due to eccentric loading in the function of a_3.

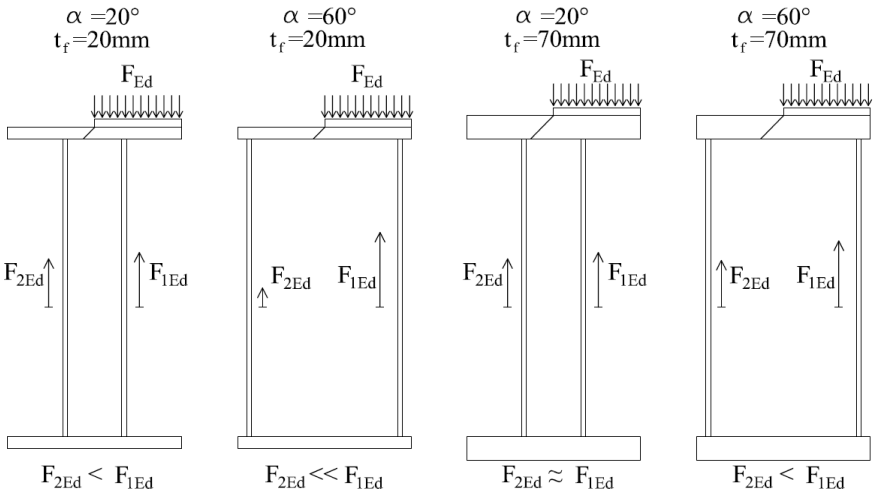

Figure 105: Investigated geometries.

The first case shows if the a_3 distance is relative small a thin flange can also distribute the applied force between the web folds almost uniformly ($F_{1Ed} \approx F_{2Ed}$). If the a_3 distance is larger and the flange thickness is small the loaded web fold has to carry a larger part of the applied load ($F_{2Ed} << F_{1Ed}$) which leads to a resistance decrease. If the flange thickness is larger the stress distribution along the loaded web folds is more uniform and it leads to a larger patch loading resistance and the girder has higher efficient against loading eccentricities. The stress distribution along three web folds are presented in Fig. 106, studying two different a_3 distances.

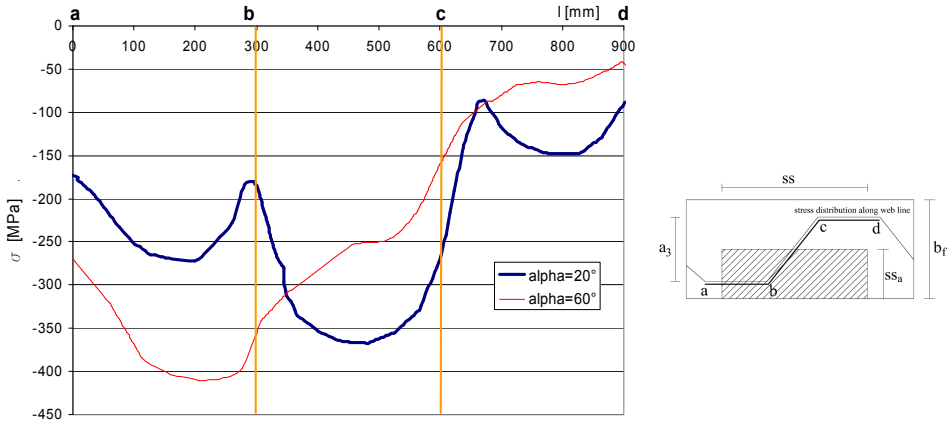

Figure 106: Stress distribution along three web folds.

The blue dotted curve shows the stress distribution by a_3=102 mm. Loaded fold is the middle inclined fold, and the applied load has an eccentricity in the direction of the previous parallel fold. The largest stress arises in the middle inclined fold. In the parallel folds there is a roughly uniform stress distribution with a little bit larger stresses under the loaded fold, but the flange is able to distribute the applied force to the web part on the other side as well. The red thin line shows the stress distribution if the a_3 distance is larger (a_3=260 mm). The diagram proves the previously introduced phenomenon that the small flange cannot distribute the applied load between the web folds and the loaded fold has to carry the largest part of the applied load. The same can be observed on the failure modes in Fig. 107. If a_3=102 mm the local buckling occurs in more folds on both side of the web and if the a_3=260 mm local buckling occurs mainly on the loaded side.

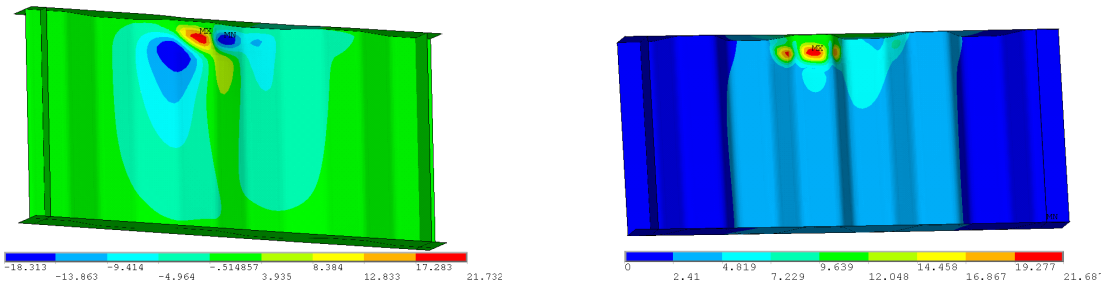

α=20° α=60°

Figure 107: Comparison of failure modes.

Based on the numerical calculations it can be concluded that the t_f and a_3 values should be always handled together. By constant flange thicknesses due to the increase of the a_3 distance the stress distribution is less uniform and it results that the loaded web fold carry a larger part of the applied load and it leads to resistance decrease. Larger flange thickness leads to more uniform stress distribution, but in the case of too large a_3 distance, small resistance decrease can be also observed. These investigations and observations are valid only in the cases if the loading width has such a geometry that by the maximal eccentricity only one side of the corrugated web is loaded ($ss_a < \frac{a_3 + b_f}{2} - t_f$). If the loading width is larger than $ss_a > \frac{a_3 + b_f}{2} - t_f$, the above described tendency can be also observed but the scale of the phenomenon is much smaller and the resistance decreasing effect due to loading eccentricities remains in all analyzed cases under 5%.

The third parameter which has influence on the resistance decreasing is the loading width. Calculation showed that for large loading widths the eccentricity has no influence on the patch loading resistance. The same is observed for short loading lengths. If the loading width is smaller the eccentricity can be larger and it results in a larger influence on the patch loading resistance reduction. The resistance reduction effect in the function of the loading width is analyzed by different flange thicknesses (t_f=30; 40; 60mm) and by different a_3 values (a_3=150; 193; 230mm). The character of the resistance decrease can be seen in Fig. 108. The resistance reduction is expressed by the ratio of the patch loading resistance under centric loading and under a constant eccentricity by e/b_f=0.2. It can be seen, that if the loading width is larger the eccentricity has a negligible influence on the resistance reduction tendency. Smaller loading width results in larger patch loading reduction and by small loading widths the reduction does not increase.

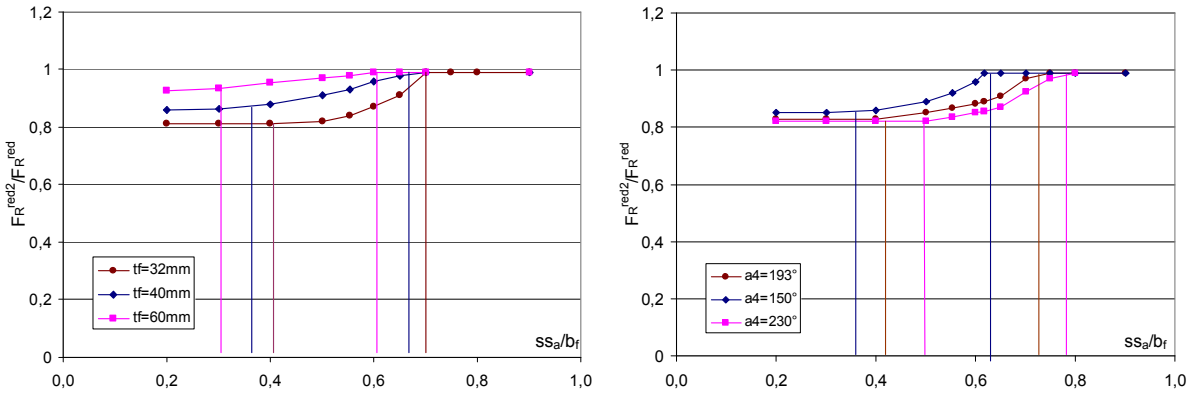

Figure 108: Effect of the loading width on the eccentricity influence.

The upper and lower limits of the functions can be expressed by Eqs. (44) and (45), respectively:

upper limit: $$\frac{a_3 + b_f}{2} - t_f \tag{44}$$

lower limit $$d \cdot \left(\frac{a_3 + b_f}{2} - t_f \right) \tag{45}$$

where: $$d = 0{,}43 + 0{,}004 \cdot \frac{a_3}{t_f} \ . \tag{46}$$

Further calculations shows that the loading position has no effect in the case of long loading lengths, neither the flange width (b_f), nor the loading length (ss) on the resistance reduction due to eccentric loading.

5.5.2. Design method development

Numerical and experimental results of flat web girders showed that the character of the decreasing tendency is changing in the function of the flange thickness. For small flange thicknesses (t_f<20mm) the decreasing tendency is parabolic, between 20mm<t_f<40mm the relationship is almost linear and for larger flange thicknesses it is nearly a square root function. This changing of the character can be hardly followed in the design proposal. In the case of bridges the flange thickness is mostly larger than 20 mm, therefore the character of this function is described linearly. For geometries used in the praxis this assumption leads to a good approximation. For larger flange thicknesses (t_f>40mm) this approximation remains on the safe side and the difference is in all analyzed cases smaller than 5%. The linear approximation can be expressed in the form of Eq. (47).

$$F_R^{red\,2} = F_{R.}^{red} \cdot \left(1 - m_3 \cdot \frac{e}{b_f} \right) \tag{47}$$

where: F_R^{red} : patch loading resistance according to Eq. (30),
m_3: slope of the resistance decreasing tendency,
e: eccentricity of the applied load,
b_f: flange width.

Decreasing tendency (m_3) is depending on 3 parameters, as introduced previously. These parameters are the flange thickness (t_f), the wave height (a_3) and the loading width (ss_a). At first the effect of the flange thickness is analyzed with constant a_3 and ss_a values. Resistance decreases by a constant e/b_f=0,25 eccentricity can be seen in Fig. 109. If t_f decreases the resistance reduction increases nearly linearly. This relationship can be expressed by Eq. (48).

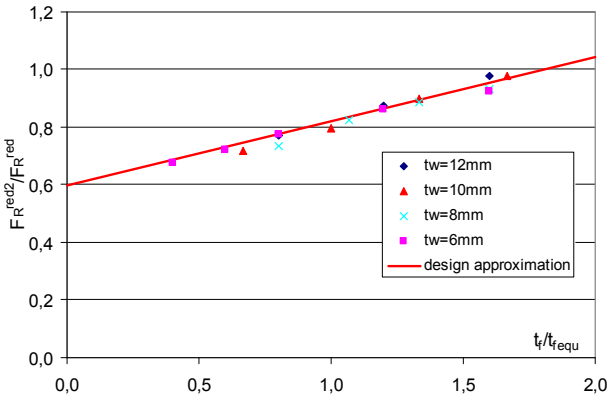

Figure 109: Effect of the flange thickness on the resistance decrease.

$$m_{tf} = 0{,}6 + \frac{t_f}{4{,}5 \cdot t_{fequ}} \tag{48}$$

where t_{fequ}=30mm, which is a lower limit of the flange thicknesses used in bridge design.

The effect of a_3 in the case of different flange thicknesses is also analyzed. Results can be seen in Fig. 110. The relationship between resistance decrease and corrugation wave height is nearly linear. Many parallel lines are in the function of the different flange thicknesses on the diagram. Based on these assumptions the previous expression can be modified in form of Eq. (49).

$$m_{tf2} = 0{,}78 + \frac{t_f}{4{,}5 \cdot t_{fequ}} - \frac{a_3}{5 \cdot a_{3equ}} \tag{49}$$

where a_{3equ}=200mm. This value matches to a usual corrugation profile with a_1=300mm and corrugation angle equal to 40°.

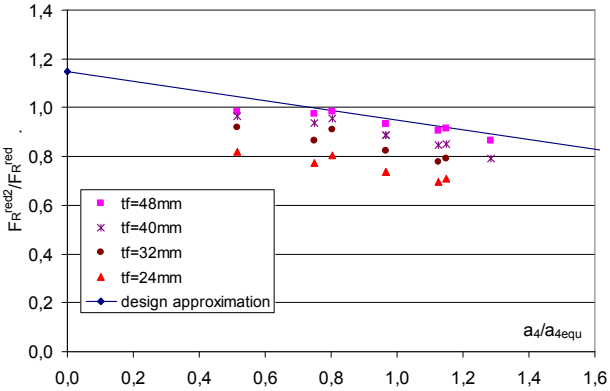

Figure 110: Effect of a_4 value on the resistance decrease.

Eq. (49) is developed for the eccentricity of e/b_f=0.25, therefore the expression has to be specified to this value and it gives the patch loading resistance and not the resistance decrease and therefore it should be subtracted from 1. According to these relationships the decreasing tendency can be described in the form of Eq. (50).

$$m_3 = \frac{0{,}22 - \frac{t_f}{4{,}5 \cdot t_{fequ}} + \frac{a_3}{5 \cdot a_{3equ}}}{0{,}25} = 0{,}88 - 0{,}89 \cdot \frac{t_f}{t_{fequ}} + 0{,}8 \cdot \frac{a_3}{a_{3equ}} \tag{50}$$

Finally the effect of the loading width is taken into account. If the loading plate is wide enough there is no resistance reduction due to eccentricity, expressed by Eq. (52). If the

loading width is small Eq. (54) can be applied. In the transition zone the decreasing tendency can be determined by Eq. (53) which considers a linear changing due to loading width. The general design proposal is summarized in Eqs. (51)-(55).

$$F_R^{red\,2} = F_R^{red} \cdot \left(1 - m_3 \cdot \frac{e}{b_f}\right) \tag{51}$$

where: $m_3 = 0$ if: $ss_a > \frac{a_3 + b_f}{2} - t_f$ (52)

$$m_3 = \left(0{,}88 - 0{,}89 \cdot \frac{t_f}{t_{fequ}} + 0{,}8 \cdot \frac{a_3}{a_{3equ}}\right) \cdot \left(\frac{\frac{a_3 + b_f}{2} - t_f - ss_a}{\frac{a_3}{2} - t_f}\right) \quad \text{if:} \quad d \cdot \left(\frac{a_3 + b_f}{2} - t_f\right) < ss_a < \frac{a_3 + b_f}{2} - t_f \tag{53}$$

$$m_3 = 0{,}88 - 0{,}89 \cdot \frac{t_f}{t_{fequ}} + 0{,}8 \cdot \frac{a_3}{a_{3equ}} \qquad \text{if:} \quad ss_a < d \cdot \left(\frac{a_3 + b_f}{2} - t_f\right) \tag{54}$$

where: $d = 0{,}43 + 0{,}004 \cdot \frac{a_3}{t_f}$ (55)

As a summary 250 numerical simulation results are compared to the proposed design method, and results showed a good agreement. Comparison is presented in Fig. 111. Mean value and standard deviation is also calculated and these are 1.01 and 0.05, respectively.

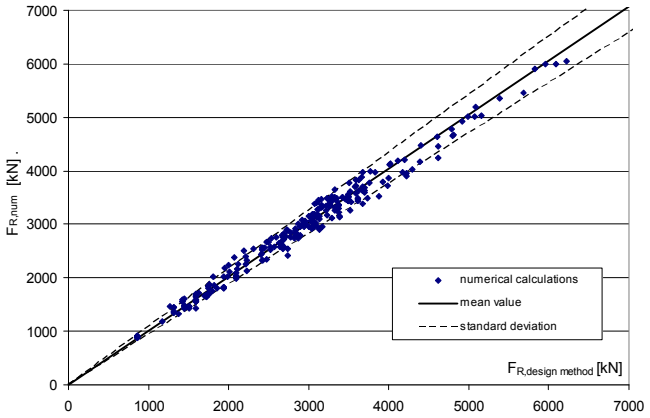

Figure 111: Comparison of design method with numerical calculations.

5.6. Application of the results

Both developed design methods can be applied directly in the patch loading design of girders with corrugated webs in the considered parameter range. The patch loading resistance can be determined by the first proposed design method if the flange is partially loaded along its flange width. The second design proposal determines the patch loading resistance under eccentric loading. The determined tendencies and conclusions based on the numerical parametric studies can also be used in the design of corrugated web girders.

5.7. Summary

The focus of the current research presented in this Chapter is the determination of the patch loading resistance of corrugated web girders under eccentric transverse loading. Based on the experimental background introduced in Chapter 3 a numerical model is developed and the patch loading resistance is determined by nonlinear finite element simulation.

The structural behaviour and failure mechanism are studied under centric patch loading along the whole flange width, along a smaller loading width and under eccentric loading. Load-

deflection and load-horizontal displacement diagrams are studied and compared in the three analyzed cases. Failure mechanism under the centric loading are the same, only the first yielding and the plastic hinge developments evolve at lower load levels due to the more concentrated load introduction. The structural behaviour under eccentric loading has a different character in the post-ultimate branch than under centric loading. The reason of it is an extra yield line which develops in the descending branch along the loading plate in longitudinal direction.

In the frame of numerical parametric studies the resistance decreasing effect due to reduced loading width and loading eccentricity are investigated. Effect of each investigated geometric parameters are determined and the resistance decreasing tendencies are appointed. If the loading width reduces the patch loading resistance reduces as well. The character of the reduction tendency can be described by two parameters, the first one is the breaking point and the second one is the decreasing tendency of the resistance decreasing effect. In the case of short loading length the decreasing tendency depends on the flange thickness and the breaking point is situated always at a_3. In the case of long loading length the decreasing tendency depends on the flange thickness and the shifting ratio of the breaking point from a_3 depends on the t_f/t_w and a_1/t_w ratios. Based on the observed tendencies in the numerical parametric study a design method is developed which takes the resistance decreasing effect due the loading width into account.

In the frame of a second numerical parametric study parameters which have influence on the resistance decreasing effect due to eccentric loading are determined. Numerical calculation shows that the patch loading resistance decreases with increasing loading eccentricity. The decreasing tendency is parabolic in the case of small flange thicknesses (t_f<20mm). Between 20<t_f<40mm the relationship is nearly linear and for larger flange thicknesses it has a square root function character. Results showed that the effect of the eccentric patch loading depends on three parameters in the case of corrugated web girders. The first one is the flange thickness. The results show that the effect of the eccentricity reduces with increasing flange thickness. In the case of corrugated web girders the lateral stiffness of the web plate has also an important effect. If the lateral stiffness of the web is higher, eccentric loading leads to a larger resistance reduction. The third parameter which has influence on the eccentric loading is the loading width: for large loading widths the eccentricity has no influence on the patch loading resistance. If the loading width is smaller the eccentricity can be larger and it results in a larger influence on the patch loading resistance reduction.

6. Determination of the partial factor to the developed design methods

6.1. General

Design methods introduced and developed in the previous chapters determine always the mean value of the patch loading resistance. In the design of structures engineers calculate with the design values therefore this Chapter focuses on the determination of the design resistance levels. All design proposals introduced in this thesis are statistically evaluated. Mean values, standard deviations and coefficient of variations are determined. Probability distribution functions are developed and evaluated. EN1990 Annex D [34] gives a detailed determination method of the partial factor if results are coming from experiments. If the resistance model is developed based on numerical calculations its specialties can be considered in the statistical evaluation method. These specialties are taken into account and based on the numerical and experimental results the partial factors are determined.

6.2. Review of different determination methods of the partial factor

6.2.1. Determination methods according to EN1990 Annex D

EN1990 Annex D (Design assisted by testing) [34] gives a detailed description on the determination of partial factors, if experimental results are available. There are two different methods:

- statistical evaluation of a single property (EN1990 Annex D Chapter 7),
- statistical evaluation of a resistance model (EN1990 Annex D Chapter 8).

The first method can be applied if the analysed function depends only on one statistical property (for example: material properties, geometric data, etc.). The second method can be applied to determine the partial factor of a resistance model. A short overview about both methods is given in the following.

Statistical evaluation of a single property (EN1990 Annex D Chapter 7)

This method can be applied to determine the partial factor of a single property. It means that the studied function has only one statistical variable. The mean value, the standard deviation and the 5% and 1% fractil values of the probability distribution function can be determined according to the following expressions. In the case of a normal distribution these values can be calculated by Eqs. (57)-(58).

characteristic value: $$X_k = F_{R,mean} \cdot \left(1 - k_n \cdot V_x\right) \quad (57)$$

design value: $$X_d = F_{R,mean} \cdot \left(1 - k_{d,n} \cdot V_x\right) \quad (58)$$

where:
V_x: coefficient of variation of the design resistance,
$F_{R,mean}$: mean value of n samples of the design resistance,
k_n: characteristic fractile factor
1.64, if β=3,8 and more than 30 experiments are available,
$k_{d,n}$: design fractile factor
3.04, if β=3,8 and more than 30 experiments are available,
β: reliability index (3,8 for structures with 50 years reference period in the reliability class RC2).

The partial factor (γ_{M1}) can be determined by Eq. (59), as the ratio of the characteristic and design values.

$$\gamma_{M1} = \frac{X_k}{X_d} = \frac{\mathrm{F}_{R,mean} \cdot \left(1 - k_n \cdot V_x\right)}{\mathrm{F}_{R,mean} \cdot \left(1 - k_{d,n} \cdot V_x\right)} \quad (59)$$

Statistical evaluation of resistance models (EC1990 Annex D Chapter 8)

EN1990 Annex D Chapter 8 [34] gives partial factor determination method if the resistance model is calibrated by experimental results. This method has 7 steps.

1. Development of the design model.
2. Comparison of experimental and theoretical values. The vertical axis of the Fig. 112 shows the patch loading resistances according to the numerical calculations ($F_{R,num}$) or the experimental values ($F_{R,exp}$). The vertical axis of the diagram illustrates the patch loading resistances calculated by different design methods ($F_{R,design\_method}$).

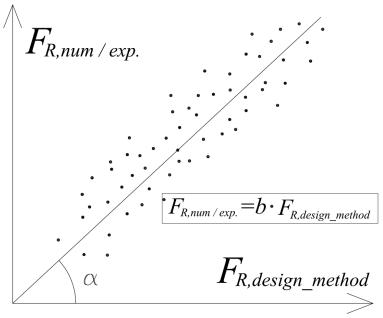

Figure 112: Comparison of experimental and theoretical values, from [34].

3. Estimation of the mean value correction factor *b.*

   If the resistance function results in the same values as the experimental or numerical results, than all of the presented points would lie on a line with a gradient of 45° (b=1.00). In the practice the points show some scatter giving the errors of each results. Normally in the practice these points are located around a line which gradient differs from 45°. The value b takes this difference into account.

$$b = \frac{\sum F_{R,num} \cdot F_{R,design\_method}}{\sum F_{R,design\_method}^{\,2}} \tag{60}$$

4. Estimation of the coefficient of variation of the errors

   If the gradient of the mean line (b) is known, errors of all results can be calculated and statistically evaluated, as detailed in the following:

   error term for each value: $$\delta_i = \frac{F_{R,num,i}}{b \cdot F_{R,design\_method,i}} \tag{61}$$

   logarithm of the error terms: $$\Delta_i = \ln(\delta_i) \tag{62}$$

   mean value of logarithm of the error terms: $$\overline{\Delta} = \frac{1}{n} \cdot \sum_{i=1}^{n} \Delta_i \tag{63}$$

   standard deviation of the error terms: $$s_\Delta{}^2 = \frac{1}{n-1} \cdot \sum_{i=1}^{n} \left(\Delta_i - \overline{\Delta}\right)^2 \tag{64}$$

   coefficient of variation of the error terms: $$V_\delta = \sqrt{\exp\left(s_\Delta{}^2\right) - 1} \tag{65}$$

5. Analysis of compatibility

   It should be tested, that the mean value, standard deviation and coefficient of variation are in the whole analysed parameter range approximately equal. It should be checked that the resistance model works in the whole analyzed parameter range with the same accuracy. If differences are larger the parameter which has the largest influence on the scatter should be determined and investigated and the test results may be split into subsets with respect to this parameters.

6. Determination of the coefficients of variation (V_{xi}) of the basic variables
   The investigated resistance model depends on different variables. The coefficient of variation of the basic variables in the resistance functions is determined in this point.

7. Determination of the characteristic and design value of the resistance model
   From the product of coefficient of variations given in point 4 and 6 the coefficient of variation of the whole resistance model can be calculated by Eq. (66).

$$V_r^2 = \left(V_\delta^2 + 1\right) \cdot \left[\prod_{j=1}^{n} \left(V_{Xi}^2 + 1\right)\right] - 1 \tag{66}$$

   Alternatively, for small values of V_δ^2 and V_{xi}^2 the approximation of Eq. (67) can be used.

$$V_r^2 = V_\delta^2 + \cdot \sum_{i=1}^{j} V_{Xi}^2 \tag{67}$$

   If a large number of tests (n>100) are available, the characteristic and design resistances can be obtained from Eqs. (68)-(70).

$$F_{R,k} = b \cdot F_{R,design\_method} \cdot e^{-k_\infty \cdot Q - 0.5 \cdot Q^2} \tag{68}$$

$$F_{R,d} = b \cdot F_{R,design\_method} \cdot e^{-k_{d,\infty} \cdot Q - 0.5 \cdot Q^2} \tag{69}$$

where $$Q = \sqrt{\ln\left(V_r^2 + 1\right)} \tag{70}$$

k_∞ is the value of k_n for $n \to \infty$ (k_∞=1.64),
$k_{d,\infty}$ is the value of $k_{d,n}$ for $n \to \infty$ ($k_{d,\infty}$=3.04).

The partial factor can be determined according to Eq. (71).

$$\gamma_{M1} = \frac{F_{R,k}}{F_{R,d}} = \frac{b \cdot F_{R,design\_method} \cdot e^{-k_\infty \cdot Q - 0.5 \cdot Q^2}}{b \cdot F_{R,design\_method} \cdot e^{-k_{d,\infty} \cdot Q - 0.5 \cdot Q^2}} \tag{71}$$

6.2.2. Modifications of the standardized determination method

The determination method of the partial factor according to EN1990 [34] is developed for evaluation of resistance models based on the experimental results. If the developed resistance model is based on numerical calculations the determination method of the probability variables are different from the standardized method. This section introduces the modification possibilities which are found in the literature.

The first possible modification proposal is found in the diploma thesis of Gabeler [35] supervised by Mirambell/Chacón, UPC Barcelona and Kuhlmann/Braun, University of Stuttgart on the topic of statistical evaluation of patch loading resistance models for welded steel girders. Different design models of the patch loading resistance are investigated and statistically evaluated. Gabeler used the standardized partial factor determination method according to EN1990 Annex D [34] with a small modification. The modified method takes into account that the resistance model is compared to numerical and not to experimental results. The numerical calculations and the experimental results do not match exactly, there are always differences. The mean value, standard deviation and coefficient of variation of these differences are calculated and the results were taken into account in the coefficient of variation of the whole resistance model by a newly introduced factor called as V_{FEM}. This new factor is implemented in Eq. (66) in form of Eq. (72).

$$V_r^2 = \left(V_\delta^2 + 1\right) \cdot \left[\prod_{j=1}^{n} \left(V_{Xi}^2 + 1\right)\right] \cdot \left(V_{FEM}^2 + 1\right) - 1 \tag{72}$$

In the literature a detailed description can be found about the determination method of partial factor for lateral torsional buckling of I-girders, made by Rebelo et al. [36] and L. da Silva et al. [37]. Basis of the investigation was more than 1000 numerical calculations beside some experimental results. Since the bases of the investigations were mainly numerical calculations, the partial factor was separated into two parts as presented in Fig. 113 and in Eq. (73). γ_m takes the material uncertainties into account and γ_{Rd} covers the uncertainties of the resistance model and the geometric deviations if these are not modeled explicitly. EN1990 [34] considers the same separation methodology of the partial factor γ_M.

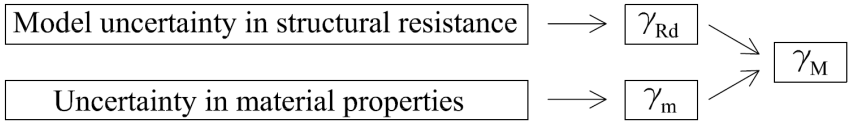

Figure 113: Separation of the partial factor according to EN1990.

The reason of the separation is, that the numerical model calculates with the given material properties and geometry exactly, therefore the difference between the numerical and experimental resistances does not consider their uncertainties and that they should be handled separately.

$$F_{R,d} = \frac{F_{R,k}}{\gamma_{M1}} = \frac{F_{R,k}}{\gamma_m \cdot \gamma_{Rd}} \tag{73}$$

γ_{Rd} was determined for lateral torsional buckling of I-girders in [36] based on numerical calculations and theoretical resistances, therefore it considers only the uncertainty of the resistance model. Value of γ_m was determined separately in another article [37] based on 5000-6000 experimental results on material tests. The γ_m determination method does not take the uncertainty of geometry and the finite element model into account.

6.2.3. Evaluation of the literature overview

All three literature sources give determination methods for partial factor, but all of them have differences. The differences are summarized in Table 8. The first three rows of this table consists the different methods found in the literature and the last row shows the methodology used in this thesis. If the resistance model is developed based on experimental results the separation of the γ_m and γ_{Rd} is not reasonable as proposed in EN1990. But the design methods studied in the current thesis are based mainly on numerical calculations; therefore γ_m and γ_{Rd} are determined separately similar as by Rebelo et al. [36] and L. da Silva et al. [37]. There are some differences between numerical calculations and experimental results, what is taken into account by a factor (V_{FEM}) as introduced by Gabeler [35]. The third difference is that the uncertainties of the geometry are also taken into account, because in the numerical model this is not considered.

Table 8: Comparison of the different methods

Method	Based on experiments	Based on FEM V_{FEM} developed	Separation of γ_{Rd} and γ_m	Uncertainty of geometry
EN1990 Annex D	✓	-	-	✓
Gabeler	-	✓	-	✓
Rebelo et al	-	-	✓	-
used method in this thesis	-	✓	✓	✓

It seems important that all effects which are basically of importance in γ_M should be taken into account. These are the followings:

- uncertainty of resistance model,
- uncertainty of material properties,

- uncertainty of geometry,
- uncertainty of numerical model.

All of these effects are taken into account in the determination of the partial factors to the resistance models developed and introduced in the previous chapters (Chapter 3 and 5). All three resistance models are investigated and statistically evaluated. At first the value of the γ_{Rd} is calculated by the single property method to get a rough estimation about the probability distribution function of the design proposals and about the mean values and standard deviations. Partial factors are also calculated to get a comparison background to the evaluation of the resistance model method. The calculation with the single property method is a rough estimation, therefore γ_{Rd} is calculated by the multiple property method as well according to EN1990 Annex D Chapter 8 [34] supplemented by the modifications presented in Table 8, which takes all possible uncertainties into account.

The studied resistance models give the mean value of the patch loading resistances and not the characteristic value. Therefore the ratio of the mean and design values is determined what is signed by γ_{Rd}^{*} and it can be calculated in the form of Eq. (74).

$$\gamma_{Rd}^{*} = \frac{F_{R,mean}}{F_{R,d}} = \frac{b \cdot F_{R,design\_method}}{b \cdot F_{R,design\_method} \cdot e^{-k_{d,\infty} \cdot Q - 0.5 \cdot Q^2}} = \frac{1}{e^{-k_{d,\infty} \cdot Q - 0.5 \cdot Q^2}} \tag{74}$$

The mean value of the patch loading resistance calculated by the proposed design proposals doesn't coincide with the patch loading resistances of the numerical calculations or the experimental values. This misalignment is expressed by the mean value correction factor *b* and it can be taken into account in the partial factor γ_{Rd}^{**} according to Eq. (75).

$$\gamma_{Rd}^{**} = \frac{\gamma_{Rd}^{*}}{b} = \frac{1}{b \cdot e^{-k_{d,\infty} \cdot Q - 0.5 \cdot Q^2}} \tag{75}$$

After determination of γ_{Rd}^{**} the value of γ_m is also determined, to allow to calculate the γ_{M1}^{**} (Eq. 76). The partial factor of the material uncertainties (γ_m) does not depend on design methods, it is only depending on material properties, therefore it is taken here from literature.

$$\gamma_{M1}^{**} = \gamma_{Rd}^{**} \cdot \gamma_m \tag{76}$$

6.3. Determination of partial factor of model uncertainties - γ_{Rd}^{**}

6.3.1. Background databases for the statistical evaluation

Three different design proposals are developed in the previous chapters of this thesis. General closed forms are collected in Eqs. (77)-(79). The first equation gives the patch loading resistance of corrugated web girders (F_R) if the whole flange is loaded along the flange width. The second one takes the effect of the loading width into account (F_R^{red}) and the third one considers the resistance reduction effect due to load eccentricities (F_R^{red2}). The used notations are introduced in the previous chapters.

$$F_R = 2 \cdot \sqrt{n \cdot M_{plf} \cdot t_w \cdot \delta \cdot f_{yw}} + \delta \cdot t_w \cdot f_{yw} \cdot ss \cdot k_\alpha \tag{77}$$

$$F_R^{red} = F_R \cdot \{1 - m \cdot [a_4 \cdot (1-b) - ss_a]\} \tag{78}$$

$$F_R^{red2} = F_R^{red} \cdot \left(1 - m_3 \cdot \frac{e}{b_f}\right) \tag{79}$$

The separation of these design models is important, because they depend on each other, it means that the second design method refers to the first one and the third to the second one.

Due to the interference of design methods they are including all individual errors as well, which may lead to the fact, that standard deviation can increase and it results in a significantly bigger partial factor. Therefore separated partial factors are determined for F_R, F_R^{red} and F_R^{red2}, respectively.

All numerical and experimental results conducted in this topic are collected. Patch loading resistances are recalculated for each analyzed girder geometry with the relevant design method. In this way a huge database is developed which consists of 4 sub-databases:

1, sub-database for patch loading resistance; 174 numerical results,
2, sub-database for effect of loading width; 325 numerical results,
3, sub-database for effect of loading eccentricity; 250 numerical results,
4, 26 experimental results (taken from literature and from own tests).

The total database consists of 775 numerical and experimental results.

6.3.2. Statistical determination using the single property method

The statistical evaluation according to EN1990 Annex D Chapter 7 is executed for all three design methods. The property distribution function gives an assessment of the safety level of each analyzed design method, and the partial factors determined by the single property method provide a comparison background to the evaluation according to the improved and previously introduced determination method. The ratio of the numerical results and design methods are calculated for each analyzed girders (Eq. 80).

$$r_i = \frac{F_{R,num/\exp,i}}{F_{R,Design\_method,i}} \tag{80}$$

The probability distribution function of r_i, mean values, standard deviations and coefficient of variations are calculated for all sub-databases, and results are presented in Figs. 114-117. The first diagram of each figures shows the probability distribution function of r_i and the second one presents the comparison of the numerical or experimental results and the proposed design methods.

After the evaluation of each sub-database coupled databases are studied. Figure 118 shows the probability distribution function for evaluation of F_R, what is based on 174 numerical and 26 experimental data (database parts 1+4). Figure 119 presents the statistical evaluation of F_R^{red} based on 174+325=499 numerical and 26 experimental data (sub-databases 1+2+4). Evaluation of F_R^{red2} is shown in Fig. 120 based on 174+325+250=749 numerical and 26 experimental data (sub-databases 1+2+3+4).

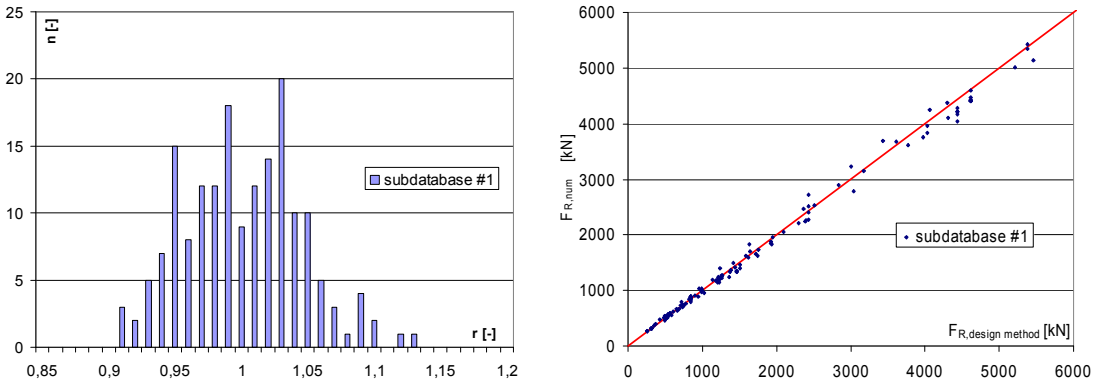

Figure 114: Statistical evaluation of sub-database #1 (174 data).

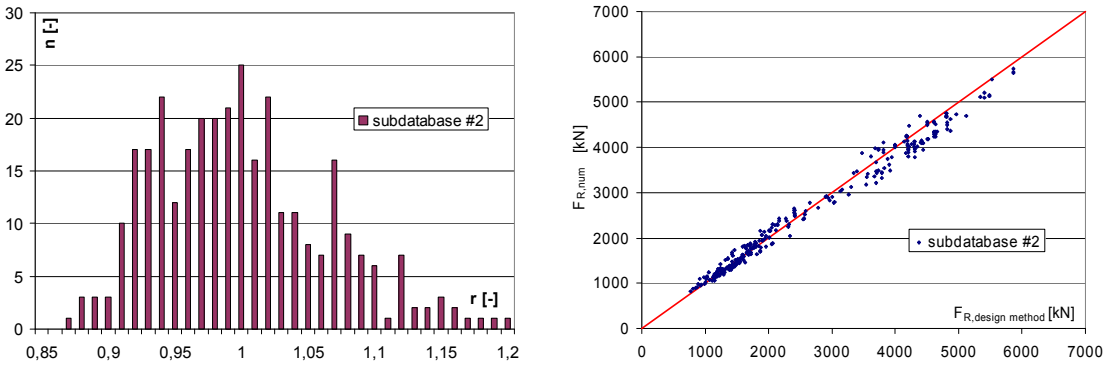

Figure 115: Statistical evaluation of sub-database #2 (325 data).

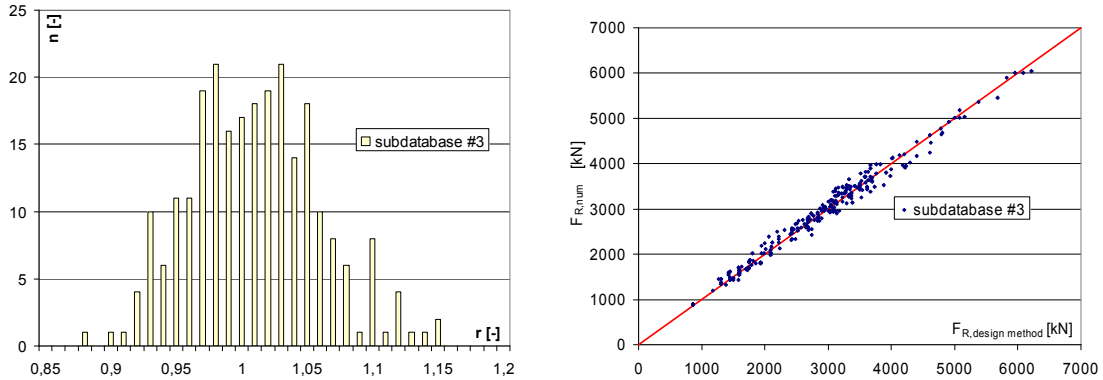

Figure 116: Statistical evaluation of sub-database #3 (250 data).

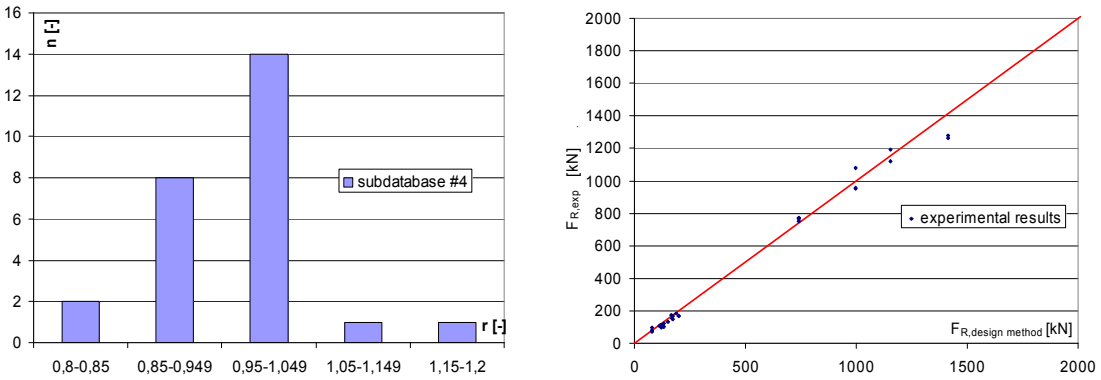

Figure 117: Statistical evaluation of sub-database #4 (26 data).

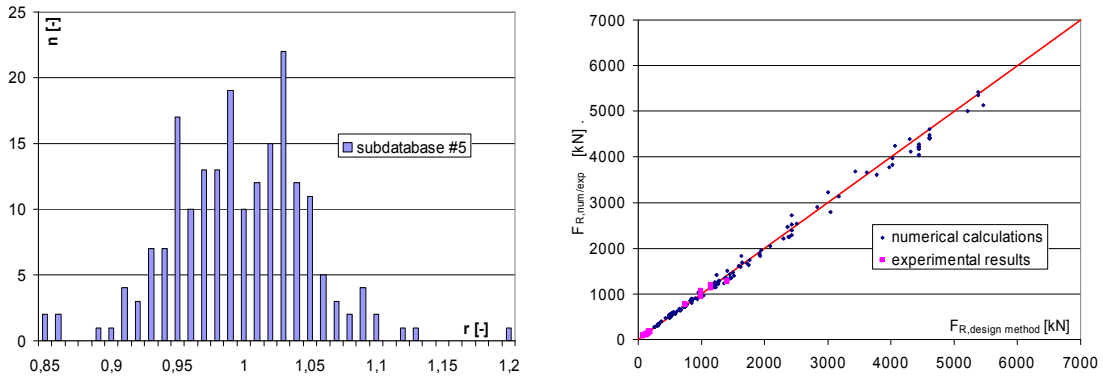

Figure 118: Statistical evaluation of F_R (based on 200 data).

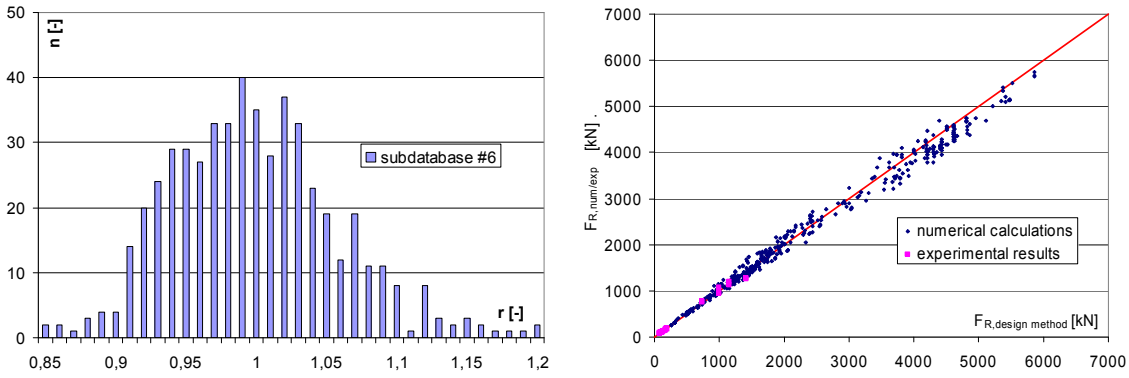

Figure 119: Statistical evaluation of F_R^{red} (based on 525 data).

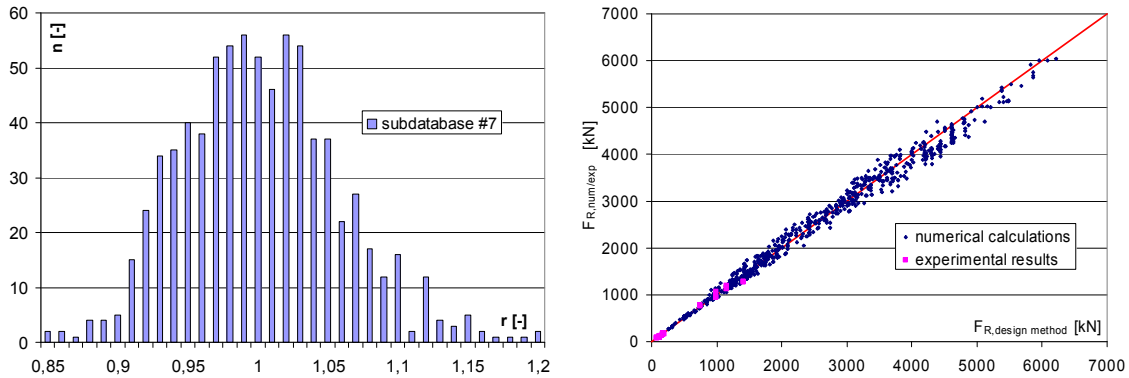

Figure 120: Statistical evaluation of F_R^{red2} (based on 775 data).

For each sub-databases the mean values, standard deviations and coefficient of variations are determined. Based on these values the partial factors (γ_{Rd}^{**}) for all three resistance models are calculated. Calculation steps are presented for the first case in Eqs. (81)-(87) and the results are summarized in Table 9.

average of the ratios: $$m_X = \frac{\sum_{i=1}^{n} r_i}{n} = \frac{\sum_{i=1}^{174} r_i}{174} = 1.00114 \quad (81)$$

standard deviation: $$s_X = \frac{1}{n-1} \cdot \sum \left(r_i - m_X\right)^2 = 0.0443 \quad (82)$$

coefficient of variation: $$V_X = \frac{s_X}{m_X} = 0.0442 \quad (83)$$

design value: $$X_d = m_X \cdot \left(1 - 3.04 \cdot V_X\right) = 0.8664 \quad (84)$$

mean value: $$X_m = m_X = 1.00114 \quad (85)$$

The design value of the resistance model can be determined according to Eq. (86). The partial factor separation methodology and the meaning of the γ_{Rd}^{*} and γ_{Rd}^{**} are here also explained. This section focuses only on the determination of the γ_{Rd}^{**}, the value of γ_m is determined in Section 6.4.

$$F_{Rd} = \frac{F_{R,mean}}{\gamma_{M1}^{*}} = \frac{F_{R,design\_method} \cdot m_x}{\gamma_{M1}^{*}} = \frac{F_{R,design\_method}}{\gamma_{M1}^{**}} = \frac{F_{R,design\_method} \cdot m_x}{\gamma_m \cdot \gamma_{Rd}^{*}} = \frac{F_{R,design\_method}}{\gamma_m \cdot \gamma_{Rd}^{**}} \quad (86)$$

The value of the γ_{Rd}^{**} can be determined by Eq. (87). The calculation results for all sub-databases are summarized in the Table 9.

$$\gamma_{Rd}^{**} = \frac{1}{X_d} = \frac{1}{m_X \cdot (1 - 3.04 \cdot V_X)} = 1.1542 \tag{87}$$

Table 9: Statistical evaluation and determination of γ_{Rd}^{**} using the single property method

	Subdatabases	m_x	s_x	V_x	$\gamma_{Rd,1}^{**}$
1	Numerical calculations for patch loading	1.00114	0.04433	0.04427	**1.1542**
2	Numerical calculations for patch loading with effect of ss_a	0.99934	0.06406	0.06410	**1.2429**
3	Numerical calculations for patch loading with effect of loading eccentricity	1.01032	0.04992	0.04941	**1.16474**
4	Experimental database	0.96054	0.09154	0.09530	**1.46578**
5	Evaluation of F_R (1+4)	0.99568	0.05461	0.05484	**1.20528**
6	Evaluation of F_R^{red} (1+2+4)	1.00024	0.05825	0.05823	**1.21481**
7	Evaluation of F_R^{red2} (1+2+3+4)	1.00191	0.05765	0.05754	**1.20969**

The smallest partial factor resulted based on the sub-database #1. It means that the developed design model has the smallest difference and standard deviation in this area, however the difference between the calculated partial factors are relative small. The largest value resulted in the case of the experimental database. It comes from the relatively small number of samples and from the material and geometrical uncertainties which are covered in the experimental results. These partial factors cannot be applied for the design these are only rough approximations but they give a comparison background for the detailed investigation in the following section. In addition the statistical evaluation and the property distribution function presented a characteristic feature of the safety level of each analyzed design method.

6.3.3. Statistical determination using the resistance model method

EN1990 [34] divides this determination method into 7 steps. It is completed in this thesis by one more step (determination of V_{FEM}) and the uncertainty of the material property is handled separately. Calculation steps for the first sub-database are presented here in details and the final results for the other cases are presented in Tables 13 to 15.

1. step: Development of resistance model

$$F_R = 2 \cdot \sqrt{n \cdot M_{plf} \cdot t_w \cdot \delta \cdot f_{yw}} + \delta \cdot t_w \cdot f_{yw} \cdot ss \cdot k_\alpha \tag{88}$$

2. step: Comparison of experimental and theoretical values (Fig. 121)

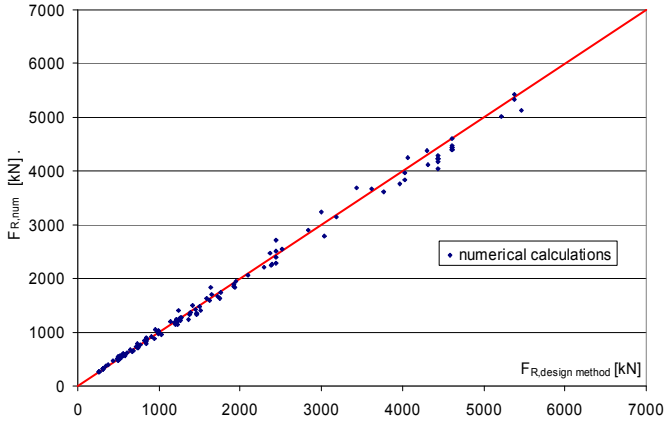

Figure 121: Comparison of numerical calculations and design method for sub-database #1.

3. Estimation of the mean value correction factor *b*

$$b = \frac{\sum F_{R,num} \cdot F_{R,design\_method}}{\sum F_{R,design\_method}^{2}} = 0.9777 \tag{89}$$

4. Estimation of the coefficient of variation of the errors

error term for each value: $$\delta_i = \frac{F_{R,num_i}}{b \cdot F_{R,design\_method_i}} \tag{90}$$

logarithm of the error terms: $$\Delta_i = \ln(\delta_i) \tag{90}$$

mean value of logarithm of the error terms: $$\overline{\Delta} = \frac{1}{n} \cdot \sum_{i=1}^{n} \Delta_i = 0.0227 \tag{92}$$

standard deviation of the error terms: $$s_\Delta{}^2 = \frac{1}{n-1} \cdot \sum_{i=1}^{n} \left(\Delta_i - \overline{\Delta}\right)^2 = 0.0195 \tag{93}$$

coefficient of variation of the error terms: $$V_\delta = \sqrt{\exp\left(s_\Delta{}^2\right) - 1} = 0.04414 \tag{94}$$

5. Analysis of compatibility

One of the most dominant effects on the patch loading resistance is represented by the loading length, therefore the compatibility analysis is executed for this parameter. All results according to the loading length are rearranged and subgroups are created for different loading lengths. The mean value, standard deviation and coefficient of variations for all subgroups are calculated and the results are listed in Table 10. The small difference in the mean values and coefficient of variations proves that the studied resistance model has the same accuracy in the whole analyzed parameter range, therefore the compatibility check is fulfilled.

Table 10: Results of the compatibility check

loading length ranges	*b*	s_Δ	V_δ
$ss/h_w<0.4$	0.9962	0.0007	0.0257
$0.4<ss/h_w<0.6$	0.9741	0.0008	0.0287
$0.6<ss/h_w<0.8$	0.9733	0.0010	0.0323
$0.8<ss/h_w<1.0$	0.9655	0.0005	0.0223

6. Determination of the coefficient of variation of the basic variable of resistance model

According to EN1990 the material and geometrical uncertainty should be taken here into account. The material property is handled separately, but the geometric uncertainty is considered. The mean value and coefficient of variation of the geometrical parameters are needed to determine this parameter. Two different proposals are found in the literature to solve it.

The first proposal is found in the diploma thesis of Gabeler [35].

Mean value: $t_{mean}=t_{nom}$, $b_{mean}=b_{nom}$,

Coefficient of variation: $V_{geom1}=0.005$ for plate width,

$V_{geom2}=0.05$ for plate thickness.

Second available proposal is the approximation of the "Joint Committee of Structural Safety" JCSS [38], which is relevant for hot rolled steel sections.

Mean value: $-1.0\text{mm} \le X_m \le +1.0\text{mm}$

Standard deviation: $s_X \le 1.0\text{mm}$

In the case of a usually used plate in bridges 400 mm x 40 mm the coefficients of variations are:

$$V_{geom1} = \frac{s_x}{t_{mean}} = \frac{1}{400} = 0.0025 \tag{95}$$

$$V_{geom2} = \frac{s_x}{t_{mean}} = \frac{1}{40} = 0.025 \tag{96}$$

The uncertainties of the plate width and thickness can be calculated according to the own experiments as well. The geometry of all specimens is measured in different locations and the measured values are statistically evaluated, the results are summarized in Table 11.

Table 11: Statistical evaluation of plate sizes

	plate thickness		plate width	
t_{nom} [mm]	20	30	225	500
n [-]	104	38	45	13
t_{mean} [mm]	20.44	30.01	225.00	499.33
s_x	0.1651	0.1115	0.5317	0.6513
V_{geom}	0.0081	0.0037	0.0024	0.0013
$\boldsymbol{V_{geom,mean}}$	**0.0059**		**0.0018**	

Three different values for the geometrical uncertainty are calculated according to 3 different sources. Calculations are executed with all different V_{geom} values. The uncertainty of the corrugation angle should also be taken into account, but there are no available information about it. Due to the fact that its effect in the resistance model is small comparing to the loading length and plate thicknesses, it can be neglected.

7. Coefficient of variation of the FE model

The value of V_{FEM} is calculated based on the experiments of Elgaaly and Seshadri [9] and based on the 12 own test results which are recalculated by numerical models. The calculation steps are the same as in the steps 3 and 4. Calculation for one specimen is detailed in Eqs. (97)-(102), and the result for all studied specimens can be found in Table 12.

$$b_{FEM} = \frac{\sum F_{R,\exp} F_{R,num}}{\sum F_{R,num}^{\ 2}} = 1.01924 \tag{97}$$

$$\delta_{FEM,i} = \frac{F_{R,\exp}}{b_{FEM} \cdot F_{R,num}} \tag{98}$$

$$\Delta_{FEM,i} = \ln\left(\delta_{FEM,i}\right) \tag{99}$$

$$\overline{\Delta}_{FEM} = \frac{1}{n} \cdot \sum_{i=1}^{n} \Delta_{FEM,i} = 0.0054 \tag{100}$$

$$s_{\Delta,FEM}^{\ 2} = \frac{1}{n-1} \cdot \sum_{i=1}^{n} \left(\Delta_{FEM,i} - \overline{\Delta}_{FEM}\right)^2 = 0.00046 \tag{101}$$

$$V_{FEM} = \sqrt{\exp\left(s_{\Delta,FEM}^{\ 2}\right) - 1} = 0.0214 \tag{102}$$

Table 12: Calculation of V_{FEM}

Determination of V_{FEM}								
		$F_{R,exp}$ [kN]	$F_{R,num}$ [kN]	$F_{R,exp}$*$F_{R,num}$	$F_{R,num}^2$	$\delta_{num,i}$	$\Delta_{num,i}$	$(\Delta_{num,i}-\Delta_{num})^2$
Experiments of Elgaaly and Seshadri .	1	131.3	126.943	16664	16115	1.015	0.0145	0.00008
	2	82.3	79.737	6564	6358	1.013	0.0129	0.00006
	3	102.4	99.79	10214	9958	1.006	0.0063	0.00000
	4	95.7	87.354	8358	7631	1.075	0.0719	0.00443
Own experiments	1	754.2	748.95	564858	560926	0.988	-0.012	0.00030
	2	956.5	915.37	875533	837902	1.025	0.0249	0.00038
	3	764.8	762.89	583420	582001	0.984	-0.017	0.00048
	4	949.0	942.85	894784	888966	0.988	-0.013	0.00032
	5	1192.0	1168.50	1392864	1365392	1.001	0.0009	0.00002
	6	1119.3	1082.40	1211563	1171590	1.015	0.0145	0.00008
	7	1077.7	1061.20	1143676	1126145	0.996	-0.004	0.00008
	8	1263.9	1248.70	1578282	1559252	0.993	-0.007	0.00015
	9	1220.5	1196.50	1460304	1431612	1.001	0.0008	0.00002
	10	1090.0	1074.83	1171565	1155260	0.995	-0.005	0.00011
	11	1281.0	1245.29	1595204	1550747	1.009	0.0092	0.00001
	12	772.4	767.94	593149	589732	0.987	-0.013	0.00035
			összeg:	13107002	12859587	Δ_{FEM}=	0.0054	0.00046
			b_{FEM}=	**1.019**			V_{FEM}	**0.021**

8. Determination of the partial factor

Coefficient of variation of the whole resistance model can be calculated by Eqs. (103)-(105).

$$V_r^2 = \left(V_\delta^2 + 1\right) \cdot \left[\prod_{j=1}^{n} \left(V_{Xi}^2 + 1\right)\right] \cdot \left(V_{FEM}^2 + 1\right) - 1 \tag{103}$$

$$V_r^2 = \left(V_\delta^2 + 1\right) \cdot \left(V_{geom1}^2 + 1\right) \cdot \left(V_{geom2}^2 + 1\right) \cdot \left(V_{FEM}^2 + 1\right) - 1 \tag{104}$$

$$V_r^2 = \left(0.04414^2 + 1\right) \cdot \left(0.025^2 + 1\right) \cdot \left(0.0025^2 + 1\right) \cdot \left(0.0214^2 + 1\right) - 1 = 0.00304 \tag{105}$$

Based on V_r an auxiliary variable can be calculated by Eq. (106) and the partial factor is obtained by Eq. (107).

$$Q = \sqrt{\ln\left(V_r^2 + 1\right)} = \sqrt{\ln\left(0.00304 + 1\right)} = 0.05514 \tag{106}$$

$$\gamma_{Rd}^{**} = \frac{1}{b \cdot e^{-3.04 \cdot Q - 0.5 \cdot Q}} = 1.2112 \tag{107}$$

Partial factors (γ_{Rd}^{**}) for all database parts are calculated and all the calculations are executed with three different V_{geom} values according to Gabeler [35], according to the recommendation of the JCSS [38] and according to own measurements and the results are summarized in Tables 13-15.

Table 13: Determination of γ_{Rd}^{**} based on V_{geom} according to the recommendation of the JCSS (2000) [38]

	Subdatabases	b	V_δ	V_r	$\gamma_{Rd,2}^{**}$
1	Numerical calculations for patch loading	0.9777	0.04414	0.05514	**1.211**
2	Numerical calculations for patch loading with effect of ss_a	0.9722	0.06319	0.07132	**1.280**
3	Numerical calculations for patch loading with effect of loading eccentricity	1.0022	0.04903	0.05913	**1.196**
4	Experimental database	0.9680	0.0982	0.0982	**1.383**
5	Evaluation of F_R (1+4)	0.9775	0.0556	0.0646	**1.248**
6	Evaluation of F_R^{red} (1+2+4)	0.9733	0.0604	0.0689	**1.269**
7	Evaluation of F_R^{red2} (1+2+3+4)	0.9851	0.0569	0.0672	**1.242**

Table 14: Determination of γ_{Rd}^{**} based on V_{geom} according to Gabeler [35]

	Subdatabases	b	V_δ	V_r	$\gamma_{Rd,3}^{**}$
1	Numerical calculations for patch loading	0.9777	0.04414	0.07028	**1.269**
2	Numerical calculations for patch loading with effect of ss_a	0.9722	0.06319	0.08360	**1.330**
3	Numerical calculations for patch loading with effect of loading eccentricity	1.0022	0.04903	0.07345	**1.250**
4	Experimental database	0.9680	0.0982	0.0982	**1.383**
5	Evaluation of F_R (1+4)	0.9775	0.0556	0.07797	**1.300**
6	Evaluation of F_R^{red} (1+2+4)	0.9733	0.0604	0.08152	**1.320**
7	Evaluation of F_R^{red2} (1+2+3+4)	0.9851	0.0569	0.07890	**1.294**

Table 15: Determination of γ_{Rd}^{**} based on V_{geom} calculated by own tests

	Subdatabases	b	V_δ	V_r	$\gamma_{Rd,4}^{**}$
1	Numerical calculations for patch loading	0.9777	0.04414	0.04945	**1.190**
2	Numerical calculations for patch loading with effect of ss_a	0.9722	0.06319	0.06702	**1.264**
3	Numerical calculations for patch loading with effect of loading eccentricity	1.0022	0.04903	0.05386	**1.177**
4	Experimental database	0.9680	0.0982	0.0982	**1.383**
5	Evaluation of F_R (1+4)	0.9775	0.0556	0.05987	**1.229**
6	Evaluation of F_R^{red} (1+2+4)	0.9733	0.0604	0.06441	**1.252**
7	Evaluation of F_R^{red2} (1+2+3+4)	0.9851	0.0569	0.06110	**1.224**

6.3.4. Comparison and evaluation of the results

The comparison of the results are summarized in Table 16. Columns 3 to 6 consists of the results calculated in Sections 6.3.2. and 6.3.3. In the last three rows ratios of the partial factors are calculated and presented to compare the different methods.

Table 16: Calculated γ_{Rd}^{**} values according to different approximations

Subdatabases		Single property method [34]	Resistance model method			Comparison		
			V_{geom} according to JCSS [37]	V_{geom} acc. to Gabeler [35]	V_{geom} acc. to own measurements	$\gamma_{Rd,3}^{**}/\gamma_{Rd,4}^{**}$	$\gamma_{Rd,1}^{**}/\gamma_{Rd,4}^{**}$	$\gamma_{Rd,1}^{**}/\gamma_{Rd,2}^{**}$
		$\gamma_{Rd,1}^{**}$	$\gamma_{Rd,2}^{**}$	$\gamma_{Rd,3}^{**}$	$\gamma_{Rd,4}^{**}$			
1	Numerical calculations for patch loading	1.154	1.211	1.269	1.190	1.066	0.970	0.953
2	Numerical calculations for patch loading with effect of ss_a	1.243	1.280	1.330	1.264	1.052	0.983	0.971
3	Numerical calculations for patch loading with effect of loading eccentricity	1.165	1.196	1.250	1.177	1.062	0.990	0.974
4	Experimental database	1.466	1.383	1.383	1.383	1.00	1.060	1.060
5	Evaluation of F_R (1+4)	1.205	1.248	1.300	1.229	1.058	0.981	0.966
6	Evaluation of F_R^{red} (1+2+4)	1.215	1.269	1.320	1.252	1.054	0.971	0.957
7	Evaluation of F_R^{red2} (1+2+3+4)	1.210	1.242	1.294	1.224	1.057	0.989	0.974

Based on the comparison of the results the following conclusions can be drawn:

1. The single property method leads in all cases to the smallest partial factor ($\gamma_{Rd,1}^{**}$) except of the pure experimental results (4), but due to the small number of experiments reliable conclusion cannot be drawn for that.

2. From the resistance model method based on different coefficients of variations, the lowest partial factor resulted in $\gamma_{Rd,4}^{**}$ which is calculated by V_{geom} according to own measurement. The proposal of Gabeler resulted in the largest value ($\gamma_{Rd,3}^{**}$). The ratio of these two calculation methods are listed in the column 7 of Table 16. Differences are between 5 to 7%.

3. Calculation with V_{geom} according to the recommendation of the JCSS leads to a medium value in between the previous two calculations. By this method the question arises for which plate size the values V_{geom1} and V_{geom2} should be calculated. In the current calculations an average plate size of bridges is used.

4. Column 8 in Table 16 consists of the comparison of $\gamma_{Rd,1}^{**}$ and $\gamma_{Rd,4}^{**}$. Maximal difference is 3%. Column 9 shows the comparison of $\gamma_{Rd,1}^{**}$ and $\gamma_{Rd,2}^{**}$, with a maximal difference of 5%. The results prove that the single property and resistance model methods are not far from each other, if calculations are based on a good calibrated numerical model (V_{FEM} is small) and the uncertainties of the geometric parameters (V_{geom}) are also small.

5. The single property method gives an assessment of the statistical properties of the design methods and it leads to a good approximation of the partial factors. The resistance model method takes more uncertainties into account therefore it is a more complex and accurate method.

6.4. Determination of partial factor of the material properties - γ_m

To determinate γ_{M1}^{**} the partial factor of the material properties (γ_m) is calculated. The value of γ_m depends on the material uncertainties and it does not depend on the resistance model, therefore this value is taken from the literature according to Eq. (108) from [37].

$$\gamma_m = \frac{f_{y,nom}}{f_{yd}} = \frac{f_{y,nom}}{f_{y,m} \cdot \left(1 - 1.64 \cdot V_{fy}\right)} \quad , \tag{108}$$

where: $f_{y,nom}$: nominal value of the yield strength,
$f_{y,m}$: mean value of the yield strength,
V_{fy}: coefficient of variation of the yield strength.

In the literature 3 different proposals can be found for the determination of the $f_{y,m}$ and V_{fy} as follows:

- diploma thesis of Gabeler [35],
- recommendation of the JCSS [38],
- research work of L. da Silva et al. [37].

I determined the γ_m according to each proposal and the results are compared.

Determination of γ_m according to Gabeler [35]:

$$f_{y,m} = 1.14 \cdot f_{y,nom} \ , \tag{109}$$

$$V_{fy} = 0.07 \ . \tag{110}$$

$$\gamma_m = \frac{f_{y,nom}}{f_{yd}} = \frac{f_{y,nom}}{f_{y,m} \cdot \left(1 - 1.64 \cdot V_{fy}\right)} = \frac{f_{y,nom}}{1.14 \cdot f_{y,nom} \cdot \left(1 - 1.64 \cdot V_{fy}\right)} = 0.9909 \tag{111}$$

Determination of γ_m according to JCSS [38]:

$$f_{y,m} = \alpha \cdot f_{y,nom} \cdot e^{(-u \cdot v)} - 20 \tag{112}$$

$$V_{fy} = 0.07 \tag{113}$$

where: α=1.05 for webs of hot rolled sections,
α=1.00 otherwise (this value is used in the followings),
-1,5<u<-2 optional value (u=-2 is used in the followings).

According to this proposal γ_m depends on the nominal yield strength ($f_{y,nom}$); the calculation results are summarized in Table 17.

Table 17: Determination of γ_m according to the recommendation of the JCSS [38]

Steel grade ($f_{y,nom}$)	$f_{y,m}$ [MPa]	γ_m
S235	250.32	1.061
S275	296.33	1.048
S355	388.35	1.033
S460	509.14	1.021
S690	773.71	1.008

Determination of γ_m according to L. da Silva et al. [37]:

Results of material tests of different steel grades were collected by the authors from all over the word. More than 6000 experimental data are statistically evaluated and γ_m are calculated for different steel grades. The results are summarized in Table 18, which are valid for plate thicknesses smaller than 40 mm.

Table 18: Determination of γ_m according to L. da Silva et al. [37]

Steel grade ($f_{y,nom}$)	n [-]	$f_{y,m}$ [MPa]	V_{fy}	γ_m
S235	795	284.74	0.064	0.922
S275	4333	316.23	0.055	0.956
S355	1879	405.01	0.044	0.945
S460	666	474.63	0.040	1.037
S690	36	793.19	0.050	0.948

Evaluation of the results show that differences between γ_m values calculated by different proposals is quite small. According to the approximation of Gabeler [35] γ_m does not depend on the yield strength. According to proposal of JCSS [38] increasing f_y results in a decrease of γ_m. Statistical evaluation of the huge number of experiments did not confirm this assumption and the trend of γ_m with the yield strength is not clear according to the experiments. The proposal of the JCSS [38] lead almost in all cases to the largest partial factor, therefore staying on the safe side these values of γ_m are used in the followings.

6.5. Determination of the partial factor - γ_{M1}^{**}

The partial factor (γ_{M1}^{**}) can be calculated as the product of γ_m and γ_{Rd}^{**} according to Eq. (114).

$$\gamma_{M1}^{**} = \gamma_m \cdot \gamma_{Rd}^{**} \tag{114}$$

The results are summarized in Table 19, where the value of the γ_m depends on the steel grade of the applied material. The tendency of the results is unchanged by the multiplication of γ_m, therefore conclusions introduced in Section 6.3.4. are also here valid. Results of the resistance model method using the recommendations of the JCSS [38] are proposed for application, because this method is the most accurate and the recommendations of the JCSS are based on the largest research background. Results showed that the differences between the different subdatabases are small, especially in case of the subdatabases #5, #6 and #7. Therefore a uniform partial factor is recommended for all the three design methods, which is equally assumed by 1.27 γ_m. As the standardized partial factor γ_{M1}=1.1 for bridges is defined in EN1993-2 [39], therefore the calculated values are integrated in the resistance model. The modified resistance models are summarized in Eqs. (115) to (118).

$$F_{Rd,new} = \frac{F_R}{\gamma_{M1}^{**}} = \frac{2 \cdot \sqrt{n \cdot M_{plf} \cdot t_w \cdot \delta \cdot f_{yw}} + \delta \cdot t_w \cdot f_{yw} \cdot ss \cdot k_\alpha}{\gamma_K \cdot \gamma_{M1}}\ , \tag{115}$$

$$F_{Rd,new}^{red} = \frac{F_R^{red}}{\gamma_{M1}^{**}} = \frac{F_R \cdot \{1 - m \cdot [a_4 \cdot (1-b) - ss_a]\}}{\gamma_K \cdot \gamma_{M1}}, \tag{116}$$

$$F_{Rd,new}^{red2} = \frac{F_R^{red2}}{\gamma_{M1}^{**}} = \frac{F_R^{red} \cdot \left(1 - m_3 \cdot \frac{e}{b_f}\right)}{\gamma_K \cdot \gamma_{M1}}\ , \tag{117}$$

where γ_{M1}=1.1

$$\gamma_K = \frac{1.27 \cdot \gamma_m}{\gamma_{M1}} = 1.155 \cdot \gamma_m\ . \tag{118}$$

The values of the γ_K are calculated for the different steel grades in the Table 19.

Table 19: Determination of γ_K to different steel grades

Steel grade ($f_{y,nom}$)	γ_m	γ_K
S235	1.061	1.225
S275	1.048	1.210
S355	1.033	1.193
S460	1.021	1.179
S690	1.008	1.164

6.6. Summary

Design methods introduced in the previous chapters determine the mean value of the patch loading resistances. To be able to determine the design resistances the developed design proposals are statistically evaluated and partial factors are derived. The determination method of the partial factor according to EN1990 [34] is developed for evaluation of resistance models based on experimental results. If the investigated resistance model is developed based on numerical calculations the specialities in the uncertainties have to be taken into account. This Chapter introduces modification possibilities in the partial factor determination method which are found in the literature. All effects which are basically built in γ_M are considered in the determination of the partial factors to the investigated resistance models, which are the uncertainties of the resistance model, material properties, geometry, and the numerical model.

If the resistance model is developed based on numerical calculations the separation of the γ_m and γ_{Rd} is used, because the numerical model does not consider the material and geometrical uncertainties. There are also some differences between numerical calculations and the experimental results, what is taken by a factor (V_{FEM}) into account. The third difference is that the uncertainty of the geometry is also considered, since the numerical model does not consider it.

At first all three resistance models are statistically investigated using the single property method in order to get an estimation about the probability distribution function of the design proposals and about the mean values and standard deviations. These partial factors lead also to a comparison background to the evaluation by the resistance model method. The partial factors are calculated also by the multiple property method according to EN1990 Annex D Chapter 8 supplemented by the modifications introduced above.

The results show that the single property method gives a characterization about the statistical properties of the design methods and leads to a good approximation. The resistance model method takes more uncertainties into account therefore it is a more complex and accurate method. The results prove that the single property and resistance model methods are not far from each other, if the resistance model is developed based on a calibrated numerical model (V_{FEM} is small) and the uncertainties of the geometric parameters (V_{geom}) are also small.

Finally partial factors for all the tree proposed resistance models are derived and recommended to used it in the design.

7. Interaction between shear and transverse force

7.1. General

In the practice during launching of a bridge structure large shear and transverse force can be introduced at the same cross section as shown in Fig. 5. In this case the corrugated web is loaded by large shear and transverse forces, so that the interaction should be considered in the design. In case of bridge structures, which have mostly high webs, the main part of the shear resistance comes from the contribution of the web. Bridges which are erected by incremental launching have mostly thick webs and long loading lengths at the launching device, therefore the main part of the patch loading resistance comes also from the web contribution. In case of corrugated web girders it is especially true because due to the corrugation profile the web contribution in the patch loading and in the shear resistance is increased. Due to the enlarged role of the web in both resistances the interaction of shear and patch loading of corrugated web girders should be investigated.

The interaction behaviour of steel girders subjected to combined shear and patch loading was studied only scarcely by researchers in the past. No considerations of the interaction is made in standards neither for flat web nor for corrugated web girders. Therefore the aim of the current research is to study the interaction behaviour of corrugated web girders under combined shear and patch loading. A comprehensive parametric study is conducted in this topic, the structural behaviour of the analyzed girders are investigated and the transition between the shear and patch loading failure modes are studied. Effect of each parameters on the interaction behaviour are analyzed and tendencies are determined. Results are compared to the previously developed interaction curves and a new design interaction equation is proposed.

7.2. Review of previous investigations

7.2.1. General

Because only one paper is available for corrugated web girders [9] the literature overview is done in the field of flat web girders. All studies on the interaction between shear and patch loading have in common that the combined load is subdivided into two basic load cases ("pure patch loading" and "pure shear force"). Figure 122 shows the separation methodology. Basis of the separation is that the shear stresses due to "pure patch load" are already included in the patch loading resistance model and a reduction of the load carrying capacity is caused only by the additional shear stresses coming from "pure shear force".

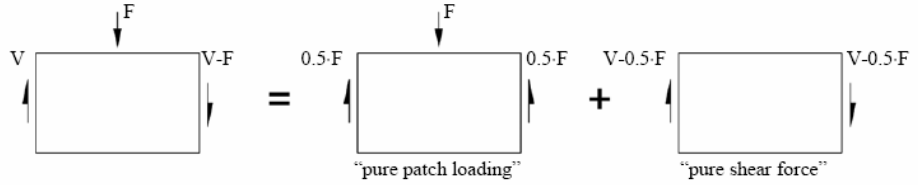

Figure 122: Subdivision of the combined load into two basic load cases [7].

7.2.2. Previous investigations on flat web girders

A compact literature overview can be found in [7] about the shear and patch loading interaction of flat web girders made by Kuhlmann and Braun. A short summary about all the available previously developed interaction curves are listed and compared in this section. The first available experimental investigation in this topic is made by Elgaaly in the 1970s [40]. Zoetemeier conducted special experiments on hot-rolled I-girders in 1980 [41]. Experimental research activity is continued by Oxfort and Weber on 3 welded test specimens in 1981 [42]. In 2000 Roberts and Shahabian made experiments on 24 welded I-girders and developed an

interaction equation which is published in [43], [44] and [45]. Kuhlmann and Braun made an extensive research in this topic in 2006 [7]. Based on a large number of numerical calculations a new interaction curve is developed, which can be used in an extended parameter range. This interaction equation is based on a larger analyzed parameter range while the previous interaction equations were based only on experimental results or only on a limited number of numerical calculations. The interaction curve developed by Kuhlmann and Braun is stricter than the previous ones and covers a wider application field. All the previously developed interaction equations are summarized in the followings.

Elgaaly (1970s): Based on 18 experiments.

$$\left(\frac{V-0.5\cdot F}{V_R}\right)^{1.8}+\left(\frac{F}{F_R}\right)^{1.8}\le 1.0\ . \tag{119}$$

Zoetemeier (1980): Investigated only hot-rolled I-profiles by testing.

$$\left(\frac{V-0.5\cdot F}{V_R}\right)^{2.0}+\left(\frac{F}{F_R}\right)^{2.0}\le 1.0\ . \tag{120}$$

Oxfort and Weber (1981): Based on 3 experiments.

$$\left(\frac{V-0.5\cdot F}{V_R}\right)\le 0.8 \tag{121}$$

Roberts and Shahabian (2000): Based on 24 experiments.

$$\left(\frac{V-0.5\cdot F}{V_R}\right)^{2.0}+\left(\frac{F}{F_R}\right)\le 1.0 \tag{122}$$

Kuhlmann and Braun (2006): 2 experiments, huge number of numerical calculations.

$$\left(\frac{V-0.5\cdot F}{V_R}\right)^{1.6}+\left(\frac{F}{F_R}\right)\le 1.0 \tag{123}$$

Where: V: shear force acting on the loaded panel,
F: transverse force acting on the loaded panel,
V_R: shear buckling resistance of the loaded web panel,
F_R: patch loading resistance of the loaded web panel.

Available test results are collected and presented in Fig. 123. All the previously developed interaction curves are also presented in this diagram.

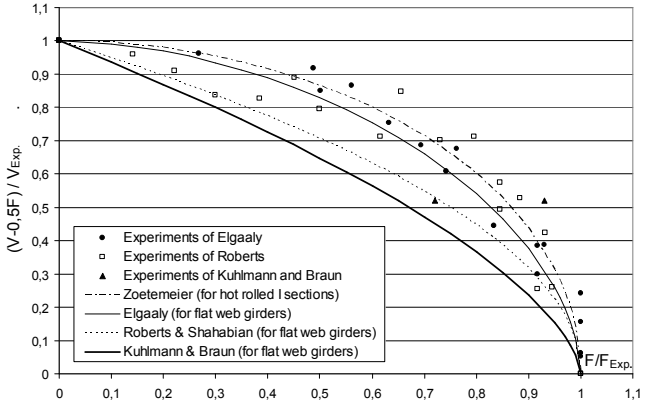

Figure 123: Experimental results on flat web girders and suggested interaction curves.

It can be seen that the interaction proposal of Zoetemeier developed for hot-rolled I-girders gives the lightest limit. Experiments made on welded structures gives a much stricter

interaction criterion. The strongest one is suggested by Kuhlmann and Braun, this interaction criterion is based on the largest numerical and experimental database.

Three conclusions can be drawn from the previous investigations:

1. The scatter (standard deviation) of the experimental results are large.
2. The larger parameter range was investigated the stronger interaction curve was needed according to the experimental and numerical calculations.
3. One of the most effective parameter is the loading length.

7.2.3. Previous investigations on corrugated web girders

Elgaaly and Seshadri [9] investigated the shear and patch loading interaction of corrugated web girders in 1997. The main aim of their research was the determination of the patch loading resistance of corrugated web girders. They conducted experiments on 5 test specimens and the pure patch loading resistance was determined. Based on the experiments a numerical model was built. The pure patch loading resistance and the interaction between bending, shear and patch loading was studied in the frame of a numerical research program. The studied parameter range was strongly limited and only 20 calculations are conducted to analyze the shear and patch load interaction. Based on the numerical calculations the following suggestion (Eq. 124) was derived for corrugated web girders:

$$\left(\frac{V-0.5\cdot F}{V_R}\right)^{1.25}+\left(\frac{F}{F_R}\right)^{1.25}\le 1.0 \tag{124}$$

Results of the numerical calculations and the recommended interaction curve of Elgaaly and Seshadri [9] can be seen in Fig. 124.

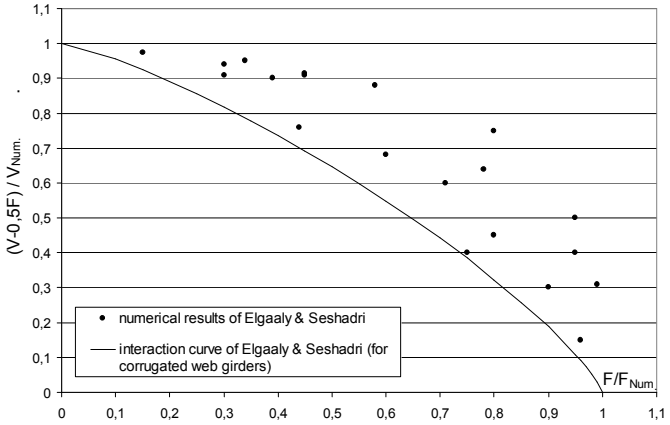

Figure 124: Numerical results on corrugated web girders and suggested interaction curve.

7.2.4. Evaluation of the previous investigations

Only a limited number of investigations are available in the literature which are dealing with shear and patch loading interaction even for flat web girders and only one for corrugated web girders. There are no experimental results available in this topic for corrugated web girders, and only results of 20 numerical calculations can be found in the literature. There are no standard recommendations in EN1993-1-5 [4].

The aim of the current investigation is to extend the previously analyzed parameter range, to study the interaction behaviour of corrugated web girders and finally to develop an interaction proposal. More corrugation profiles, longer loading lengths and a larger range of web and fold ratios are investigated. The effect of all analyzed parameters are studied and tendencies are determined. Based on the numerical results an interaction curve is developed which is based on the extended parameter range and permits an economical design.

7.3. Numerical investigations

7.3.1. General

Panels loaded by combined patch load and shear force can be classified into four classes according to [7]. The schematic overview of the subdivision is illustrated in Fig. 125. The basis of the classification is the different V_1/V_2 ratio.

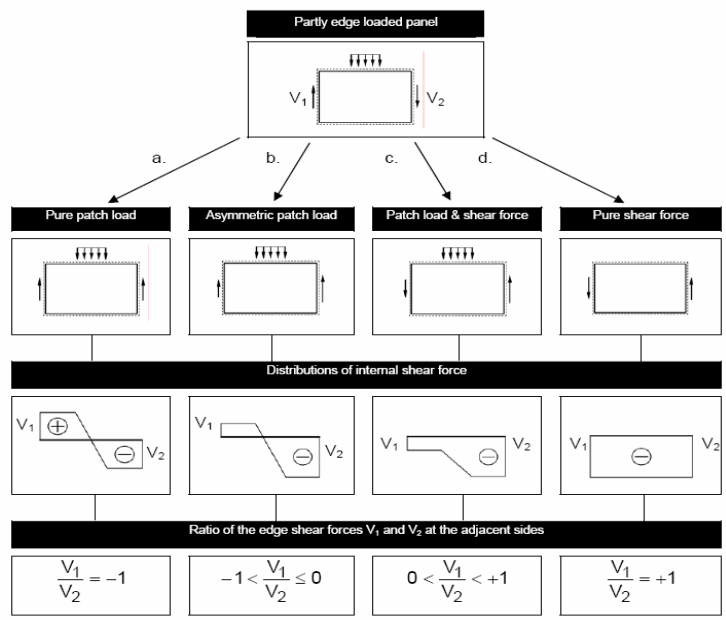

Figure 125: Subdivision of panels loaded with combined shear and patch load [7].

Case “a” shows the pure patch loading situation if the girder is loaded along a small part of the flange. In this case V_1 and V_2 forces are equal, and the V_1/ V_2 ratio is equal to -1.

Case “b” corresponds to the patch loading situation with an interacting shear force. The dominant effect is the patch load and the shear force makes the V_1 and V_2 reaction force distribution asymmetrical. The ratio of V_1/V_2 varies between 0 and -1.

Case ”c” represents the loading situation if the shear force is dominant and an interacting patch loading is also applied on the structure. In this case the shear force diagram does not change sign and the ratio of the V_1 and V_2 changes between 0 and 1.

Case “d” shows the situation of pure shear without patch loading. The ratio of the V_1/V_2 forces is equal to 1.

This classification does not mean four independent classes of the structural behaviour of the loaded panel. In the first class (pure patch loading) the failure mode is web crippling. In class "d" (pure shear force) the failure mode is shear buckling of the web. In the interaction zone there is a uniform transition between these two failure modes.

7.3.2. Numerical model development and verification

Numerical calculations are executed on the same finite element model which is introduced in Chapter 4. The applied finite element, the used material model and support conditions are the same as detailed previously. The used finite element mesh has the same density as in the case of the previous models which are verified based on experimental background introduced in Chapter 3.

The subdivision of the problem shown in Fig. 125 suggests, that it is sufficient if only half of the girder (only one web panel) is modelled (Fig. 126) using symmetry conditions.

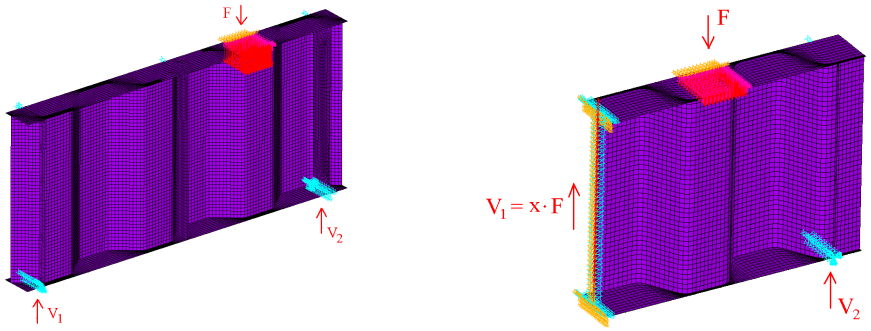

Figure 126: Applied numerical models.

By this simplification the calculation time is significantly reduced. The second advantage is that both applied forces (V_1 shear force and F transverse force) are input data of the model. V_1 and F are the applied forces on the girder and V_2 might be calculated as a vectorial sum of these two forces, therefore the V_1/V_2 ratio can be controlled easily during the calculation steps. Defining $V_1 = x \cdot F$ the numerical parametric study can be automatized. By changing the value of x the whole interaction domain ($-1 < V_1/V_2 < 1$) can be analyzed uniformly step by step. Based on the classification in Fig. 125 it can be stated that in case of bridge launching the asymmetric patch loading (case "b") has the most frequent occurrence, therefore this parameter range is analyzed with special regard.

Due to the model simplification and due to defining a symmetry plane at the midspan a new model verification is needed. In case of pure shear force the analyzed loading situation is symmetrical therefore the definition of the symmetry plane is correct. If patch load is also applied the loading situation is asymmetrical and the equivalence of the calculation results made on the total and on the half girder has to be proved. Model verification is executed through the comparison of the load bearing capacities calculated on the full and on the half girder under several loading situations. Comparison is made for several girder geometries on three levels: ultimate loads, load-deflection diagrams and failure modes are compared. Calculated ultimate loads are presented in Table 20 for one example. The results show that only minor differences are observed between the two calculations (0,34%). It proves that the symmetry plane can be applied in the case of the unsymmetric loading situation as well, because it has no influence on the structural behaviour and on the ultimate loads in case of combined shear and patch loading.

Table 20: Comparison of the ultimate loads.

	$F_{R,num}$ [kN]	difference
Full girder modeled	2451,35	0,34%
Half girder modeled	2459,77	

Failure modes are compared and presented in Fig. 127.

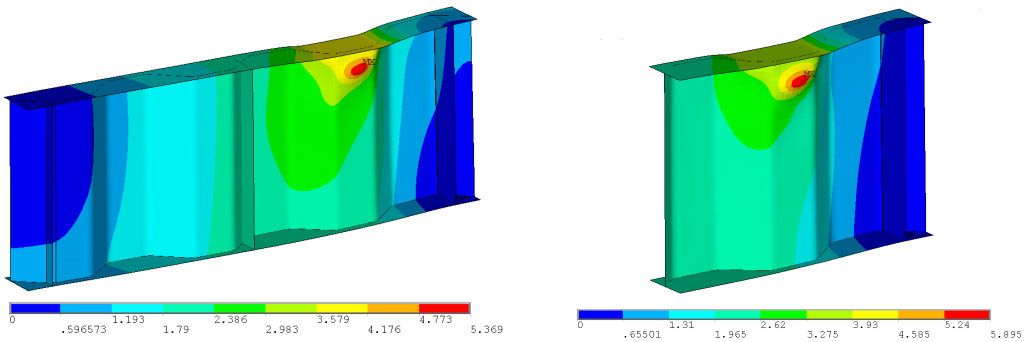

Figure 127: Comparison of the ultimate shapes.

It can be seen that the ultimate shapes and failure modes are the same, and the symmetry plane does not change the failure mode in the cases of the analyzed models. The results prove that both models show the same structural behaviour and failure load. It means that this modelling simplification can be used to analyze the interaction of shear and transverse force of corrugated web girders.

7.3.3. Structural behaviour

To obtain the structural behaviour of the shear and patch loading interaction, different failure modes under pure patch loading, pure shear force and combined loading are analyzed and compared to each other. The comparison is presented in Fig. 128. In the case of pure patch loading the failure mode is local web crippling (case V_1/V_2=-1), in the case of pure shear force the failure mode is shear buckling of the web (case V_1/V_2=1). In the interaction zone a uniform transition between the two failure modes can be observed, and no strict limit can be drawn between the two failure modes.

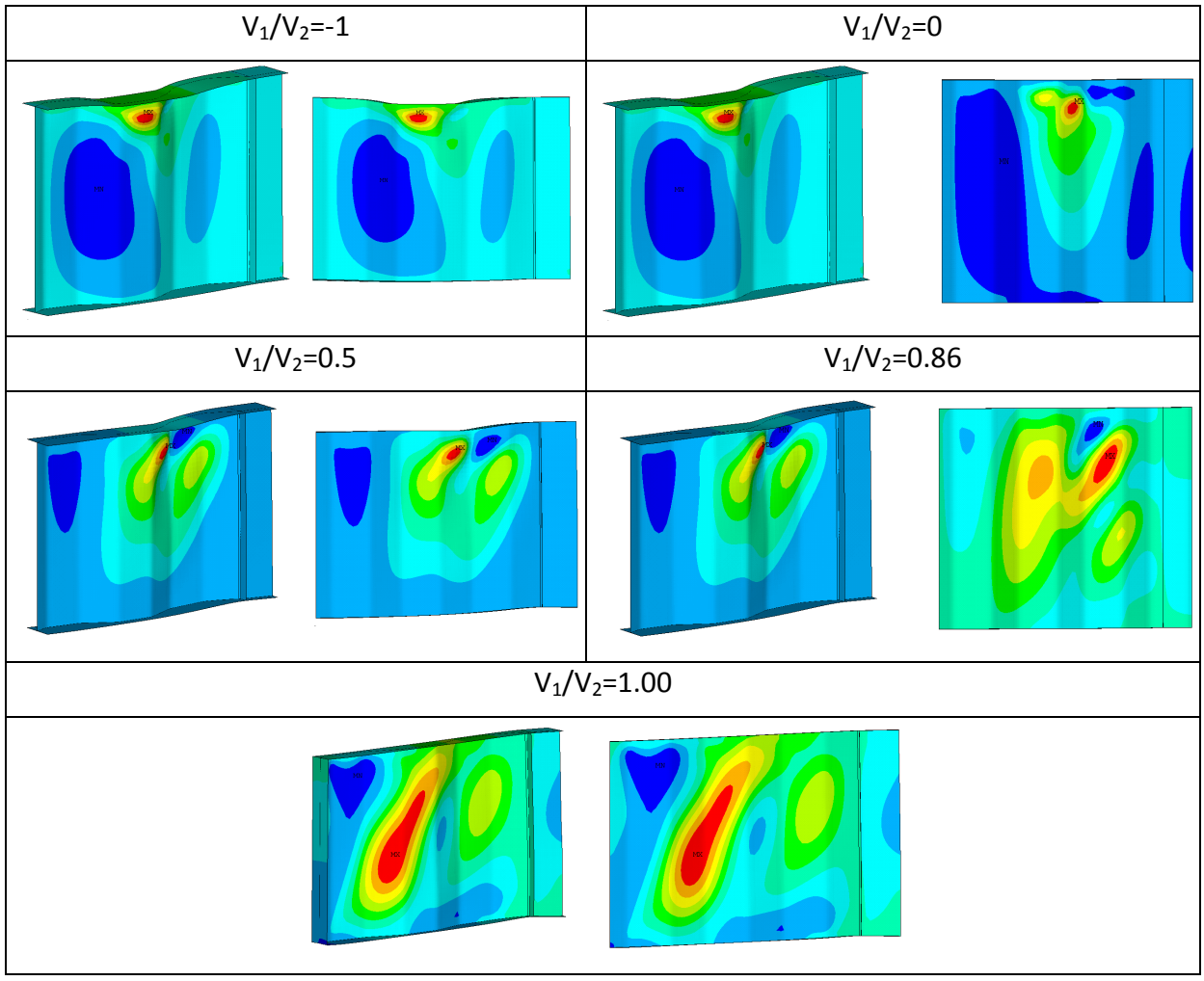

Figure 128: Comparison of different failure modes.

The lateral displacements in the loaded web folds are analyzed under different loading conditions. Figures 129 and 130 show the lateral displacements along the web height in a parallel and in an inclined fold, respectively. In the case of pure web crippling there is only one peak in the diagrams under the loaded flange (V_1/V_2=-1). In the case of pure shear force (V_1/V_2=1) the maximal lateral displacement is at the position of the tension band. In the interaction range coming from pure patch loading to the pure shear force the effect of the shear buckling is more dominant. In the case of asymmetric patch loading ($-1<V_1/V_2\leq 0$) there

are two peaks on the diagrams, one belongs to web crippling and one to the tension band of the shear buckling. In the case of $0<V_1/V_2<1{,}0$ the shear buckling is more dominant and only one peak can be seen on the diagrams.

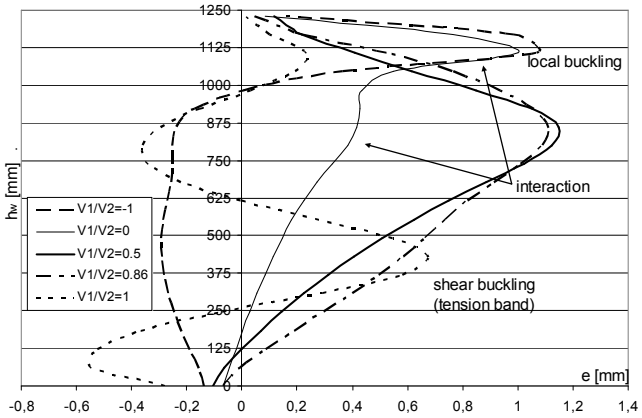

Figure 129: Comparison of the lateral displacements – parallel fold.

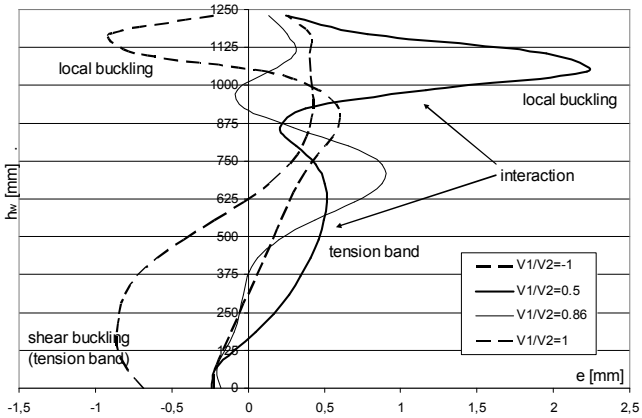

Figure 130: Comparison of the lateral displacements – inclined fold.

7.3.4. Evaluation of the results and development of interaction curves

In the frame of the numerical parametric study the interaction between shear and patch loading is investigated. In the case of all analyzed girder geometry the ratio of F and V_1 is changed. At first the pure patch loading and shear buckling resistances are determined and the observed failure modes are studied. After it 7-8 calculations are executed with different F and V_1 ratios for each geometry. By this way about 10 calculations are conducted in average for each girder geometry, and in total 370 calculations are executed. By this study the analyzed parameter range of Elgaaly and Seshadri [9] is extended as follows:

- h_w/t_w : 100 - 125 - 150 - 200 - 250
- a_1/t_w : 15 - 20 - 25 - 30 - 35
- α : 20° - 30° - 40° - 60°
- ss/h_w : 0.2 - 0.4 - 0.5 - 0.6 - 0.8

The obtained results, together with Elgaaly´s numerical calculations are presented in two diagrams. The evaluation of the results is implemented by two different ways. The first (Fig. 131) is completed using the above mentioned method with subdivision of the combined loading situation according to Fig. 122.

The horizontal axis of the diagram shows the transverse force divided by the patch loading resistance. The vertical axis shows the subdivided shear force divided by the shear buckling resistance of the web panel. Figure 131 shows that the given interaction curve of Kuhlmann

and Braun developed for flat web girders overestimates the interaction behaviour in some cases for corrugated web girders. It can be explained by the fact, that the corrugation profile of the web results in an increase in the patch loading and shear buckling resistance of the web, therefore the web should carry a larger part of the whole applied load and it indicates a stronger interaction criterion.

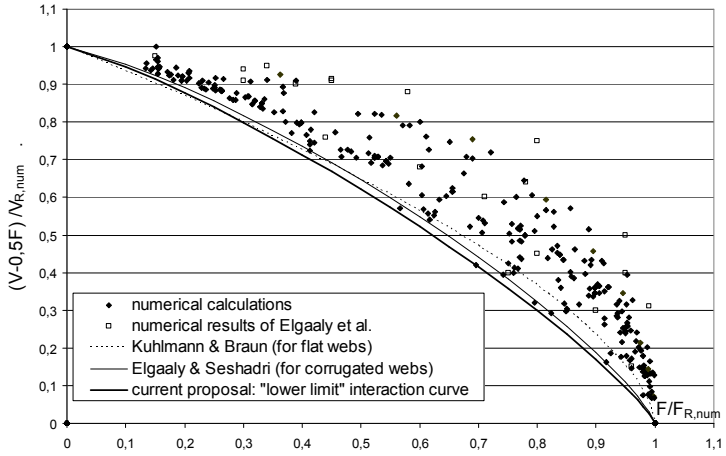

Figure 131: Interaction of shear and patch loading – evaluation method #1.

Results proved that the recommended interaction curve of Elgaaly and Seshadri gives a good approximation in the extended parameter range. From all the numerical calculations only 3 results are under this interaction curve and all of them are at the edges of the analyzed parameter range (long loading length; large α value and large a_1 at the same time). According to take these special cases into account, a lower limit interaction curve is proposed in form of Eq. 125.

$$\left(\frac{V-0.5\cdot F}{V_R}\right)^{1.2}+\left(\frac{F}{F_R}\right)^{1.2}\le 1.0 \tag{125}$$

There is an another possible evaluation method if the load subdivision method according to Fig. 122 is not used. In this case the vertical axis of the diagram shows the maximum shear force (V_2) divided by the shear buckling resistance. Results, based on this evaluation method are presented in Fig. 132.

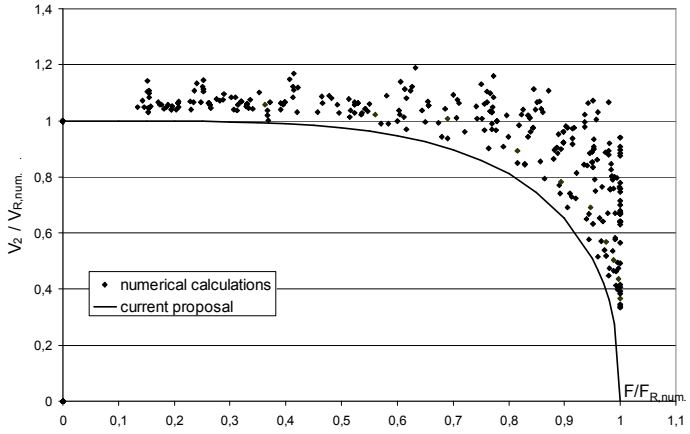

Figure 132: Interaction between shear and patch loading – evaluation method #2.

The shear force due to pure patch loading is not subtracted from the maximum shear force and therefore a significant interacting shear force is present in the case of pure patch loading, too. Points on the diagram are significantly higher than in the case of the first evaluation method. The developed interaction curve may be expressed by Eq. 126. The interaction proposal of

Eq. 121 can be also useful, but the general shear and patch loading interaction evaluation method is based on the load subdivision procedure, therefore only method #1 is studied further.

$$\left(\frac{V_{\max}}{V_R}\right)^{2.5}+\left(\frac{F}{F_R}\right)^{4}\le 1.0 \tag{126}$$

7.3.5. Influence of the analyzed parameters

Due to the relative large scatter of the numerical results, shown in Figs. 131 and 132 each parameters are separately studied, to get to know their effects on the interaction criterion. All together four geometric parameters are studied in the current research work, and this section gives an overview about their influences on the interaction behaviour.

Figure 133 shows the results in the function of the web depth and thickness ratio (h_w/t_w). In the case of the presented calculation results all the other geometric parameters are constant, and only the h_w/t_w ratio is varied.

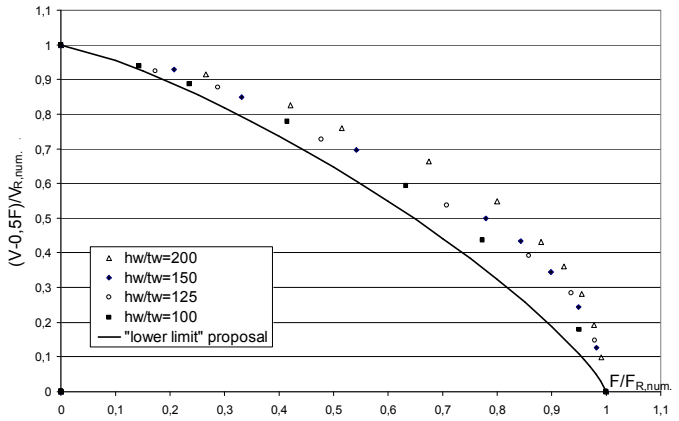

Figure 133: Effect of h_w/t_w on the interaction behaviour.

Diagram shows that smaller h_w/t_w leads to stronger interaction criterion. The same conclusion was drawn for flat web girders by Kuhlmann and Braun, but its effect was smaller for flat web girders than for corrugated web girders. The physical explanation can be the following: the patch loading resistance does not depend on the web depth and therefore the buckling patterns are always the same (length of the yield lines are the same). In the case of higher girders the tension band and the web crippling yield lines do not overlap each other therefore both failure can occur separately and the interaction criterion is weaker. In the case of smaller web depths the tension band can overlap the area of the web crippling and therefore the interaction is stronger. The illustration of the two different cases can be seen in Fig. 134.

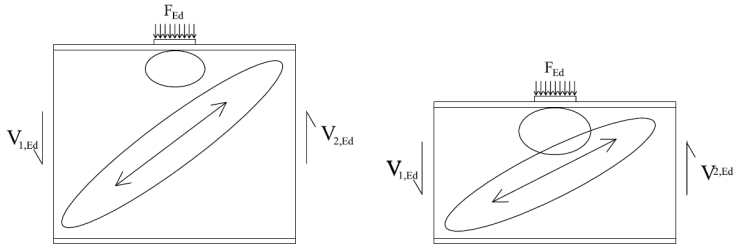

Figure 134: Illustration of the influence of h_w on the interaction behaviour.

The second analyzed parameter is the corrugation angle. Figure 135 shows the effect of it on the interaction behaviour between α=20°-60°. It can be observed that the corrugation angle has a significantly smaller influence and for larger α values the interaction is stronger. The reason of it is that larger corrugation angle increases the patch loading resistance of the web

panel. The patch loading resistance of the flange remains the same, therefore a larger part of the total patch load is carried from the web and with coexisting shear force it leads to resistance decrease. The absolute resistance of the girder is larger for larger corrugation angles, only the interaction is moderately stronger.

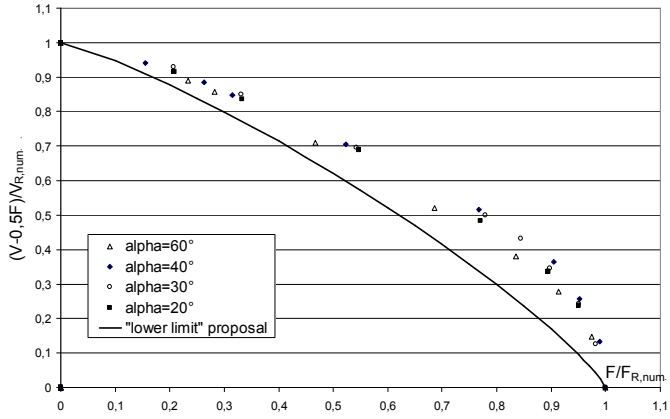

Figure 135: Effect of α on the interaction behaviour.

The third analyzed parameter is the fold width and thickness ratio (a_1/t_w). The effect of this parameter is also relatively small, as presented in Fig. 136. It is in the same order of magnitude as the corrugation angle.

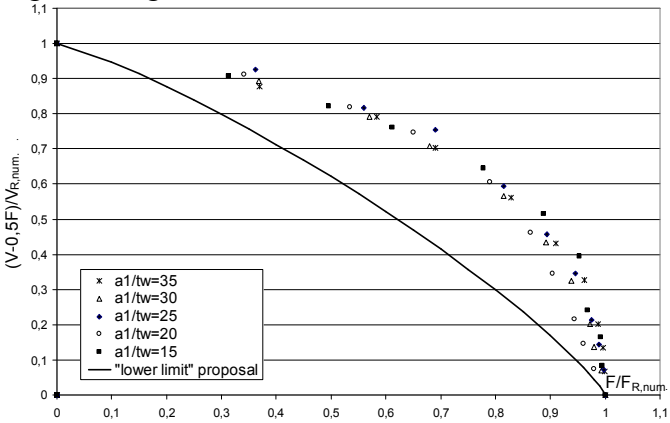

Figure 136: Effect of the a_1/t_w on the interaction behaviour.

The fourth analyzed parameter is the loading length, its influence is presented in Fig. 137. Investigations showed that this parameter is the most dominant, and it results in the largest influence on the interaction behaviour. Larger loading length leads to stronger interaction criterion. The same was observed by Kuhlmann and Braun for flat web girders.

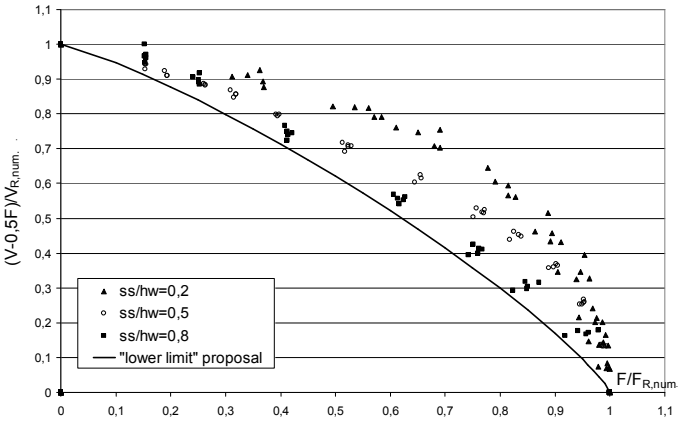

Figure 137: Effect of ss/h_w on the interaction behaviour.

It can be explained by the same reason as before, that larger loading length increases the patch loading resistance of the web. It means that the web carries a larger part from the total patch loading resistance and with coexisting shear force it results stronger interaction. This observation is significant in the development of the design interaction curve. The three analyzed parameters showed that the interaction criteria depends on the ratio of flange and web patch loading resistance. If the flange can carry a larger part of the applied load, the smaller part should be carried from the web and it can be more efficient against the combined loading situation. If the flange can carry only a smaller part of the applied load, the web carries more and it results in a resistance decrease.

Based on this assumption the evaluation of the results is executed in the function of the $F_{R,w}/F_{R,fl}$ ratio (web to flange patch loading resistance). The ratio of the flange and web patch loading resistances are calculated based on the design proposal developed by Kuhlmann and Braun and modified and finalized in the current research introduced in Sections 2.5.2. and 3.4.

The ratio of the web and flange patch loading resistances are calculated by Eqs. (18) and (19) for all analyzed girder. All the calculated results are characterized by this ratio and evaluation is made in the function of it. Results showed that if the $F_{R,w}/F_{R,fl}$ ratio is larger, the interaction criteria is stronger, as shown in Fig. 138. A ”lower limit” interaction curve can be given which is on the safe side for all analyzed girder geometries, but it is uneconomical in some cases. Based on the assumption that the interaction criteria depends on the $F_{R,w}/F_{R,fl}$ ratio, a ”moving” interaction curve is also developed, what always matches to the analyzed girder geometry. It can be expressed in the form of Eq. (127).

$$\left(\frac{V-0.5\cdot F}{V_R}\right)^a+\left(\frac{F}{F_R}\right)^b\le 1.0 \tag{127}$$

Numerical calculations showed that the results are nearly symmetrical on a line beginning from zero with a gradient of 45°, therefore indexes *a* and *b* can be set to equal (*a*=*b*) with a good approximation. Previous investigations of Elgaaly and Seshadri also proved this assumption.

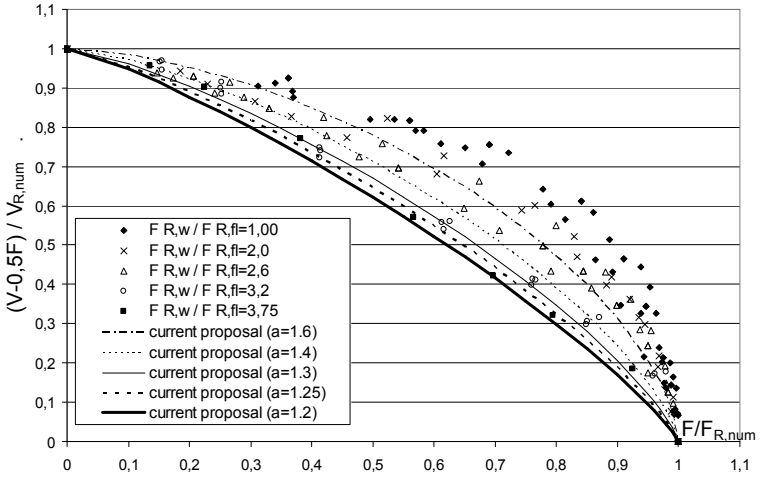

Figure 138: Effect of $F_{u,w}/F_{u,fl}$ ratio on the interaction behaviour.

Figure 138 shows the applicable interaction curves for different $F_{R,w}/F_{R,fl}$ ratios, and indexes are noted on the diagram. The lowest index is 1.2, stronger interaction is not needed in the analyzed parameter range. If the web and flange resistance ratio is smaller, the exponent of the interaction equation can be larger. Applicable exponents are presented in the function of $F_{R,w}/F_{R,fl}$ in Fig. 139. Relationship can be approximated by an exponential function and the shear and patch loading interaction can be calculated by Eq. (128).

$$\left(\frac{V-0.5\cdot F}{V_R}\right)^a+\left(\frac{F}{F_R}\right)^a\le 1.0 \tag{128}$$

where: $a=e^{-0.25\cdot\left(\frac{F_{R,w}}{F_{R,fl}}\right)}+0.8$ but $a\ge 1.2$. (129)

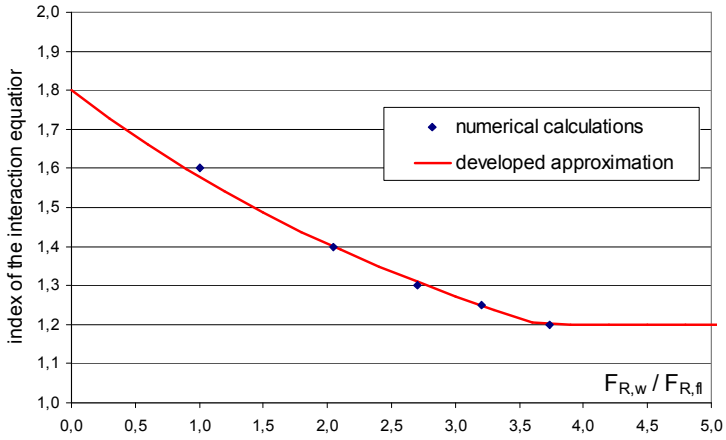

Figure 139: Necessary indexes in the function of $F_{R,w}/F_{R,fl}$.

Using the exponent of 1.2 leads to the ”lower limit” interaction curve, because it can be applied in the whole analyzed parameter range independent from the web and flange patch loading resistances. If the applied exponent is calculated according to Eq. (129), the ”moving” interaction curve is used which takes the effect of the interaction influential parameters into account and leads to a more economical design.

7.4. Statistical evaluation of the proposed interaction curve

The misalignments between interaction curves and numerical results are calculated in this Section. Vector lengths which goes from the zero point to each result are calculated (r_e). The intersection of this vector and the analyzed interaction curve is calculated and the vector length of the intersection point is determined (r_t). The ratio of the two lengths is called by r, which gives a good diagnostic about the distance of the calculated results and the interaction curve. The schematic overview of this calculation method can be seen in Fig. 140.

$$r=\frac{\overline{r_e}}{\overline{r_t}} \tag{130}$$

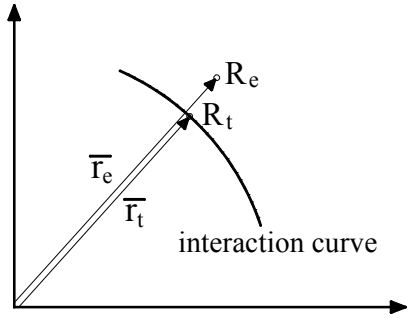

Figure 140. Schematic overview of the calculation method.

Interaction curve can be interpreted on the way that both axis of the diagram are divided by the pure patch loading or shear buckling resistances which comes from experiments or numerical calculations. In this case the results of the numerical calculations are substituted in V_R and F_R.

$$\left(\frac{V-0.5\cdot F}{V_{R,num}}\right)^{a}+\left(\frac{F}{F_{R,num}}\right)^{a}\le 1.0 \tag{131}$$

Results of all numerical calculations and proposed interaction curve of Elgaaly and Seshadri and the ”lower limit” interaction curve are shown in Fig. 141.

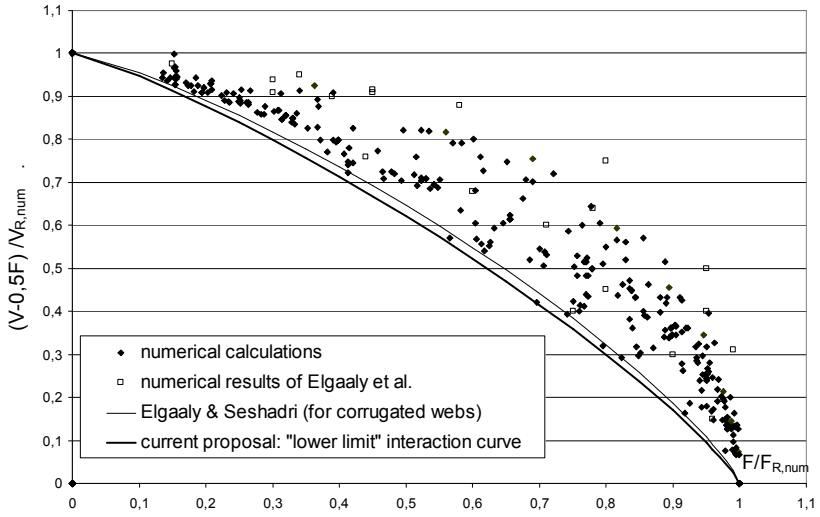

Figure 141: Interaction by numerical resistances of $V_{R,num}$ and $F_{R,num}$.

The *r* values are calculated for all numerical results, where pure patch loading and shear resistances are taken from the numerical calculations ($V_{R,num}$ and $F_{R,num}$). Mean value, standard deviation, coefficient of variation, 5% fractile and minimum and maximum values of *r* are calculated and listed in Table 21. The calculation is executed based on the interaction curve of Elgaaly and Seshadri, based on the currently proposed ”lower limit”, and ”moving” interaction curve.

Table 21: Statistical evaluation based on the resistances of V_{R_Ansys} and F_{R_Ansys} .

	Interaction curve of Elgaaly et al	Current proposal „lower limit“	Current proposal „moving limit“
Mean value	1.071	1.086	1.042
Standard deviation	0.066	0.073	0.038
Coeff. of variation	0.062	0.067	0.037
5% lower fractile	0.963	0.967	0.979
5% upper fractile	1.179	1.206	1.105
maximum	1.350	1.381	1.145
minimum	0.980	1.000	0.986

Results show that the mean value of the *r* is the nearest to 1.00 in case of the moving interaction curve and the standard deviation is also here the smallest. It means that this interaction curve gives the best approach of the numerical calculations. Table 21 shows that the proposed „lower limit“ interaction curve gives a slightly stronger interaction criteria, and this curve can be applied for all girder geometry in the analyzed parameter range.

7.5. Conclusions

In the frame of the presented research work the combined shear and patch loading of girders with corrugated steel web is analyzed. In advance the previous experiments, numerical investigations and existing interaction curves are studied. Only one investigation is available in the literature dealing with this interaction type for corrugated web girders and it was focused only on a narrow parameter range and no experiments were executed. Therefore the focus of the current research is the determination of the shear and patch loading interaction behaviour of corrugated web girders by nonlinear finite element simulation for an extended parameter range.

Based on previous patch loading experiments conducted at the Budapest University of Technology and Economics a finite element model is developed and verified for all test specimens. The load carrying capacities are determined by geometrical and material nonlinear analysis using imperfections. Based on the verified numerical model a parametric study is executed to investigate the shear and patch loading interaction behaviour of corrugated web girders in a large parameter range.

The analyzed parameters are the web depth and thickness, the corrugation angle, the fold and loading lengths. The effect of each parameters on the interaction behaviour is analyzed and tendencies are determined. Results are compared to the previously developed interaction curves and a new design interaction equation is proposed which is applicable for corrugated web girders in the analyzed parameter range. The analyzed parameters showed that the interaction criteria depends significantly on the ratio of the flange and web patch loading resistances. If the flange can carry a larger part of the applied load, the smaller part should be carried from the web and it can be more efficient against the combined loading situation. If the flange can carry only a smaller part of the applied load, the web carries more and it results in a stronger interaction criteria.

Using the lowest developed index in the interaction equation (1.2), it leads to a „lower limit“ interaction curve, and it can be applied in the whole analyzed parameter range independent from the web and flange patch loading resistances. If the applied index is calculated according to the currently developed relationship, the „moving“ interaction curve is used which takes the effect of the interaction influential parameters into account and leads to a more economical design.

Interaction of bending moment and transverse force is also an important aspect of the load bearing capacity as proved by several researchers in the past [45], [46], [48], [49] and [50]. Mainly the flanges are responsible to carry the bending moments and at the same time flanges can have an important role in the patch loading resistance as well, especially in case of bridges where the flanges are relative thick. Therefore the interaction of these two effects, or the interaction of all three effects (bending moment, shear and transverse forces) should be also considered in the design. In the current research the interaction of shear and transverse force is investigated, the interaction with bending moment is the subject of future investigations.

8. Summary and conclusions

8.1. New scientific results

Results of the presented research work is summarised in the following new scientific results.

8.1.1. The thesis of the dissertation in English

Thesis 1.

I identified the geometric parameters which have influence on the patch loading resistance and I determined the behavioural tendencies of them by nonlinear finite analysis.

a, I developed a numerical database where the patch loading resistance of trapezoidally corrugated web girders is determined in a parameter range what is typical for bridges.

b, I determined and characterised the failure modes which can be local buckling of the folds or global bucking of the whole web.

c, I determined the relationships between the patch loading resistance and the loading length, local web ratio, corrugation angle, flange width, flange thickness, loading width and the loading eccentricities if the failure mode is local buckling of the corrugated web.

Publications linked to the thesis: [1], [5], [6], [7].

Thesis 2.

A modified analytical design method is developed to determine the patch loading resistance of girders with corrugated webs in the cooperation between the University of Stuttgart, Institute of Structural Design and BME Department of Structural Engineering. The design method development is based on experimentally verified finite element simulations and on experimental results taken from literature. The following part of the thesis focuses only on my research results.

a, I investigated the previously developed design models and I determined that the design method of Kähönen gave the best approach in the analysed parameter range if the failure mode is local buckling of the corrugated web.

b, I extended the design method to take the effect of the load introduction width, and the loading eccentricities into account. I developed and determined the parameter range of the application for the proposed design methods.

c, The developed design methods are statistically evaluated and partial factors are derived to determine the design resistance level.

d, I determined the constructional rules to avoid the local transverse flange bending failure mode.

Publications linked to the thesis: [1], [10].

Thesis 3.

I designed and executed an experimental research program on 12 large scale test specimens to determine the patch loading resistance of girders with corrugated webs.

a, I analysed and described the observed failure modes and structural behaviours in the function of the investigated parameters.

b, I determined that the patch loading resistance is depending also on the flange and web thickness ratio (t_f/t_w) and the tendency of it is clarified.
c, I modified the resistance model developed by Braun and Kuhlmann based on the experimental results.

Publications linked to the thesis: [1], [2].

Thesis 4.

I developed a finite element based design method to determine the patch loading resistance of girders with corrugated web.

a, I determined the effect of the equivalent geometric imperfection on the structural behaviour (stiffness, patch loading resistance, post-ultimate behaviour and failure modes).
b, I analysed three different imperfection shapes and I determined their effects on the structural behaviour. I developed a new equivalent geometric imperfection shape which is based on the first local buckling mode and what can be given in a closed form equation.
c, I determined the proposed scaling factor of the equivalent geometric imperfection shape based on the imperfection sensitivity analysis and the experimental results.

Publications linked to the thesis: [2], [9].

Thesis 5.

I developed an interaction equation to determine the resistance of the corrugated web girders under combined shear and transverse forces.

a, I proved that the interaction proposal of Elgaaly and Seshadri gives a good "lower limit" interaction approximation for corrugated web girders in a larger parameter range than they analysed.
b, I developed and introduced an "moving" interaction equation which takes the girder geometry and the loading conditions also into account, therefore it leads to a more economic design.

Publication linked to the thesis: [3].

8.1.2. The thesis of the dissertation in Hungarian

1. tézis

Meghatároztam azokat a geometriai paramétereket, melyek befolyásolják a trapézgerincű tartók beroppanási ellenállását és meghatároztam ezek hatását a szerkezeti viselkedésre nemlineáris végeselemes analízis alapján.

a, Kidolgoztam egy adatbázist, mely a trapézgerincű tartók beroppanási ellenállási értékeit tartalmazza a hídszerkezetekre jellemző paraméter-tartományban.

b, Meghatároztam a keresztirányú erő hatására létrejövő lehetséges tönkremeneteli módokat, mely lehet az egyes lemezmezők lokális horpadása, valamint a teljes gerinclemez globális horpadása.

c, Meghatároztam a beroppanási ellenállás és a vizsgált paraméterek közti összefüggéseket, ha a tönkremenetel módja a gerinclemez lokális horpadása. A vizsgált paraméterek az erőbevezetési hossz, a lemezmező szélesség/vastagság aránya, a hajlítási szög, az övlemez szélessége és vastagsága, valamint az erőbevezetés szélessége és a külpontosság.

A tézishez kapcsolódó publikációk: [1], [5], [6], [7].

2. tézis

A trapézlemez gerincű tartók beroppanási ellenállásának meghatározására egy módosított méretezési eljárás lett kidolgozva a BME Hidak és Szerkezetek Tanszéke és a Stuttgarti Egyetem Konstruktion und Entwurf Tanszékének együttműködésében. A méretezési eljárás szakirodalmi kísérleteken és a kísérletek által verifikált numerikus számítások alapján lett kidolgozva. A tézis a témakörben elvégzett saját kutatási eredményeket foglalja össze.

a, Megvizsgáltam és elemeztem a korábban kidolgozott trapézgerincű tartók beroppanási ellenállását meghatározó méretezési eljárásokat, és megállapítottam, hogy Kähönen méretezési eljárása adja a legjobb eredményt a vizsgált paramétertartományban, ha a tönkremeneteli mód a gerinclemez lokális horpadása.

b, Kiegészítettem a méretezési módszert az erőbevezetési szélesség teherbírást befolyásoló hatásának, valamint az erőbevezetés külpontosságából származó teherbíráscsökkenés figyelembe vételével. Kidolgoztam és meghatároztam a kidolgozott méretezési módszerek alkalmazási tartományát.

c, A méretezési eljárás eredményeit statisztikailag kiértékeltem és meghatároztam az alkalmazandó parciális tényező értékét az ellenállás tervezési szintjének meghatározásához.

d, Megadtam azokat a szerkesztési szabályokat, melyek alkalmazásával a lokális keresztirányú övhajlítási tönkremenetel elkerülhető.

A tézishez kapcsolódó publikációk: [1], [10].

3. tézis

Megterveztem és végrehajtottam egy kísérleti programot trapézlemez gerincű tartók beroppanási ellenállásának meghatározására 12 nagy léptékű próbatesten.

a, Meghatároztam és jellemeztem a kísérletben tapasztalt tönkremeneteli módokat és szerkezeti viselkedéseket a vizsgált paraméterek függvényében.

b, Megállapítottam, hogy a beroppanási ellenállásban az övlemez ellenállása függ az öv- és gerinclemez vastagságának arányától (t_f/t_w) is, és a köztük lévő összefüggést meghatároztam.

c, A kísérletek alapján a Braun és Kuhlmann által kidolgozott méretezési eljárást pontosítottam.

A tézishez kapcsolódó publikációk: [1], [2].

4. tézis

Kidolgoztam egy végeselem alapú méretezési eljárást trapézgerincű tartók beroppanási ellenállásának meghatározására.

a, Meghatároztam a helyettesítő geometriai imperfekció hatását a szerkezeti viselkedésre (a merevségre, a beroppanási ellenállásra, a leszálló ágra, valamint a tönkremeneteli módra).
b, Három különböző imperfekciós alakot vizsgáltam és meghatároztam a hatásukat a szerkezeti viselkedésre. Egy módosított alakot dolgoztam ki a helyettesítő geometriai imperfekció felvételére, mely a lokális horpadáshoz tartozó sajátalakon alapszik és zárt képlet formájában megadható.
c, Az imperfekcióérzékenységi vizsgálat és a kísérleti eredmények alapján ajánlást dolgoztam ki a helyettesítő geometriai imperfekció nagyságának felvételére.

A tézishez kapcsolódó publikációk: [2], [9].

5. tézis

Interakciós görbét dolgoztam ki a koncentrált keresztirányú erő és nyíróerő kölcsönhatásának figyelembe vételére.

a, Igazoltam, hogy az Elgaaly és Seshadri által kidolgozott ajánlás a nyírás és a koncentrált keresztirányú erő interakciójának figyelembe vételére egy jó közelítést ad egy, az általuk vizsgált paramétertartománynál sokkal szélesebb tartományban is.
b, Kidolgoztam és bevezettem egy u.n. „mozgó” interakciós görbét, mely figyelembe veszi az interakciót befolyásoló geometriai paraméterek hatását és a tartó terhelési viszonyát, mely eredményeként gazdaságosabb tervezést tesz lehetővé.

A tézishez kapcsolódó publikáció: [3].

8.2. Publications on the subject of the thesis

International journal papers

1. B. Kövesdi, B. Braun, U. Kuhlmann, L. Dunai: „Patch loading resistance of girders with corrugated webs", *Journal of Constructional Steel Research*. (accepted for publication)
2. B. Kövesdi, L. Dunai: „Determination of the patch loading resistance of girders with corrugated webs using nonlinear finite element analysis", *Computers and Structures*. (submitted for publication)
3. B. Kövesdi, U. Kuhlmann, L. Dunai: „Combined shear and patch loading of girders with corrugated webs", *Periodica Polytechnica - Civil Engineering*. (accepted for publication)

Hungarian journal papers

4. B. Kövesdi, L. Dunai: „Trapézlemez gerincű tartók fáradási viselkedése – kísérleti vizsgálat ", *MAGÉSZ Acélszerkezetek*, VI. évfolyam, 1. szám, pp. 38-43, 2009.

International conference papers

5. U. Kuhlmann, B. Braun, B. Kövesdi: „The patch loading resistance of girders with corrugated webs", Proceedings of the Fifth International Conference on Coupled Instabilities in Metal Structures CIMS2008, Volume 1, June 23-25, 2008, Sydney, Australia, pp. 309-316, 2008. ISBN 978-0-646-49439-5.
6. B. Kövesdi, B. Braun, U. Kuhlmann, L. Dunai: „Enhanced design method for the patch loading resistance of girders with corrugated webs", Proceedings of the 5th European Conference on Steel and Composite Structures, EUROSTEEL 2008, Volume B, September 3-5, 2008, Graz, Austria, pp. 1155-1160. ISBN 92-0147-000-90.
7. B. Kövesdi: „Model development for determination of the patch loading resistance of hybrid girders with corrugated webs", Proceedings of the 7th International PhD Symposium in Civil Engineering, September 11-13, 2008, Stuttgart, Germany, full paper on CD, pp.39-48.
8. B. Kövesdi, L. Dunai: „Experimental fatigue analysis of girders with corrugated web", Proceedings of the 25th Danubia-Adria Symposium on Advances in Experimental Mechanics, September 24-27, 2008, Ceske Budejovice (Budweis) and Cesky Krumlov, Czech Republic, pp. 127-128. ISBN 978-80-01-04162-8.
9. B. Kövesdi, L. Dunai: „Determination of the patch loading resistance of girders with corrugated webs using nonlinear finite element analysis", Proceedings of the Twelfth International Conference on Civil, Structural and Environmental Engineering Computing, September 1-4, 2009, Funchal, Portugal, Stirlingshire: Civil-Comp Press, 18 p. Paper No. 16. ISBN:978-1-905088-32-4.
10. B. Kövesdi, L. Dunai, U. Kuhlmann: „Analysis and design of corrugated web girders under eccentric patch loading", Proceeding of the 8th International PhD Symposium in Civil Engineering, June 20-23, 2010, Lyngby, Denmark, pp. 159-164. ISBN 9788778773012.

Presentations

1. „Trapézlemez gerincű hibrid hidak beroppanásvizsgálatának numerikus modellezése”, VII. ANSYS Conference, April 17, 2008, Budapest, Hungary.
2. „Enhanced design method for the patch loading resistance of girders with corrugated webs” 5th European Conference on Steel and Composite Structures, EUROSTEEL 2008, September 3-5, 2008, Graz, Austria,
3. „Model development for determination of the patch loading resistance of hybrid girders with corrugated webs”, 7th International PhD Symposium in Civil Engineering, September 11-13, 2008, Stuttgart, Germany.
4. „Experimental fatigue analysis of girders with corrugated web”, 25th Danubia-Adria Symposium on Advances in Experimental Mechanics, September 24-27, 2008, Ceske Budejovice (Budweis) and Cesky Krumlov, Czech Republic.
5. „Trapézlemez gerincű tartók vizsgálata”, PhD Seminar at the BME Department of Structural Engineering, October 7, 2008, Budapest, Hungary.
6. „Trapézlemez gerincű tartók beroppanásvizsgálata”, PhD Seminar at the BME Department of Structural Engineering, March 24, 2009, Budapest, Hungary.
7. „Imperfections for use with corrugated webs”, 8th Official Meeting of ECCS-TWG 8.3, April 24, 2009, Stuttgart, Germany.
8. „Lokale Krafteinleitung in Trägern mit trapezförmig profillierten Stegen”, Workshop Presentation at the University of Stuttgart, Institute of Structural Design, October 26, 2009, Germany.
9. „Beroppanás és nyírás interakciójának vizsgálata trapézgerincű tartókon”, PhD Seminar at the BME Department of Structural Engineering, March 5, 2010, Budapest, Hungary.
10. „Combined shear and patch loading of girders with corrugated webs”, 10th Official Meeting of ECCS-TWG 8.3, April 30, 2010, Cottbus, Germany.

8.3. Proposal for further study

On the bases of the results presented in the thesis the research is planed to be extended on the following way:

The actually developed design method of the patch loading resistance does not consider the possible interaction of the different effects acting on the loaded girder. Separated interaction equation is developed in this thesis for combined shear and transverse force, but the interaction of the bending moment and transverse force and the interaction of all the three effects could be investigated. Interaction of the combined bending and transverse force should be especially investigated because the bending moment can reduce significantly the flange contribution in the patch loading resistance.

The presented results, evaluations and conclusions in this thesis can be appiled only for girders with trapezoidally corrugated web. Investigations could be extended for sinusoidally corrugated web girders. The patch loading failure mechanism and structural behaviour of both structure types are the same, therefore the patch loading resistance model and the developed interaction criterias could have the same bases.

Further research topic could be the investigation of the effect of the concrete deck on the patch loading resistance. It is possible that the launching of the bridge structure is executed by finished conrete decks. In this case the concrete deck takes part in the patch loading resistance and the ultimate load can be increased. The magnitude of this resistance increase could be studied.

References

[1] http://www.psmic.co.jp/ps_english/gijyutu

[2] http://de.structurae.de/structures/data/index.cfm?ID=s0000849

[3] U. Kuhlmann, B. Braun: „Berechnungs- und Konstruktionsgrundlagen für sandwichähnliche Verbundträger mit Trapezstegen im Brückenbau", Part of the Final Report, Project No. P 645, Forschungsvereinigung Stahlanwendung (FOSTA), Düsseldorf, Germany, 2008.

[4] EN 1993-1-5:2005; EUROCODE 3: Design of steel structures Part 1-5: Plated structural elements.

[5] A. Kähönen: „Zur Einleitung von Einzellasten in I-Träger mit trapezförmig profilierten Stegen", *Stahlbau 57*, No. 8, pp.250-252, 1988.

[6] L. Davaine: „I-girders launching – Influence of load eccentricity", COMBRI project, RFCS Contract RFS-CR-03018, Document COMBRI-Report-SETRA-001, 2007.

[7] U. Kuhlmann, B. Braun: „Combined Shear- and Patch Loading: Numerical Studies and Development of an Interaction Equation", COMBRI project, RFCS Contract RFS-CR-03018, Document COMBRI-Report-USTUTT-002, 2006.

[8] L. Leiva-Aravena, B. Edlund: „Buckling of trapezoidally corrugated webs", Proceedings of the ECCS Colloquium on Stability of Plates and Shells. Ghent, Belgium, 1987.

[9] M. Elgaaly, A. Seshadri: „Girders with corrugated webs under partial compressive edge loading", *Journal of Structural Engineering*, No. 6, pp.783-791, 1997.

[10] R. Luo, B. Edlund: „Ultimate strength of girders with trapezoidally corrugated webs under patch loading", *Thin-Walled Structures*, Vol. 123, No. 6, pp.135-156, 1996.

[11] T.M. Roberts, K.C. Rockey: „A mechanism solution for predicting the collapse loads of slender plate girders when subjected to in-plate patch loading", *Proc. Instn. Civil Engineers*, Vol. 67, No. 2, pp.155-175, 1979.

[12] B. Kövesdi, B. Braun, U. Kuhlmann, L. Dunai: „Enhanced design method for the patch loading resistance of girders with corrugated webs", Proceedings of the 5th European Conference on Steel and Composite Structures, EUROSTEEL 2008, Volume B, September 3-5, 2008, Graz, Austria, pp.1155-1160.

[13] ANSYS® v10.0, Canonsburg, Pennsylvania, USA.

[14] Kövesdi B. „The patch loading resistance of corrugated steel webs used in bridge building", Diploma Thesis. Cooperation between the Institute of Structural Design, University of Stuttgart, Germany and Department of Structural Engineering, Budapest University of Technology and Economics, Hungary, 2007.

[15] L.G. Vigh: „Virtual and real test based analysis and design of non-conventional thin-walled metal structures", PhD thesis, Budapest University of Technology and Economics, p. 128, Budapest, Hungary, 2006.

[16] L.G. Vigh, L. Dunai: „Finite element modelling and analysis of bolted joints of 3D tubular structures", *Computers & Structures*, Vol. 82, pp.2173-2187, 2004.

[17] L.G. Vigh, L. Dunai: „Advanced stability analysis of regular stiffened plates and complex plated elements", keynote lecture, Proc. SDSS 2010 International Colloquium on Stability and Ductility of Steel Structures, September 8-10, 2010, Rio de Janeiro, Brasil. (in press)

[18] L. Pavlovčič, A. Detzel, U. Kuhlmann, D. Beg: „Shear resistance of longitudinally stiffened panels - Part 1: Tests and numerical analysis of imperfections", *Journal of Constructional Steel Research*, No. 63, pp.337-350, 2007.

[19] H. Degée, A Detzel, U. Kuhlmann: „Interaction of global and local buckling in welded RHS compression members", *Journal of Constructional Steel Research*, No. 64, pp.755-765, 2008.
[20] R. Chacón, E. Mirambell, E. Real: „Influence of designer-assumed initial conditions on the numerical modelling of steel plate girders subjected to patch loading", *Thin-walled structures*, No. 47, pp.391-402, 2009.
[21] D. Dubina, V. Ungureanu: „Effect of imperfections on numerical simulation of instability behaviour of cold-formed steel members", *Thin-walled structures*, No. 40, pp.239-262, 2002.
[22] E. Maiorana, C. Pellegrino, C. Modena: „Imperfections in steel girders with and without perforations under patch loading", *Journal of Constructional Steel Research*, No. 65, pp.1121-1129, 2009.
[23] J. Oxfort: „Versuche zum Beul- und Krüppelverhalten von unversteiften Trägerstegbleche unter zentrischen und excentrischen Einzellasten auf dem Obergurt", *Stahlbau*, No. 10, pp.309-312, 1983.
[24] M. Elgaaly, W. Nunan: „Behaviour of rolled section web under eccentric edge compressive loads", *Journal of Structural Engineering*, ASCE, Vol. 115, No. 7, July 1989.
[25] M. Elgaaly, R. Salkar: „Behaviour of webs under eccentric compressive edge loads", Proc. of IUTAM Symposium on Contact Loading and Local Effects in thin-walled plated and shell structures, Prague, 1990.
[26] M. Elgaaly, R. Salkar, M. Eash: „Webs under compressive edge loads", *Research transformed into practice*, pp. 591-600, 1995.
[27] M. Drdacky: „On two particular problems of plate girder webs under partial edge loads", *Journal of Constructional Steel Research*, Vol. 20, pp.183-190, 1991.
[28] J. Raoul, I. Schaller, J.N. Theillout: „Tests of buckling of panels subjected to in-plane patch loading", Proceeding of IUTAM Symposium on Contact Loading and Local Effects in thin-walled plated and shell structures, Prague, 1990.
[29] D. Lučić, B. Šćepanović: „Experimantal investigation on locally pressed I-beam subjected to eccentric patch loading", *Journal of Constructional Steel Research*. Vol. 60, pp.525-534, 2004.
[30] D. Lucic: „Experimental research on I-girders subjected to eccentric patch loading", *Journal of Constructional Steel Research*, Vol. 59, pp.1147-1157, 2003.
[31] B. Sćepanović, S. Aleksic, D. Lucic: „An experimental research "ekscentro 2007" - experimental testing of eccentrically patch loaded steel I-girders", Proceedings of the 5th European Conference on Steel and Composite Structures, EUROSTEEL 2008, Volume B, September 3-5, 2008, Graz, Austria, pp.1149-1154.
[32] B. Šćepanović, L.M. Gil-Martín, E. Hernández-Montes, M. Aschheim, D. Lučić: „Ultimate strength of I-girders under eccentric patch loading: Derivation of a new strength reduction coefficient", *Engineering Structures*, Vol. 31, pp.1403-1413, 2009.
[33] L. Davaine: „Competitive steel and composite bridges by improved steel plated structures: I-girders launching; Influence of load eccentricity", COMBRI project, RFCS Contract RFS-CR-03018, Document COMBRI-Report-SETRA-001, 2006.
[34] EN 1990:2001; EUROCODE: Basis of structural design.
[35] L. Gabeler: „Statistical Evaluation of Patch Loading Resistance Models for Welded Steel Girders", Diploma Thesis. University of Stuttgart, Institut of Structural Design, Germany, 2009.
[36] C. Rebelo, N. Lopes, S.L. da Silva, D. Nethercot, P.M.M. Vila Real: „Statistical evaluation of the lateral-torsional buckling resistance of steel I beams, Part 1: Variability

of the Eurocode 3 resistance model", *Journal of Constructional Steel Research*, Vol. 65, pp.818-831, 2009.
[37] S.L. da Silva, C. Rebelo, D. Nethercot, L. Marques, R. Simoes, P.M.M Vila Real: „Statistical evaluation of the lateral-torsional buckling resistance of steel I beams, Part 2: Variability of steel properties", *Journal of Constructional Steel Research*, Vol. 65, pp.832-849, 2009.
[38] http://www.jcss.ethz.ch/publications/PMC/RESISTANCES/DIMEN00.PDF
[39] EN 1993-2:2006; EUROCODE 3: Design of steel structures Part 2: Steel bridges.
[40] M. Elgaaly: „Failure of thin-walled members under patch loading and shear", Proceedings of the 3th International Conference on Cold Formed Steel Structures, University of Missouri-Rolla, Montana, USA, pp.357-381, 1975.
[41] P. Zoetemeijer: „The influence of normal-, bending- and shear stresses on the ultimate compression force exerted laterally to European rolled sections", Report 6-80-5, Department of Civil Engineering, Delft University of Technology, Delft, 1980.
[42] J. Oxfort, N. Weber: „Versuche zum Stegblechbeulen bei Einzellasteinleitung und Biegung oder Querkraft", Bericht 7/1981, Institut für Stahlbau und Holzbau, Universität Stuttgart, 1981.
[43] T.M. Roberts, F. Shahabian: „Design procedures for combined shear and patch loading", Proceedings of the Institution of Civil Engineers, Structures & Buildings, pp.219-225, August, 2000.
[44] F. Shahabian, T.M. Roberts: „Combined Shear-and-Patch loading of plate girders", *Journal of Structural Engineering*, No. 3, pp.316-321, 2000.
[45] T.M. Roberts, F. Shahabian: „Ultimate resistance of slender web panels to combined bending shear and patch loading", *Journal of Constructional Steel Research*, No. 57, pp.779-790, 2001.
[46] P. Granath, A Thorsson, B. Edlund: „I-shaped steel girders subjected to bending moment and travelling patch loading", *Journal of Structural Engineering*, No. 54, pp.409-421, 2000.
[47] E. Maiorana, C. Pellegrino, C. Modena: „Linear buckling analysis of unstiffened plates subjected to both patch load and bending moment", *Journal of Constructional Steel Research*, No. 30, pp.3731-3738, 2008.
[48] C. Graciano, E. Casanova: „Ultimate strength of longitudinally stiffened I-girder webs subjected to combined patch loading and bending", *Journal of Constructional Steel Research*, No. 61, pp.93-111, 2005.
[49] L.G. Vigh: „Influence of flange-to-web connection on the patch load resistance of I-beams", Proc. SDSS 2010 International Colloquium on Stability and Ductility of Steel Structures, September 8-10, 2010, Rio de Janeiro, Brasil. (in press)
[50] T.M. Roberts, F. Shahabian: „Ultimate resistance of slender web panels to combined bending, shear and patch loading", *Journal of Constructional Steel Research*, No. 57(7), pp.779-790, 2001.